9-29-2014 12:00 AM

Characterization of a Contact-Stylus Surface Digitization Method Using Collaborative Robots: Accuracy Evaluation in the Context of Shoulder Replacement or Resurfacing

Sara Saud Zimmo
The University of Western Ontario

Supervisor
Dr. Louis Ferreira
The University of Western Ontario

Graduate Program in Biomedical Engineering
A thesis submitted in partial fulfillment of the requirements for the degree in Master of Engineering Science
© Sara Saud Zimmo 2014

Characterization of a Contact-Stylus Surface Digitization Method Using Collaborative
Robots: Accuracy Evaluation in the Context of Shoulder Replacement or
Resurfacing
Thesis format: Integrated Article

by

Sara S. <u>Zimmo</u>

Graduate Program in Biomedical Engineering

A thesis submitted in partial fulfillment
of the requirements for the degree of
Master of Engineering Science

The School of Graduate and Postdoctoral Studies
The University of Western Ontario
London, Ontario, Canada

Abstract

Total shoulder arthroplasty (TSA) is the third most common joint replacement. While robot-assisted hip and knee replacement technologies have enjoyed extensive development, this has been limited in the upper limb. This work focused on quantifying the localization accuracy of a robotic system, and evaluating its efficacy in the context of TSA.

A collaborative robot was fitted with a stylus tip to perform manual surface digitizations using the robot's encoder output. In the first experiment, two precision-machined master cubes, representing the working volume around a glenoid structure, were used for system validation. Next, cadaveric glenoids were digitized and compared to a 'gold standard' laser scanner. Digitization errors were 0.37±0.27 mm, showing that collaborative robotics can be used for osseous anatomy digitization.

This thesis presents two novel concepts: 1) use of collaborative robotics for manually operated surface digitizing, and 2) optical fiducial technique, allowing registration between a laser scanner and stylus digitizer.

Keywords

Acknowledgments

The completion of this thesis would not have been made possible without the support and contribution of many individuals.

Firstly, I thank my supervisor, Dr. Louis Ferreira for his guidance, advice and endless words of wisdom. I am fortunate for his patience and mentoring skills, which aided in my development and success as a graduate student. Louis's care for my work and growth provided me with opportunities to attend several talks and conferences. I also greatly appreciate his creative and insightful ideas – may he never stop creating awesome ideas.

Many thanks to Dr. Emily Lalone, who helped me with the registration process for my thesis. She was motivational, helpful, and very encouraging. She always created a very exciting environment to work in! To Nikolas Knowles, you made my time in the lab easier and enjoyable, and with your awesome advice and suggestions made my life easier. Thank you!

I would also like to thank Clayton Cook and Chris Vandelaar from the University Machine Services for taking their time to discuss our ideas and continued revisions for best value and result. Also, I appreciate the time we had together, it was never a dull moment! Thank you Chris, I learned a lot from you, especially on how to minimize cost, which was beneficial!

To the staff at the Writing Support Centre, thank you for proofreading my thesis and improving my writing skills. I definitely recommend everyone to go there!

Thanks to Maryam Mohammad who drew a few of the pictures included in my thesis to ease the work for me. They were pretty awesome. To Fatima Ba'abbad who saved me in the last minute wanting to help, thank you!

A special thank you to my best friend, Hana Dakkak, whose support from the start helped me keep going. She is truly someone I can rely on for advice, ideas, and to always put a smile on my face. To Amir Hage, I express great gratitude for your positive attitude and great proofreading skills. Your eagerness to always help is truly inspiring and motivational.

Lastly, my deepest appreciation to my family and especially my parents. To my siblings, Sahar, Kado, Soomy and Raya, you have driven me to work hard and reach high. A special

thanks to my oldest sister Sahar who has been my biggest role model and strongest advocate. To my parents, Saud Zimmo and Fatima Chahbar, thanks for going through every hardship just to get me through. Thanks for your patience and continuous support and encouragement - I am forever grateful.

Table of Contents

List of Tables

List of Figures

List of Appendices

Chapter 1

1   Introduction

1.1   Shoulder Anatomy, disease and joint replacement

The upper extremities of the human body allow interaction with surrounding environments. Specifically, the shoulder joint provides the most mobility within the whole body, and is capable of performing a variety of movements.

1.1.1   Anatomy and Function

The anatomy of a shoulder allows more movement than any other joint in the body. A shoulder is made up of three bones: the humerus, scapula and clavicle, as shown in **Figure 1.1** (1, 2).

A humerus, or upper arm bone, is a long bone in the upper limb, with a humeral head on the proximal end shaped like a ball. The humerus allows the movement and functionality of the arm as it is a link from the elbow to the shoulder. A scapula is a shoulder blade shaped in a thin, triangular bone, concaved anteriorly on the back of the upper rib. The scapula connects the humerus with the clavicle as a floating link to allow a larger range of motion. The clavicle is also known as the collarbone, and is a long curvy bone that connects the scapula to the trunk and transmits the force from the arm to trunk as well.
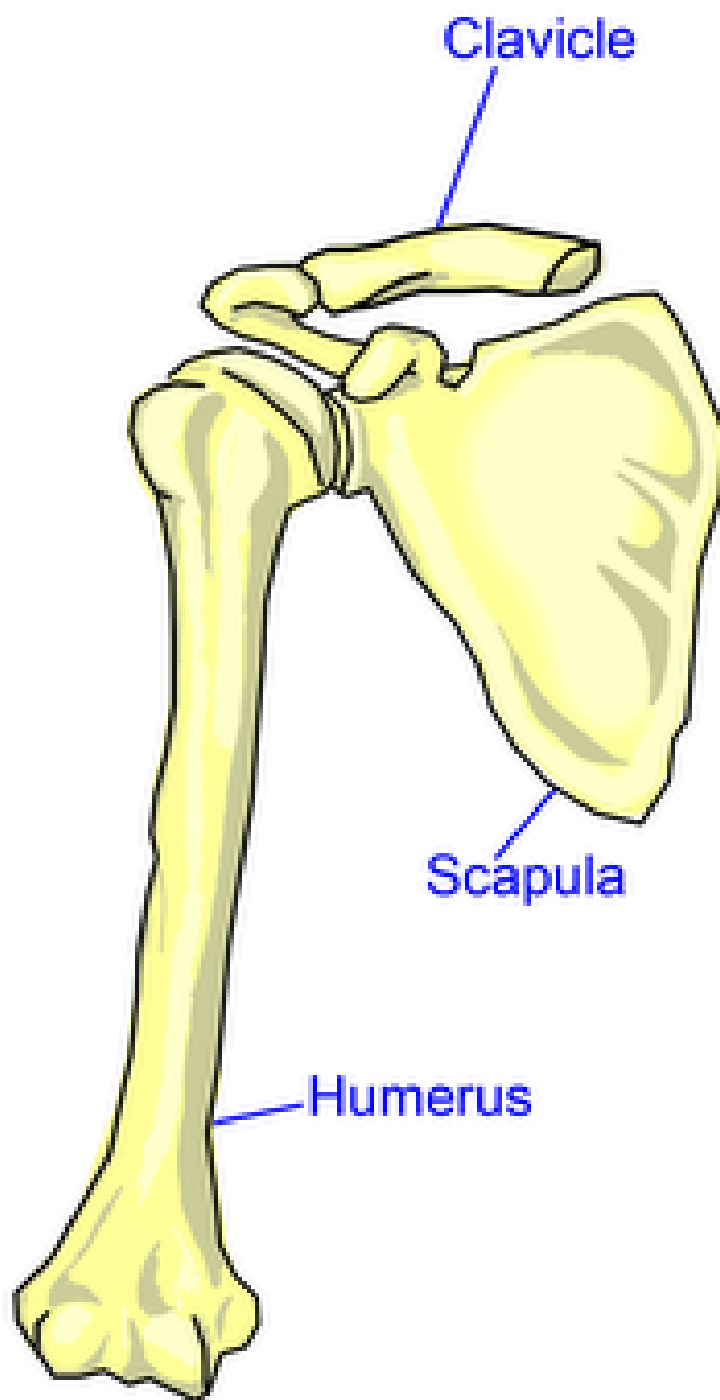
Figure 1.1: The Osseous Anatomy of a Shoulder

Illustrated is an anterior view of the right shoulder; the shoulder consists of three bones: clavicle, scapula and humerus.

Contrary to popular belief, the four joints that make up a shoulder joint are: the glenohumeral joint (GHJ), acromioclavicular joint (ACJ), sternoclavicular joint (SCJ) and scapulothoracic joint (STJ) (**Figure 1.2**). The ACJ is where the clavicle meets the acromion, a bony process on the posterior and superior side of the scapula. It is the only articulation between the clavicle and scapula, providing extra flexibility in the shoulder joint as it allows the ability to raise the arm above the head. The SCJ controls the axial skeleton on the front of the chest and the upper extremity. The STJ is formed where the scapula glides against the thorax, more commonly known as the rib cage. This joint is usually not defined in many sources, as it is not a true anatomic joint with no bone-on-bone motion, but it is an articulation and it keeps the glenoid lined up during shoulder movements. (3-5).

The main or true shoulder joint is the GHJ shown in **Figure 1.3**. The GHJ is a ball and socket joint formed by a glenoid and the head of the humerus (1-3). The glenoid fossa or cavity is a depression on the head of the scapula; it is also the shallow socket for the humerus ball to rotate in making the GHJ (**Figure 1.4**). The surface of a glenoid and humerus is an articular cartilage, which is a smooth substance that allows the bones to move easily, as well as protects the bones. The GHJ has a frictionless motion due to the synovial membrane, a small, thin tissue that creates a fluid to lubricate the cartilage to eliminate friction. Therefore, the GHJ is mostly unconstrained and, like a golf tee, is not very conforming; it is surrounded by a rim called the glenoid labrum and relies on soft-tissue and muscle support.

The rotator cuff is a network of muscles and tendons surrounding the shoulder to provide stability, support, and the ability to move the bones around (2). The rotator cuff surrounds the head of the humerus, attaches the humerus to the scapula, and keeps the arm in the glenoid (6). Ideally, the GHJ consists of three degrees-of-freedom (DOF): supination/pronation (yaw), flexion/extension (roll), and abduction/adduction (pitch). However, the GHJ is not purely a rotational DOF, as the GHJ consists of rotational and minimal translational movements (7), especially in any injury or pathology that may have more translation in the GHJ than usual (8, 9).
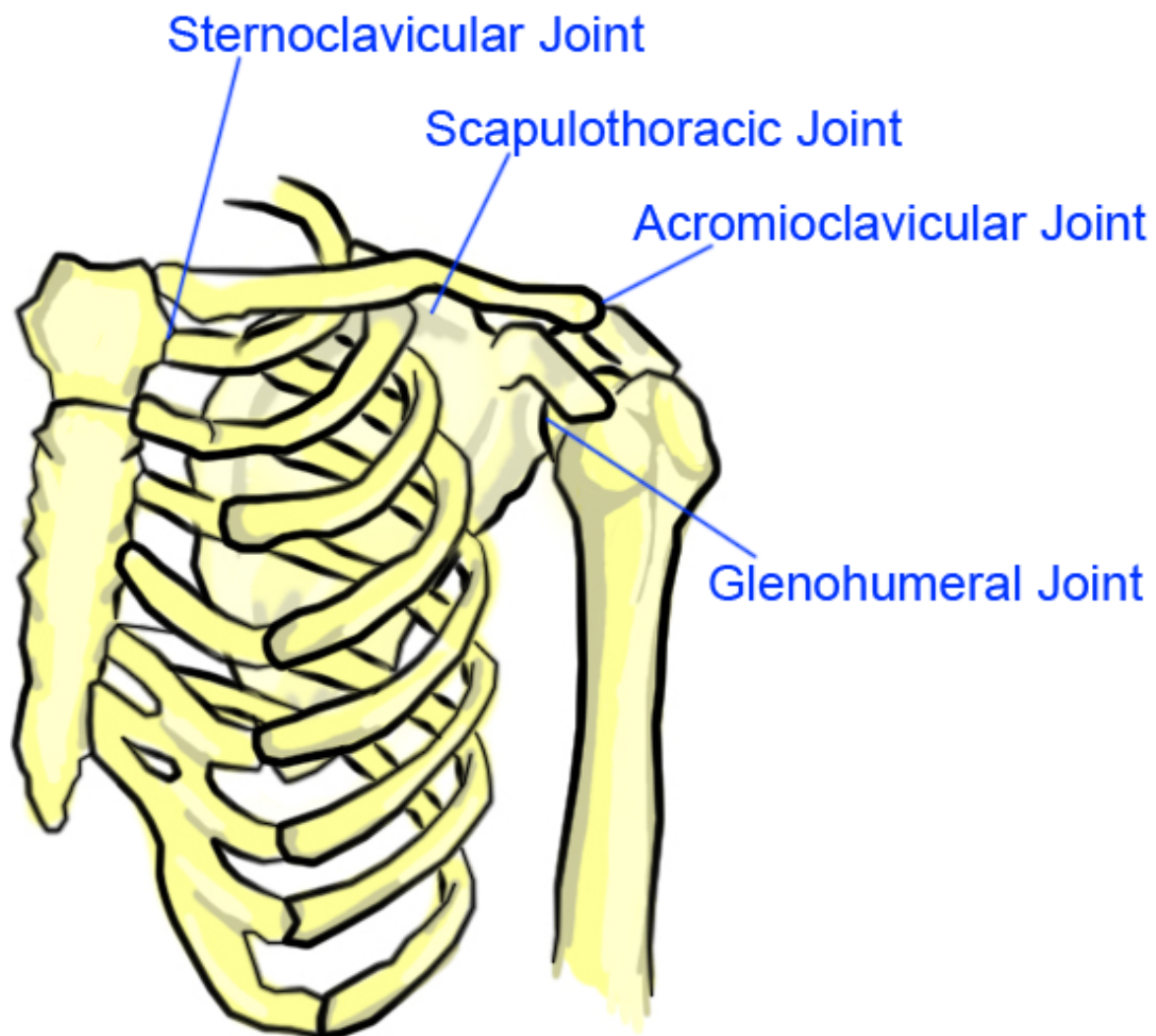
Figure 1.2: Four Different Joints in the Shoulder

The anterior view of the left shoulder is portrayed. The sternoclavicular joint, the scapulothoracic joint, the acromioclavicular joint and the glenohumeral joint are four different joints that allow movements in the shoulder.
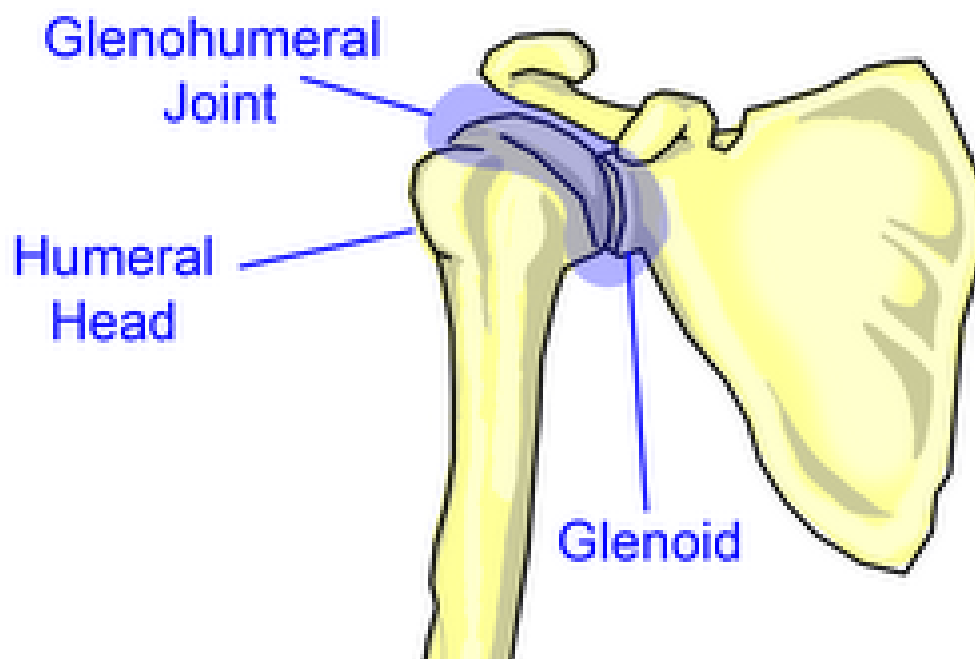
Figure 1.3: The True Shoulder Joint – Glenohumeral Joint

An anterior view of the right glenohumeral joint (GHJ) is depicted. The GHJ is most commonly known shoulder joint, and consists of the head of the humerus and the glenoid. The GHJ is a ball-and-socket joint, as shaded in the illustration.
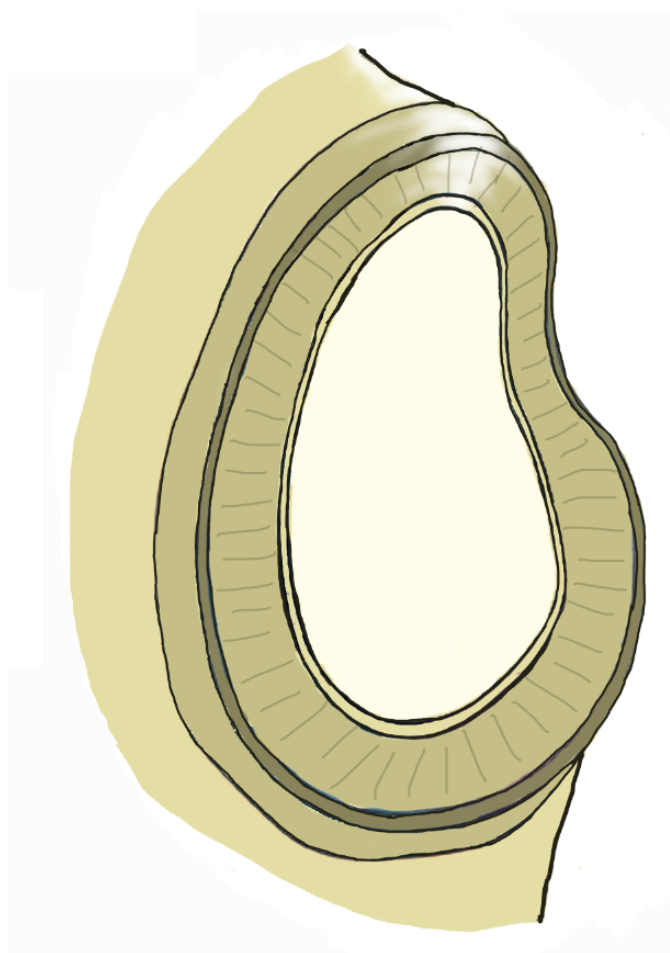
Figure 1.4: A Drawing of Glenoid Fossa

The glenoid fossa, or glenoid, is located at the lateral angle of the scapula. Glenoid is shaped as a socket for the humeral head, and has rim around the edge to contain the humeral head in the socket.

1.1.2   Shoulder Conditions

Several conditions in the shoulder may lead to shoulder arthroplasty, such as osteoarthritis, rheumatoid arthritis and rotator cuff tear arthropathy.

Osteoarthritis, known as "wear and tear" arthritis, is a degenerative joint disease in which the cartilage on the joint deteriorates. Osteoarthritis has two types: primary, which is idiopathic, and secondary caused by another condition such as an injury. In shoulder osteoarthritis, the cartilage on the humeral head and glenoid are worn, reducing the cushioning effect in the joint. As a result, the surfaces of the humeral head and the glenoid become rough, and thus the bones become exposed. Consequently, patients may experience pain and stiffness in the shoulder as the bones rub and grate against each other, limiting their physical activities, work time and functionality of the shoulder (10).

Rheumatoid arthritis is a chronic inflammatory autoimmune disease, a systematic disease that attacks specific components of the body. The synovial membrane that surrounds the joint becomes inflamed and thickened, which can cause cartilage and bone destruction in the joints. This results in severe pain and disability due to joint deformity.

Patients with rotator cuff tear arthropathy have had a rotator cuff tear for a long time, eventually causing them to have shoulder joint disease. A rotator cuff tear involves one or more torn tendons in the rotator cuff, and a humerus head that is not attached fully to the rotator cuff. If there is no early diagnosis or treatment, this can lead to arthropathy, which can result in arthritis and destruction of the joint cartilage (2, 6).

Treatments for these conditions involve medication, physiotherapy, and surgery. When the medication and physiotherapy do not improve the functionality, surgery is recommended as a last resort. The most common cause of a total shoulder replacement is osteoarthritis in the GHJ, as it directly involves the replacement of the cartilage and bones (2, 11).

1.1.3   Total Shoulder Replacement

The shoulder, after the knees and hip, is the third most common joint requiring surgical reconstruction (11). The goal of an arthroplasty is to regain the functionality of a joint

lost due to degenerative joint disease. The first successful shoulder replacement recorded was performed by Péan in 1882 to treat tuberculosis arthritis using a rubber and platinum prosthesis (12). Since then, many discoveries about total shoulder arthroplasty (TSA) have been implemented and are still undergoing research to improve the arthroplasty design. From the original design, in which the GHJ was replaced with a mechanical joint, to current total shoulder arthroplasty, in which the damaged head of the humerus is removed and is replaced by a smooth metal ball with a stem that is press-fitted into the humerus, studies have shown that the shoulder replacement surgery is still improving. In this current procedure, the glenoid is resurfaced with a high-density polyethylene component (13).

TSA is an option for those patients with osteoarthritis in the glenohumeral joint where the pain is interfering with their everyday activities and sleeping patterns, as well as for those who have had non-surgical treatments without improvement to their functionality (11). Although hemiarthroplasty, in which one bone of the joint is replaced, is much easier to perform due to glenoid complications, TSA is recommended over hemiarthroplasty; in their study of the treatment of glenohumeral osteoarthritis, Izquierdo et al. (2010) show that the global health assessment scores and pain relief of the shoulder were statistically significantly better after TSA (11). The stability and normal load transfer cannot be restored to a degraded glenoid anatomy if hemiarthroplasty is performed. Furthermore, compromising the structure or mechanical properties of cartilage of the glenoid will result in the loss of the normal load-distributing and stabilizing mechanisms of the joint, and the accelerated wear of the cartilage due to the loss of even distribution of force (14).

TSA is a highly technical procedure (13). In summary, it is performed by making an incision on the anterior of the shoulder, between two muscles, the deltoid and the pectoralis major, to access the glenohumeral joint. Once the incision is open, the scar tissue that restricted the motion of the shoulder is removed, and one of the tendons is cut to further access the joint. The damaged humeral head is removed, and prepared for a humeral component placement. A smooth metal ball with a stem is press-fitted into the humerus. The placement of the glenoid is prepared by reaming, which will shape and orientate the bone of the glenoid, and the glenoid prosthesis is inserted. Then the tendon

that was cut in the beginning of the procedure is repaired to the bone.

Glenoid complications are the most common challenge in TSA and require extensive attention to the glenoid component in the surgery. Complications include inadequate preparation of the bone surface, the prosthesis not fully seated on the prepared bone and insufficient bone left for glenoid placement (15).

1.1.3.1   Glenoid Component

Many studies show that the glenoid component remains a primary concern in TSA, as large percentages of failures of shoulder arthroplasties are related to problems in managing the glenoid socket (15-18). This complication causes post-operative pain and limited functionality of the shoulder, as well as a potential need for a revision surgery.

1.1.3.1.1   Anatomic Parameters

Anatomic parameters are considered to determine the glenoid implant and placement, including glenoid height, width, inclination, shape and version as shown in **Figure 1.5** (18, 19). A normal glenoid cavity has a pear shape (20) or is an elliptical (18). Glenoid height is defined as the distance between the most superior and inferior points of the glenoid. Glenoid width is the distance between the most anterior and posterior points on the glenoid. Glenoid inclination is defined as the slope of the glenoid surface area along the superior and inferior axis. Glenoid version is defined as the angular orientation of the axis of the glenoid articular surface relative to the long (transverse) axis of the scapula; posterior or positive angle is denoted as retroversion, while negative angle is anteversion (18, 21).

Three evaluations of the glenoid are used to report its anatomic parameters, specifically the height, weight and version. Checroun et al. (2002) evaluated 412 cadaveric scapulae (22), Iannotti et al. (1992) evaluated 96 shoulders of patients and 44 cadaveric scapulae; Iannotti et al. reported that there is no significant difference between the cadaveric glenoid and those in live patients (20). Lastly Churchill et al. (2001) evaluated 172 matched pairs or 344 cadaveric scapulae; Churchill et al. chose 50 black men, 50 white men, 50 black women and 22 white women (21).
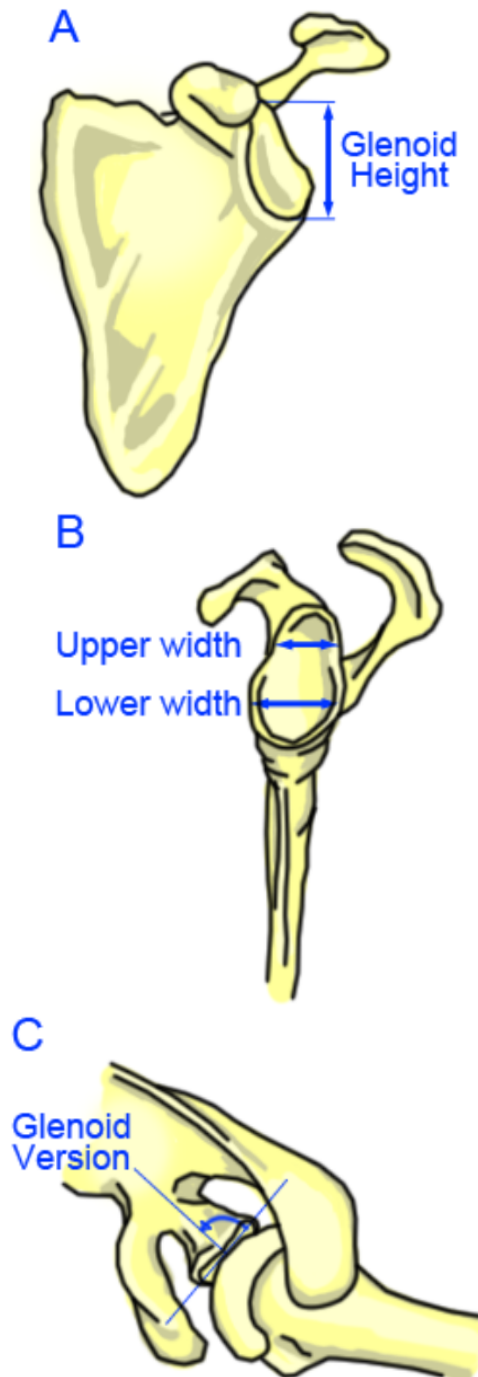
Figure 1.5: Anatomic Parameters

(A) Displays the glenoid height (B) Displays the upper and lower width if the glenoid is pear shaped, and (C) Displays the glenoid version.

In terms of glenoid shape, Checroun et al. reported that, of 412 cadaveric glenoid, 71% were pear shaped, and 29% were elliptical, and found that female glenoids were 10% smaller than male glenoids. Iannotti et al. only mentioned pear shapes, and reported a ratio of lower to upper anterior-posterior measurement of 1:0.08 ± 0.01. Churchill et al. made no mention of the shape of the glenoid.

With regards to glenoid height, Checroun et al. reported a mean glenoid height of 37.9 ± 2.7 mm. Iannotti et al. reported a mean glenoid height of 39 ± 3.7 mm. Churchill et al. found that although the two races did not vary, there was a significant difference between gender; Churchill et al. reported a mean male glenoid height of 37.5 ± 2.2 mm and female glenoid height of 32.6 ± 1.8 mm ($p < 0.001$).

Concerning glenoid width, Checroun et al. reported a mean glenoid width of 29.3 ± 2.4 mm. Iannotti et al. reported two widths for each glenoid, as he believed the glenoids were pear-shaped. Thus Iannotti et al. reported a mean upper glenoid width of 23 ± 2.7 mm and a mean lower glenoid width of 29 ± 3.1 mm. Churchill et al. reported a mean glenoid width of 27.8 ± 1.6 mm in male specimens and 23.6 ± 1.5 mm in female specimens ($p < 0.001$).

Only Churchill et al. made mention of glenoid inclination, and found that there was a variability between gender and race, although not statistically different ($p = 0.07$ between black men and white women). He found that the glenoid was superiorly inclined by 4.0 ± 3.4° in male specimens and superiorly inclined by 4.5 ± 3.8° in females.

Regarding glenoid version, Churchill et al. reported a mean glenoid retroversion of 1.23 ± 3.5°. Churchill et al. found no significant difference between gender; however there is a difference between race as white patients were more retroverted than black males (mean white, 2.66; mean black, 0.20; $p < 0.00001$). The parameter of glenoid version has been emphasized in recent studies, with a normal range varying from 2° anteversion to 9° retroversion and noted changes in version in the presence of glenohumeral pathology (18).

1.1.3.1.2   Glenoid Pathology

Glenoid arthritis is frequently associated with glenoid wear (18). Walch et al. generated a classification system to describe glenoid wear patterns in arthritic glenoid after observing 113 GHJ with primary osteoarthritis (23). Walch et al. classified the main glenoid types as A, B, and C.

Type A is classified as concentric wear, in which the humeral head is centered to allow equal distribution of the joint reaction force along the glenoid surface. The minor erosion is classified as Type A1, and the major as Type A2. Walch et al. found that the average retroversion is 11.5 ± 8.8°. Type B is categorized by a posterior humeral head subluxation with a posterior glenoid wear pattern; a joint reaction force is distributed asymmetrically. Retroversion was found to be at least 18 ± 7.2°. Type C is defined by glenoid retroversion of more than 25°, regardless of erosion.

In primary osteoarthritis, Walch et al. found that Type A was the most used in 1999; however more recent studies found that Type B, or posterior glenoid wear due to humeral head subluxation in the posterior joint, was the most common pattern (14, 18, 24). A good preoperative axillary view is used to determine the glenoid wear, as it shows the shape of the glenoid, as well as the position of the humerus, to assess for the extent and location of the glenoid wear (14).

Iannotti et al. (2005) explained that there are two main reasons for glenoid retroversion of patients with primary osteoarthritis with Type B to lead to posterior instability (25). First, increasing glenoid retroversion causes the joint reaction force to translate posteriorly, causing an off-axis moment, and posteriorly directed shear force across the glenoid face. Second, the retroverted glenoid will effectively decrease the posterior wall height or joint constraint.

1.1.3.1.3   Glenoid Design and Fixation

The primary goal in TSA is to ensure no complications in the glenoid component, specifically in the glenoid placement. Therefore, many studies have attempted to optimize the design and fixation of the glenoid component. Factors include, but are not

limited to, metal vs. polyethylene backing, in-growth vs. cemented placement, and pegged vs. keeled.

A study by Fox et al. (2009) collected 1542 primary total shoulder replacements and presented 20 years follow-up data on a number of glenoid implant designs (26). The two materials that Fox et al. evaluated were metal-backed, in which the glenoid surface is polyethylene and the implanted area of the component is metal, and polyethylene, in which the component is all polyethylene. Fox et al. found that metal-backed glenoid components have the most surgery revisions due to infection, instability, wear and loosening relative to polyethylene. The differences between the two materials are large; 2.3% of all metal-backing were infected, compared to 0.6% of all polyethylene; the instability rate was 3.5% for metal-backed, compared to 0.5% for polyethylene. Overall, 16.7% of the metal-backed required surgery revisions, compared to 2.7% of the polyethylene. Fox et al. concluded that the material used for the backing was significantly associated with revisions. Fox et al. also found that the bone in-growth, non-cemented implants are at a greater risk for failure over time due to material wear, component loosening and instability compared to cemented implants. Finally, Fox et al. discovered that aseptic loosening was the most common reason for revision, and contributed to about 42% of all revisions. Fox et al. concluded that to achieve the best survival of the glenoid component involved using polyethylene and cemented implants.

Throckmorton et al. (2010) conducted a long-term study to determine the failure rate of two types of mounting designs, pegged or keeled (27). The design of each component type is shown in **Figure 1.6**, where the pegged design has three pegs aligned in the superior-inferior axis, and the keeled design has a thick and flat trapezoid shape. Throckmorton et al. compared their findings to two studies; one of these studies reported that biomechanical analysis suggested pegged components perform better with normal bone stock, while keeled components performed better with inadequate bone stock. The other study reported that keeled components were most likely to shift in position and that glenoid erosions became worsened.
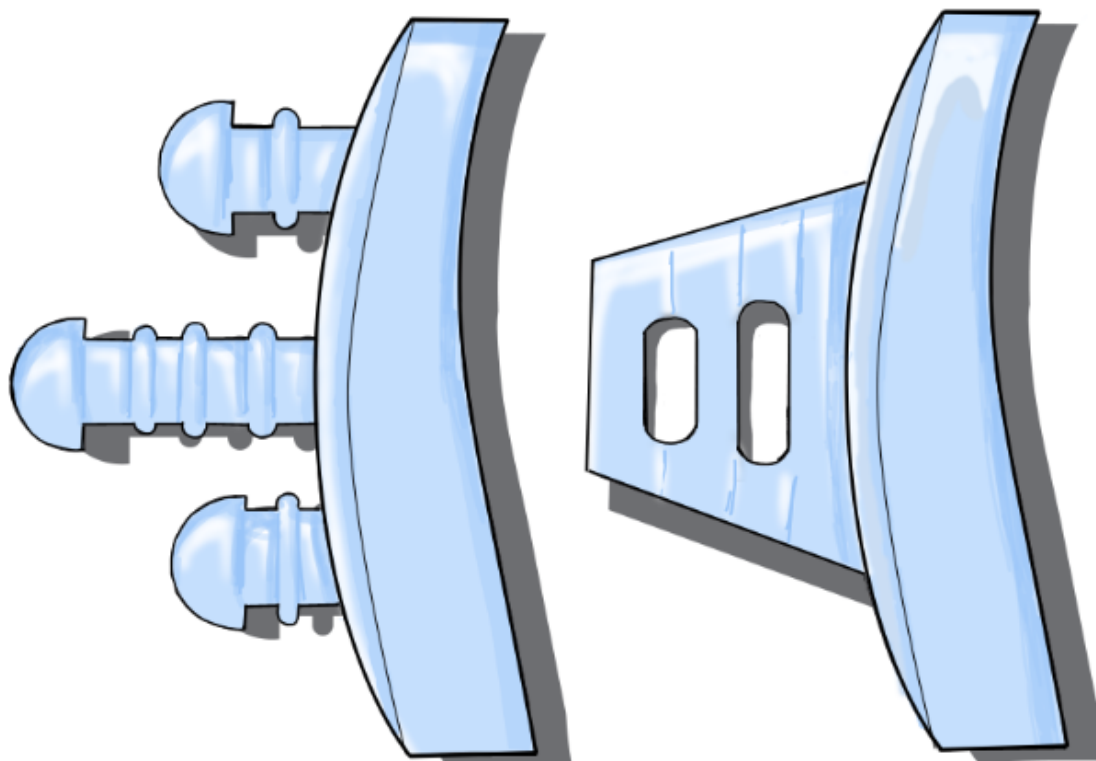
Figure 1.6: Two Types of Glenoid Component: Pegged and Keeled

The glenoid components have two different types to implant into the bone, as represented in the drawing. The left shows a pegged component, and the right shows a keeled component. Pegged component has three pegs, with small rims around each peg to secure placement of the implant. The keeled component is shaped as a trapezoid, with holes to allow cement through to secure placement.

The mean radiographic follow-up period was approximately 4 years, and found no significant difference between both groups regarding clinical or radiographic performance. Therefore, to optimize the design, polyethylene cemented design is favoured, and although there is no significant difference between pegged and keeled design, some studies prefer a pegged design as it has better seating. However, factors that limit component fixation include inadequate bone stock and low strength of the available bone (18); therefore, there is a need for further research in pegged vs. keeled design regarding the associated limiting factors. It is important to note that nonconcentric glenoid wear is often treated by eccentrically reaming the glenoid to correct the glenoid version and improve fixation; instead of compensating the glenoid retroversion with humeral anteversion, as Iannotti et al. reported that humeral component version does not affect the glenoid component wall height or joint constraint (25).

Another factor contributing to the glenoid component design is the glenohumeral implant conformity (**Figure 1.7**). Glenohumeral implant conformity is the relationship between the convexity of the humeral head and the concavity of the glenoid components. Biomechanics of the joint, specifically loading and stability, are significantly influenced by the conformity of the glenohumeral joint (19). Concavity compression refers to the stability obtained by compressing the humeral head into the concave glenoid fossa (28). Increasing the magnitude of the compression load into the glenoid concavity increases the stabilization of the GHJ, and the distributed loads is evenly spread in the glenoid. Therefore equal convexity and concavity is desired as the GHJ is conformed; however due to the compression, GHJ is constraint to humeral translation in the glenoid (14, 19). Therefore, several studies suggested reaming the glenoid to create a radial mismatch, which results in a greater glenoid radius than the humeral head radius (29-33).The radial mismatch decreases the risk of glenoid loosening, as Nho et al. reported that on a retrieval study, conformed glenoid components have greater wear than non-conformed glenoid components (33). Therefore, a trade-off is shown between polyethylene wear and GHJ stability; and as a result, the optimal radial mismatch is 6-7 mm, as discovered by Walch et al. after evaluating 319 TSA (30).
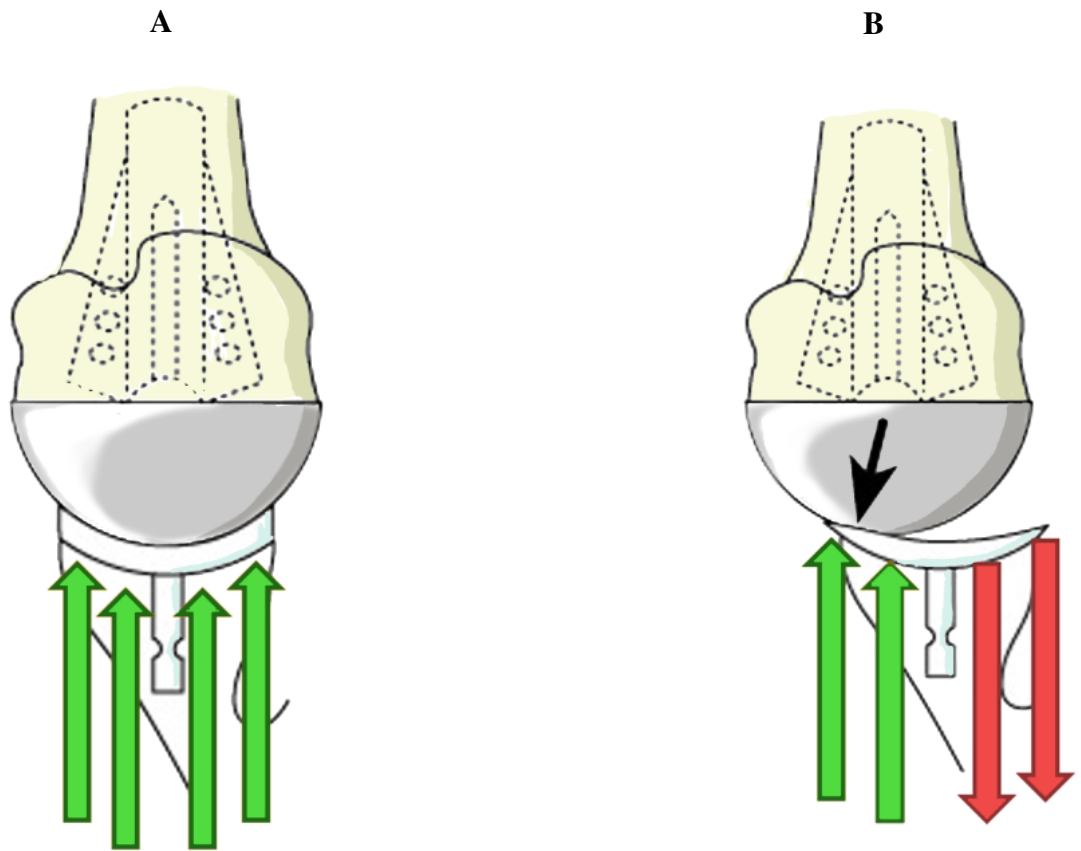
Figure 1.7: Glenohumeral Implant Conformity

A) Correct way of conforming the glenohumeral joint, as the load applied causes the reaction force to be distributed evenly along the implant. B) Case when the glenoid is incorrectly placed, the loading is applied on one side, causing the reaction force to behave like a rocking horse. This will then loosen the glenoid component as well as accelerate wear.

1.1.3.1.4   Glenoid Component Failure

Matsen et al. (2008) reported many failures involving glenoid components, including the failure of the component itself, the component seating, and the prosthetic loading (15). Failures of the component itself include pitting and erosive wear on the prosthesis surface, the fracture of the glenoid component including the keel or peg fracture, and fracture of the polyethylene body. The wear of the glenoid due to metal backing as well as the separation of the polyethylene and metal are also failures of the component itself.

Failures of the component seating include inadequate preparation of the bone surface, the prosthesis not fully seated on prepared bone and inadequate bone stock for component placement. Prostheses not fully seated on the prepared bone, which may be caused by glenoid component malalignment, is the most common reason to have surgery revisions. Glenoid component malpositioning contributes to aseptic loosening, as the distributed force is not applied on the glenoid face evenly, causing one end to elevate as the other end compresses. Matsen et al. reported a study that showed seating was much worse for the keeled component than for the pegged component, due to the precision of the match between the geometry of the design to the prepared bone. Insufficient bone stock is also an issue as there is no support to secure the fixation of the glenoid component.

Failures due to prosthetic loading include the glenohumeral implant conformity, rim loading, glenohumeral instability and rotator cuff insufficiency. Glenohumeral implant conformity can influence failure by the excessive conforming of the joint surfaces, which limits the translation of the humerus, increases the concavity compression, and increases wear of the glenoid component. Rim loading is the loading on one edge, which causes the opposite edge to elevate; continuous rim loading will cause a rocking-horse effect, and lead to aseptic loosening. Glenoid component version refers to the abnormal version of the component, which leads to eccentric loading on the glenoid and eventual increase to cement mantle stress. Finally, rotator cuff insufficiency is the instability in the glenohumeral joint, which causes rocking-horse loosening due to eccentric loading (15, 34).

1.2 Robotic joint replacement or resurfacing in other joints

Robotics is a relatively young field of modern technology that crosses traditional engineering boundaries (35). It was not until the mid-twentieth century that mechanics, controls, computers and electronics were combined to create the field of robotics (36). In 1979, The Robot Institute of America defined a robot as 'A reprogrammable, multifunctional manipulator, designed to move material, parts, tools or specialized devices through variable programmed motions for the performance of a variety of tasks' (37). Sciavicco et al. mentioned that this definition reflects the current status of robotics technology (36), and Spong et al. specifically pointed out a keyword "reprogrammable", which accounts for the utility and adaptability of the robot 'brain' (35).

The first robot used for orthopaedic surgery was ROBODOC, shown in **Figure 1.8** (Integrated Surgical Supplies Ltd., Sacramento, CA). It was also the first surgical robot approved by the US Food and Drug Administration (FDA), and was developed at the University of California-Davis from 1986 to 1992 (38, 39). ROBODOC was an active robot, designed to assist the surgeon to perform a total hip arthroplasty, with computer-aided robotic milling devices for accurate implant placement on the femoral bone. The ROBODOC procedure was performed clinically on human patients in 1991(39, 40). In hopes of satisfying the needs of the FDA, studies from 1991 to 1998 showed improvement of fit, fill and alignment of implants statistically compared to conventional total hip arthroplasty, with accuracy within 0.4 mm and 96% precision (38, 41).

However, ROBODOC complications included longer surgery times and greater learning curves for the surgeons operating with the robot (38). Also, when the monitoring system detected an error, the robot stopped its task and corrected the error before proceeding. In addition, there was a slight increase in blood loss due to the locator pins as a marker reference used for image guidance anchored on the bone (38). Currently, ROBODOC, which has been approved over the years, uses surface-matching procedures to replace the locator pins. It is commercially available by Integrated Surgical Systems Inc., Davis, CA, and has been applied in over 10,000 procedures (42).

Bone Milling Machine
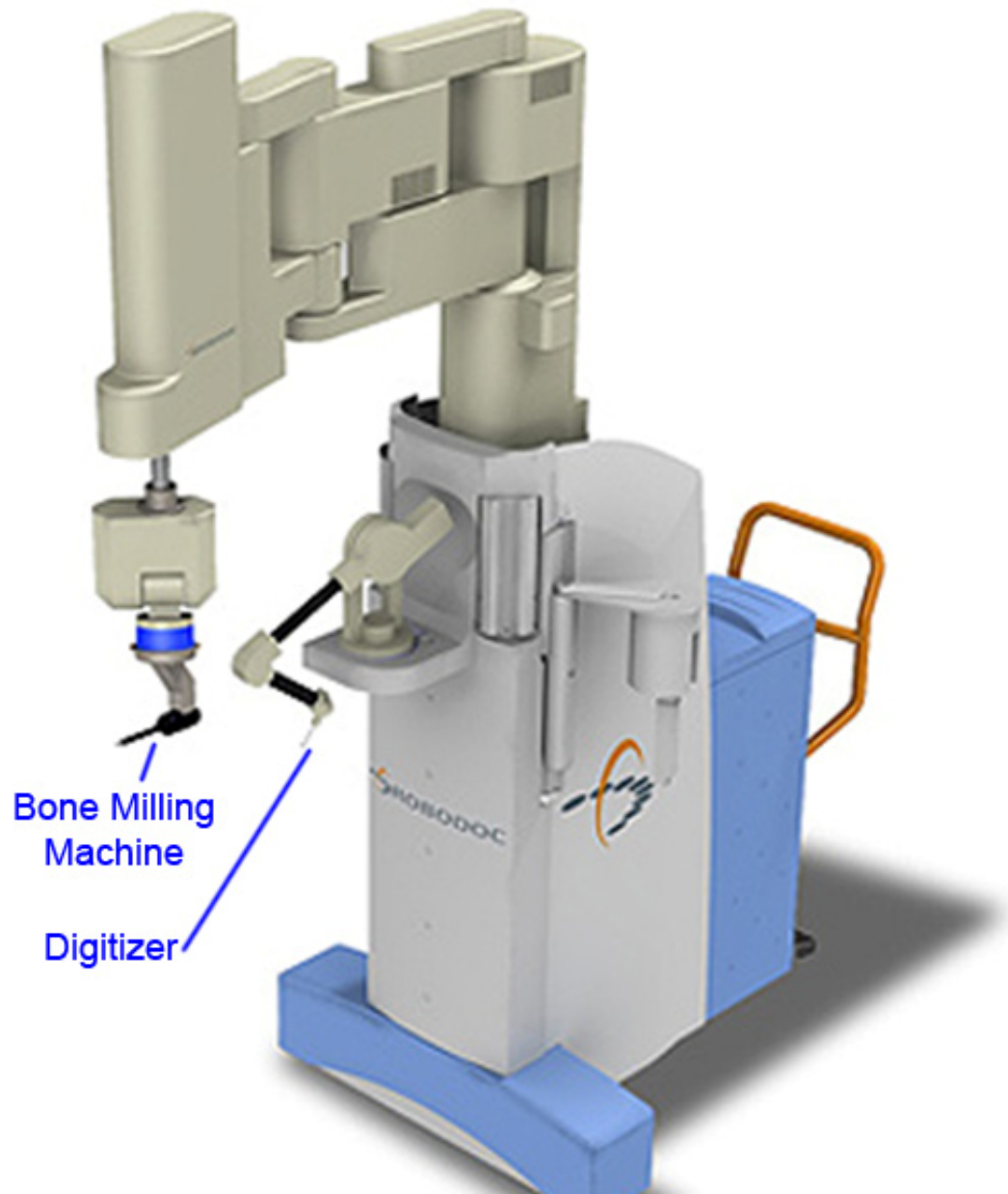
Digitizer

Figure 1.8: The Robodoc System[1]

The left-most arm with the blue band is a bone milling machine, used to prepare the placement of the implant on the bone. The middle arm is a mechanical arm digitizer with a stylus probe on the platform for digitization purposes in the pre-operative planning.

---

[1]Modified from RoboDoc 1.0 surgical system [Internet]. Pleasanton, CA: Compass Services; 2014; cited July 25, 2014]. Available from: http://compassdesign.com/robodoc1/.

Active Constraint ROBOT, or ACROBOT (The Acrobot Company Ltd, London, UK), is another early robot used for orthopaedic surgery (38, 41). ACROBOT used a different approach than ROBODOC, where ACROBOT allowed the surgeons some control in the arthroplasty surgery, making the system synergic. ACROBOT was a six DOF articulated robot arm designed for industrial robot (38, 42), and transformed into a surgical robot. ACROBOT uses a software-based motion constraint system using force feedback; this software will ensure that the bone milling process is still in a safe region for the bone preparation of the knee prosthesis bed (43). There are two skills required to work with ACROBOT: a skill of the robot to accurately cut flat surfaces in specified positions, and a skill of the surgeon to judge how much force is need to be applied to cut away the undesired bone (43). To synergize the two skills, the surgeons have complete control over the cutting process while the robot prevents the surgeons to damage the soft tissue or remove too much bone material, and guides the surgeons to registered cuts in the bone (43). ACROBOT is the first active surgical robot, and it is currently commercially available for partial knee replacement (40, 42). ACROBOT was recently acquired by MAKO as part of a settlement in intellectual property litigation (41).

Bone Resection Instrument Guidance by Intelligent Manipulator, or BRIGIT (MedTech S.A., Montpellier, FR), is an active robot intended for use in total knee arthroplasty (44). A main functionality of BRIGIT is to lock the knee in position to ensure accuracy of the knee prosthesis placement. Determining and optimizing the lock position is included in the patient specific pre-operative planning, to allow surgeons to use their tools to resurface the bone at a precise angle, and to ensure that the knee prosthesis is accurately placed without any complications. BRIGIT was developed by MedTech's Intelligent Surgical Instrument Technology, acquired by Zimmer in 2006, and cleared for FDA in 2006. However, it was believed that BRIGIT was never used clinically even after Zimmer announced the availability and price of BRIGIT (44).

MAKOplasty (Mako Surgical, Fort Lauderdale, FL, USA) is a procedure for Robotic arm Interactive Orthopaedic (RIO) systems; it is a hands-on collaborative device intended for any orthopaedic joint replacement; so far, however, it has only been performing on total hip replacement (41, 45) and knee replacement (41, 46). MAKOplasty provides both

auditory and haptic feedback, to allow surgeons to mill out bones only in the negative area from the pre-operative plan (41, 46). This system was FDA approved in May 2005, and is currently commercialized (44). In 2011, it was reported that there were 36 RIO systems in operation, and over 2300 procedures performed (41, 44).

With the vision of higher accuracy and precision in mind, the technology of surgical robots is expanding (38). One of the most recent orthopaedic surgical robots is the SpineAssist (Mazor Robotics, Caesarea, Israel), a miniature robot used to guide surgeons' placement of the bone on the vertebra. The SpineAssist is directly mounted onto the bony anatomy depending on the location obtained from the pre-operative plan, so that the SpineAssist and the spine can be treated as one rigid body (47). Recently, the FDA approved the use of the Mazor robot for brain surgery in 2012 due to its precision and simplicity (48).

1.3   Robots

1.3.1   Definition

A robot is a mechanical structure or manipulator that consists of a set of rigid bodies connected by a means of articulation (36, 49). In other words, a robot is made up of links connected by joints. There are two elementary types of joints as shown in **Figure 1.9**: 1) rotational (revolute) and 2) translational (prismatic). Each joint has one DOF, and can be combined to create a complex joint, which will result in more than one DOF. For example, a Cartesian robot has three prismatic joints to provide translation in three perpendicular axes, resulting in a three DOF robot. An articulated robot has at least three rotary joints, which can be used as a robot manipulator or a robotic arm. A robotic arm is composed of three parts: an arm for mobility, a wrist for dexterity and an end effector for tasks to be performed (36).
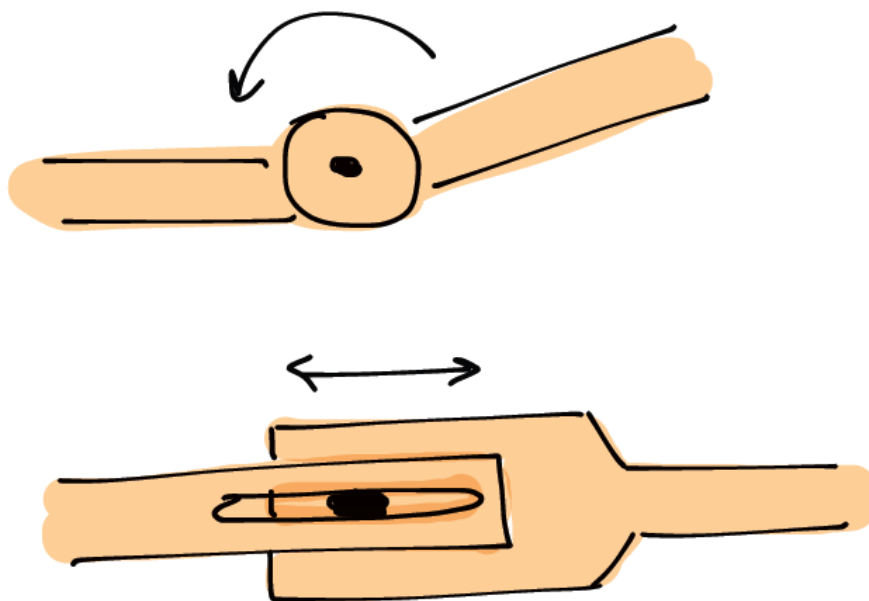
Figure 1.9: Representation of Revolute and Prismatic Joints

The two types of robot joints are revolute (top) and prismatic (bottom) joints as illustrated. The revolute joint allows rotation of a joint, whereas the prismatic joint provides linear motion, such as expansion and retraction.

Furthermore, a robot involves the study of mechanics, electronics, control theory, and computer science. For example, in computer science, the output of a robotic system is the actual task ordered by the code, which is monitored by sensors. Control theory allows the sensors to transmit task information and compare with the prescribed task. The difference is sent back into the controller, which then sends out information to correct the task in the actuators; this process is known as a feedback system (50). A mixture of mechanics and electronics allow sensors to be integrated into the system. The two main types of sensors found in each joint for this research are position and torque sensors.

Position and impedance controls are two types of robot design algorithm that are used for this study. Position control is a robot motion control, which allows the user to move the end effector to the desired location, and to define the path and trajectory planning of the robot (35). Impedance control is an interaction control, which allows the robot to interact with the environment, resulting in a collaborative robot with the user. Furthermore, impedance control regulates the mechanical impedance, such as damping and stiffness (35).

Currently, robots are widely available for industrial use as they increase productivity and precision, and decrease labour costs (35). A robot is an autonomous machine capable of executing a set of programs automatically to carry out actions. Robotics is concerned with the study of those machines that can replace human beings in the execution of a task, both physical activity and decision making (36). A robot is used to complete a job that does not require intelligence, and to make easier the work of humans.

1.3.2   Surgical Robot

Davies defines a surgical robot as 'a powered computer controlled manipulator with artificial sensing that can be reprogrammed to move and position tools to carry out a range of surgical tasks' (40). This statement implies that the robot will have the functionalities of surgeons, which is the purpose of having a robot-assisted procedure. However, the robot will not replace surgeons, as the robots do not have enough intelligence to carry out the surgery; rather, the robot will be used to assist surgeons to enhance precision in results. A robot-assisted procedure is also a minimally invasive

approach, which will reduce the surgical scar and soft tissue disruption. Also, using a robot to assist the surgeons help reduce the amount of repetitive tasks to keep surgeons focused (40).

In general, robotic systems used in surgical procedures are comprised of three phases: a) pre-operative planning, b) intraoperative intervention, and c) post-operative assessment (40). In the case of joint arthroplasty, pre-operative planning involves digitizing an anatomy to create a 3D anatomy model and superimposing the virtual implant model over the new 3D anatomy model. After superimposing and optimizing the location of the implant model, negative area, or the overlapped area between the implant model and the 3D anatomy model, can be determined for the drilling process of the robot, and the operative plan for the robot and the surgeons is created. The second phase is the intraoperative stage, in which the 3D model has been registered and negative area has been inputted into the robotic system. The robot will then drill out the negative area for implant placement. It is important to note that surgeons monitor the process of the robot to ensure that the operation runs smoothly. Finally, in the post-operative phase, the assessment is completed, the robot is removed and the patient is released.

There are five key requirements in orthopaedic surgery: 1) safety, 2) accuracy, 3) sterility, 4) integration in the operating room, and 5) measureable benefits (51). By using a surgical robot, these requirements can be achieved, and possibly improved. For example, the first criteria can be implemented by using force measurement; the robot may sense a force change when the anatomy has been moved. This detection will slow down or stop the robotic task to avoid any unnecessary problems. The second requirement is accuracy, and the robot's accuracy can be comparable to or better than the surgeon's accuracy. The accuracy of implant placement by surgeons can range from 0.5 – 1.0 mm, and in orthopaedic procedures, an accuracy of 1 mm is efficient to carry out the procedure (51). Finally, due to the high accuracy of the robot, the measureable benefits, such as less blood loss and hospital stays due to removing only undesirable regions for minimal soft tissue disruption, can be increased (52).

There are different types of surgical robots that are classified according to their surgical

tasks: passive robot, active robot, synergistic systems, and master-slave 'telemanipulator' systems (40). A passive robot is one that is fixed at a location, and is powered down or locked so that tools can be used at this fixed place. In other words, these robots can be used as tool holders at appropriate locations. The second classification is an active robot, in which the robot is programmed to complete the tasks automatically using sensors or any input commands. For example, an existing robot system for laparoscopic surgery will assist surgeons by allowing a camera to guide surgeons to view what they desire. This type of robot requires extensive research and preoperative planning since it has higher safety concerns as it performs autonomously and is in control of tasks (40). For this reason, active robots are usually developed specific to a procedure. Surgeons and surgical robots can work together to create a synergistic system, and this allows the robot to be collaborative (40, 53). Surgeons can have control over the robot, while the robot restricts surgeons from unsafe regions. The last classification is the master-slave systems, in which surgeons have complete control over the robot, and act as masters by using a joystick or a kinematic mimic system to move the robot manipulator (slave).

1.3.3   Advantages and Disadvantages

There are three main advantages of robot-assisted orthopaedic surgery over conventional surgery (39). Firstly, the precision of the robot-assisted surgery is approximately an order of magnitude better than that of the surgeons. The accuracy and safety of procedures depend on the judgement of the surgeons (51). Secondly, the robot can be more reliable and produce better outcomes in repeatable tasks. Thirdly, when combined with dynamic scanning and positioning technology, the robot has great spatial accuracy.

Moreover, the surgical robot can prevent drilling motions into critical regions or allow motions along a specified direction, such as drilling an angled hole. This is useful for orthopaedic applications, especially in cases in which drilling bones is a requirement; in such a case, one must be careful in removing undesired parts, keep the good bones and ensure that there is minimal soft tissue disruption (40).

However, surgical robots have complications, such as slower adoption rate in clinics, and the need to immobilize patients (47). Also, the operating time associated with the use of

the surgical robot is significantly longer than conventional surgery. As a result, the learning curve for surgeons operating with a robot is significantly greater than without the use of a robot (52). Longer surgical time can also raise concerns about the correlation between surgical time and infection risks (41). Also, when the robot monitoring system detects an error, the robot stops, and has to undergo many processes to confirm whether it is safe to continue, which will significantly increase surgical times (38). Another disadvantage of using a surgical robot is, due to the intensive preoperative planning required for robot navigation, patients are exposed to more radiation by CT scan, which can raise health concerns (41).

For the robot manipulator to be used in medical applications, there should be a significant benefit over conventional surgery. Surgeons are reluctant to spend more time in preoperative planning regardless of the performance of the robotic system. Therefore, it is necessary to show an improvement in outcomes and cost effectiveness, as well as safety and ease-of-use, rather than simply focus on the performance of the robot system (54).

1.3.4   Safety Considerations

The latest ISO 10218-1 and 10218-2 standards for robotic safety allow a collaborative robot to be operated unguarded (53). Collaborative robots contain features such as force feedback, which allows the robot to safely stop without damaging its surroundings if the robot detects a collision.

Najmaei et al. (2010) studied the human factors that influence the safety assessment of robots in an interactive environment (55). Furthermore, Najmaei et al. suggested that a risk assessment should be used in the path planning process to improve the safety of the robot system. Primary considerations for the safety of the collaborative robot should focus on planning and control strategies to avoid collisions with humans. Although physical factors, such as impact force based on the distance between the robot and human or obstacles, the relative velocity, and the inertia, are important considerations for preventing collision and decreasing risk with humans, human factors are also important to consider in risk assessment, such as fatigue and improper body language.

This area of research is still in its early stage; however, human factors can provide intelligence in the decision-making process. For example, by analyzing human body language, robots can have a feedback system of humans' cognitive and emotional state interpretation. This is done to enhance the safety of human-robot interactions. Firstly, human physiological signals are important factors because they have a significant effect on the risk of collision. For example, if the user is tired or stressed, then the risk of collision may significantly increase. Secondly, monitoring the direction of the humans' eye gaze and body orientation could potentially improve the risk assessment of the robot, as there is a relation between their focus and awareness of the robot. Najmaei et al. developed an algorithm to determine a risk index to include in the path planning of the robot, and found that including the physical and human factors significantly improved the performance of the robotic system.

1.4   Registration and Digitization

Registration is finding coordinate transformation from one set of data to another, in order to align important features of both sets of data (56). In the case of computer- or robot-assisted procedures in orthopaedic surgery, a virtual model of a bone in the joint is registered to the patient's computer tomography (CT) scan obtained from the pre-operative plan. Two main registration algorithms to determine the transformation of two sets of data or three-dimensional (3D) objects are point-to-point registration and surface-based registration. Firstly, point-to-point registration, also known as paired point registration, involves identifying more than three key target points on both 3D objects before registration (57). Point-to-point registration utilizes the least sum of squares errors to find the best transformation to align two 3D objects. Secondly, surface-based registration compares two 3D objects by the point clouds. The most commonly used surface-based registration is an iterative closest point (ICP) algorithm by, in which the algorithm finds the closest point in the point cloud of one 3D model to a given point of the other 3D model, and this is done for all points in both 3D models (58).

Mcdonald et al. (2007) compared three different registration procedures, including point-to-point, surface-based, and surface-based with noise reduction (59), and found that surface-based without noise reduction produced the lowest registration error, as well as

the most consistent results, and it was significantly better than the point-to-point procedure and surface-based with noise reduction.

Moreover, digitization is a representation of a 3D object in a set of points. A digitization device, or a digitizer, is a tool that measures 3D coordinates into a digital form, providing 3D position (x, y and z coordinates) and orientation (yaw, pitch and roll) data into a computer system. In this project, a digitizer utilizes a stylus probe to trace over the object, and the system then converts the digitization of the object into a 3D representation format readable by a computer; the computer samples the stylus probe movement to transmit discrete data points at different coordinates (60). A digitization device can be used as a navigational tracking system in surgery, where the ideal virtual imaging data is registered to the patient's CT scan to guide surgical procedures. In orthopaedic surgery, the digitization device can be used for localization, which is a process of pinpointing the location of the bony structures and anatomical landmarks.

1.4.1   Digitization Device

Tracking systems can be used as digitizers, as tracking systems are used to monitor six DOF with respect to a reference point in real-time. Existing tracking systems include electromagnetic, optical or mechanical arm equipped with a stylus probe (61). Electromagnetic tracking systems utilize a source, which is a transmitter that generates a magnetic field using the three orthogonal wire coils in the transmitter, and a receiver, which detects this signal that will measure the magnetic field and processes this signal in a computer for analysis. Current electromagnetic tracker systems use a six DOF stylus, such as a Polhemus Patriot Digitizer (**Figure 1.10**). The Polhemus Patriot Digitizer uses a free-form stylus tool, with a cable attached to electromagnetic coils enclosed in a plastic shell that emits a magnetic field, which is the reference frame for the stylus. The Polhemus Patriot Digitizer has a marketed absolute accuracy of 0.05" (1.3 mm).
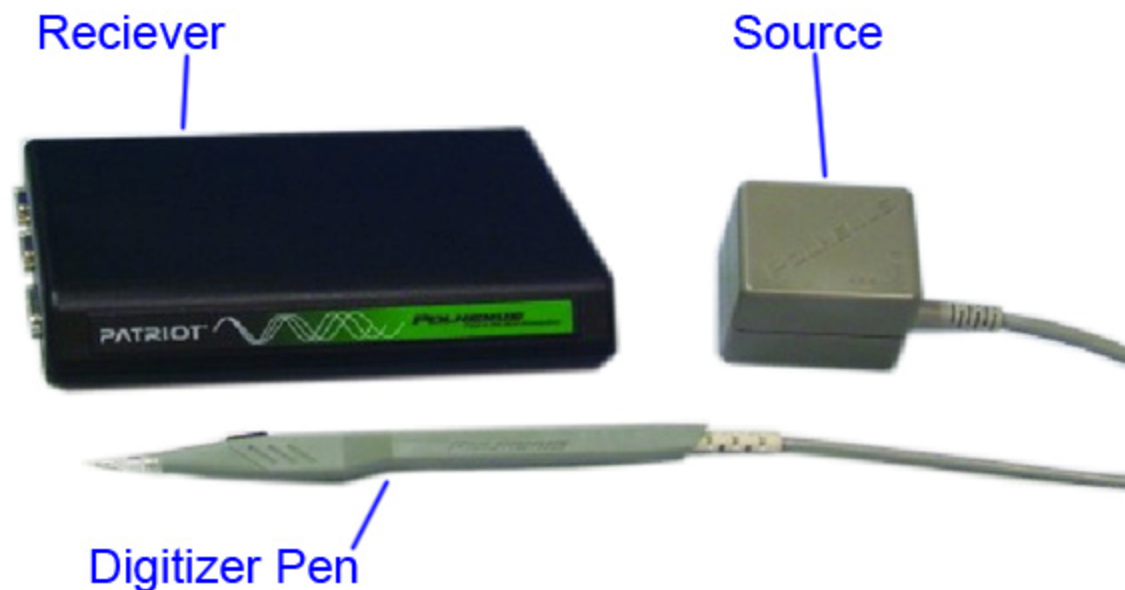
Figure 1.10: Electromagnetic Tracking System: Polhemus Patriot Digitizer[2]

The black box in the top left corner is a receiver used to detect the signal transmitted by the source in the top right corner, and then process this signal in the computer. The bottom shows a digitizer pen, which is a probe to digitize an object, and is attached to the source.

---

[2]Modified from: Polhemus announces rhinoceros plug-in for stylus based, hand-held digitizing [Internet]. China: SouVR Co.; 2008; cited July 25, 2014. Available from: http://en.souvr.com/news/200803/836.html

The optical tracking system is the most commonly used tracking modality (62, 63). The optical system contains a series of cameras and trackers that can be mounted to track motions, or equipped with a stylus probe to use as digitizers. Trackers have markers that are passive or active; passive systems utilize light-reflecting markers and active systems use light-emitting markers. Wiles et al. (2004) has shown that the difference in the accuracy between active and passive systems is minimal (64). Optical systems measure the location and orientation by triangulation and time-of-flight calculation after detecting the light emitted or reflected from the markers. An example of an optical motion analysis system is the Optotrak Certus (**Figure 1.11**). The Optotrak Certus has three cameras and various trackers with three markers and utilizes a stylus with the tracker attached as a digitizer. The Optotrak Certus has a marketed accuracy of 0.1 mm.

Finally, a last type of digitizer is a mechanical arm digitizer (**Figure 1.12**). It consists of an articulated arm design, sensors in the joints of the linkage chain, and the stylus linked to the end effector. The sensors determine the relative orientation of the linkage, and with the known link size and number of joints, the 3D coordinates can be calculated (60, 65). The Microscribe digitizer is a mechanical arm digitizer with five or six DOF stylus depending on the model. The Microscribe 3DX reported a marketed accuracy of 0.009" (0.23 mm). Currently, some surgical robotic systems implement the Microscribe, such as Robodoc and Acrobot. FARO arm is another mechanical arm digitizer and is a passive six DOF digitizer, with a 200 mm probe cylinder and a thin shaft at the end. Rohling et al. (1995) found that the accuracy of the FARO arm is less than 0.5 mm, and that the FARO arm was comparable to the Optotrak; however, the Optotrak resulted in better accuracy (65).

A

B

Figure 1.11: Optical Tracking System: Optotrak Certus[3,4]

(A) a Certus stylus with three markers in the tracker, (B) three cameras are shown in three

black circles in the horizontal bar in the **Optotrak Certus** system.

[3]Orthopaedic and spine research [Internet]. Waterloo, Ontario: Northern Digital Inc; 2014; cited July 25, 2014. Available from: http://www.ndigital.com/msci/applications/orthopaedic-spine-research/.

[4]Modified from: Optotrak certus hd dmm [Internet]. Cincinnati, OH: Exact Metrology; N/A; cited July 25, 2014. Available from: http://www.exactmetrology.com/products/ndi/optotrak-certus-hd-dmm/.

Figure 1.12: Mechanical Arm Digitizers: Microscribe 3DX[5] and FARO Arm[6]

Pictured are examples of mechanical arm digitizers; the joints in both mechanical arm digitizers are all revolute. The right side is a Microscribe 3DX, with the digitizing pen in home position for calibration purposes, and the left side is a FARO arm.

[5]Using a touch probe to acquire muscle fibre data [Internet]. Toronto, Ontario: James McCrae; 2008; cited July 25, 2014. Available from: http://www.dgp.toronto.edu/~mccrae/projects/microscribe/.

[6]Faro arm [Internet]. UK: Automation Technologies; 2011; cited July 25, 2014. Available from: http://www.automationtechnologies.co.uk/services/cimage1.html.

In this thesis, a 7-axis collaborative KUKA robot will be used as a mechanical arm digitizer. Although the manufacturers of the KUKA robot reported that it has a repeatability of 0.05 mm, for the purpose of this thesis, it is hypothesized that this KUKA robot can be competitive with the aforementioned digitizers in this review section. One of the advantages of using a KUKA robot is the reprogrammability, as the robot has other purposes than just digitization.

1.4.2   Advantages and Disadvantages of Digitizing Technologies

The advantages and disadvantages of each type of device are outlined in **Table 1.1**:

Table 1.1: Advantages and Disadvantages of Digitization Devices

	Advantage	Disadvantage
Optical	- Very high accuracy - Very high resolution - Tracked six DOF sensors are relatively large	- Need clear line of sight between source and sensors otherwise measurements are lost - Camera lens and image distortions and rough handling can decrease accuracy (66)
Electromagnetic	- Flexible due to no clear line-of-sight - Less expensive than optical tracker	- Accuracy is relatively lower, depending on the placement - Possible interference of metallic objects (67) - Wiring can be obtrusive in surgery
Articulated Arm	- Very high accuracy - No metal or radio interference - Low cost	- Small work area - Inaccurate if no calibration is done

1.4.3   Accuracy Assessments

The two most common standards in validating the accuracy of surgical guidance devices are the ISO 5725-1:1994 "Accuracy (trueness and precision) of measurement methods and results" and the ISO 9238 "Manipulating industrial robots – Performance criteria and related test methods". **Figure 1.13** summarizes the definition of accuracy in ISO 5725-1:1994, and ISO 9238 defines accuracy as the closeness of agreement between a test result and the accepted reference value. For digitization or surgical navigators, absolute position accuracy is considered the highest priority (68).

In surgical guidance devices, the literature review suggests dividing the term "accuracy" into three different types: intrinsic or technical accuracy, registration accuracy and application accuracy (69, 70). In orthopaedic applications, the technical accuracy applies to a digitizer as a localizer. The technical accuracy is the average error of the component in its operational use; in other words, how reliable is the digitizer in defining its own position in space? The registration error relates to coordinate transformation, where the fiducial of the markers is registered in image space. Application accuracy reflects the overall error in the surgical procedure, including technical and registration accuracy. In general, the acceptable range of the technical, registration and application accuracies should be 0.1 – 0.6 mm, 0.2 – 3.0 mm and 0.6 – 10 mm, respectively (69, 70).
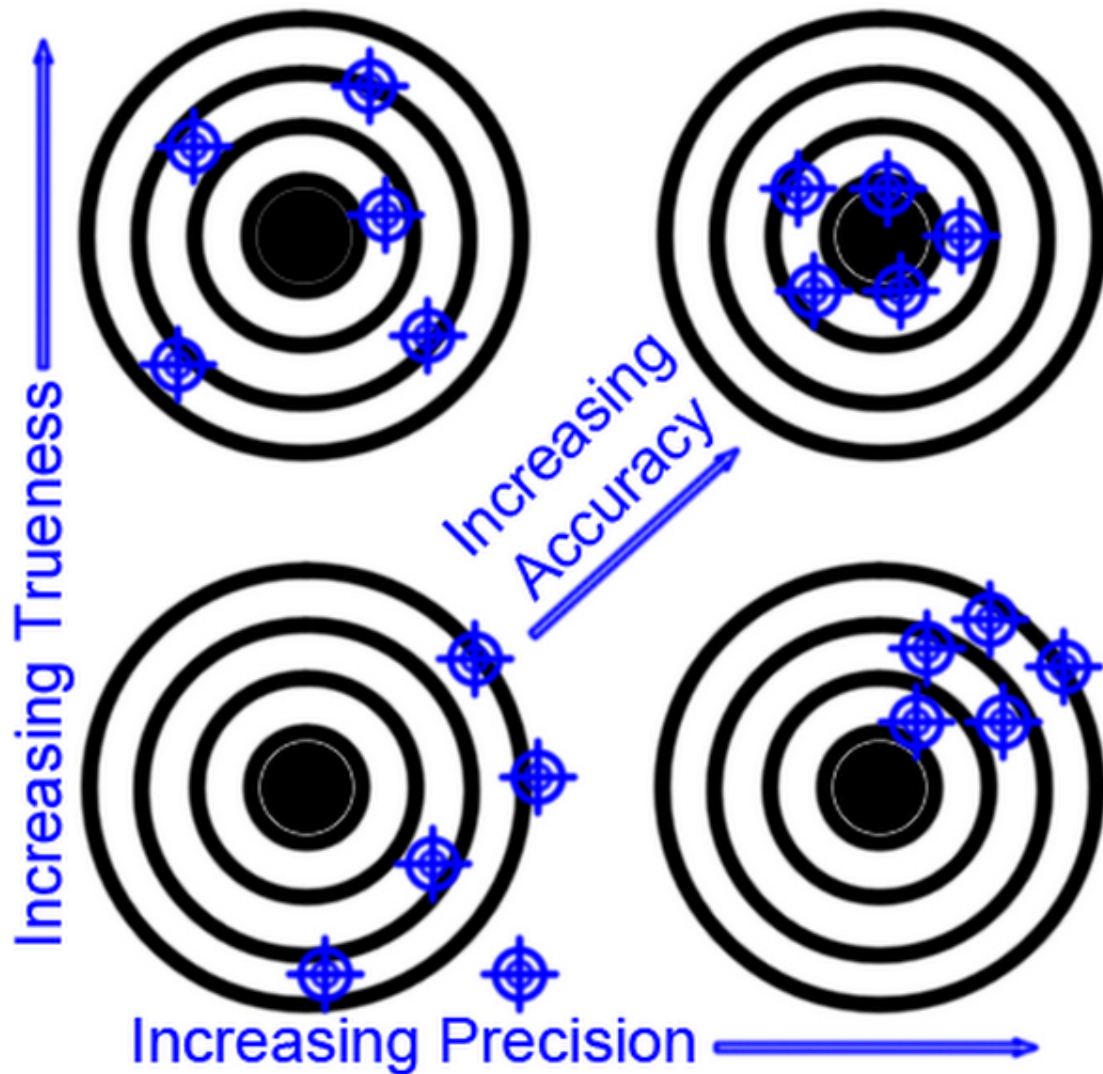
Figure 1.13: Overview of ISO 5725-1:1994

Three different terms are used to summarize ISO 5725:1994. More trueness means that the targets are closer to the ideal location, which is the black circle in the centre. Increasing precision shows the targets closer with each other. Accuracy consists of trueness and precision, and the more trueness and precision, the more accurate the results.

Methods of validating the accuracy of the digitization device have been developed and consist of a phantom and a protocol. A study by Koivukangas (2013) was found to be the most relevant to this thesis (66). Koivukangas had specially designed an accuracy assessment phantom as shown in **Figure 1.14**. This phantom has three separate levels attached with screws to form the total reference volume of 120×120×100 mm. Each level has 49 points, spaced at 20 mm, and machined with a tolerance of 0.015 mm. Using 17 points on each level, the protocol is to collect coordinate data in x, y and z directions of each point from point 1 to point 17 on each level. The center point, or point 9 in **Figure 1.14**, is the reference point. The algorithm is similar to previous studies such as Hummel el al and Frantz et al (71-73), which is a form of Euclidean Distance of accumulated measured point and theoretical point. The equation is:

$$E_{ij} = \sqrt{(X_{M,ij} - X_{M,25})^2 + (Y_{M,ij} - Y_{M,25})^2 + (Z_{M,ij} - Z_{M,25})^2} - \sqrt{(X_{ij} - X_{25})^2 + (Y_{ij} - Y_{25})^2 + (Z_{ij} - Z_{25})^2} \qquad Eq.\ 1$$

where X_{ij}, Y_{ij}, Z_{ij} are true values, X_M, Y_M, Z_M are measured values and 25 corresponds to the center point, i-th is the number of points, and j-th is the level number.
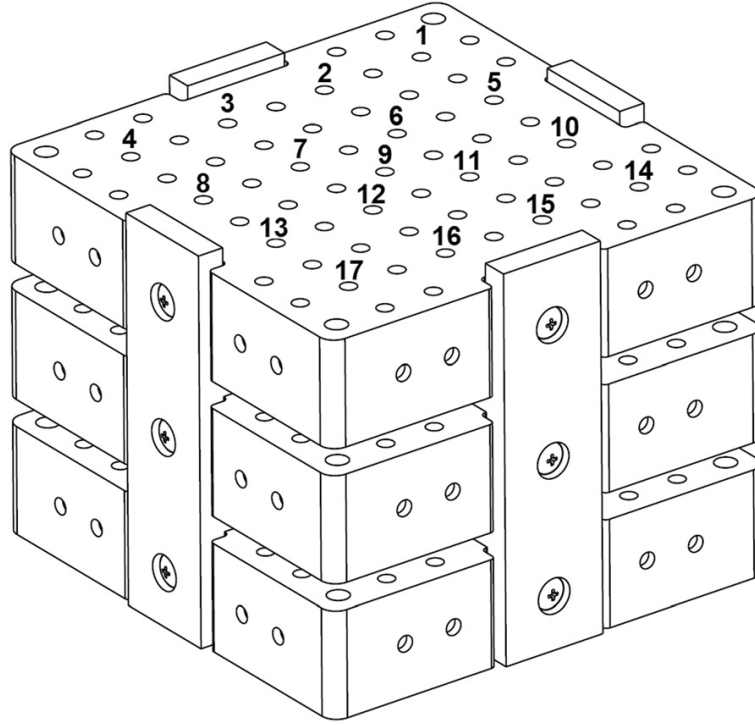
Figure 1.14: Accuracy Assessment Block

Calculations of the mean error, RMS error and 95% confidence interval are, respectively:

Average Error:

$$E_{avg} = \frac{1}{n} \sum_1^n E_{ij} \qquad\qquad Eq.\ 2$$

RMS Error:

$$E_{RMS} = \sqrt{\frac{1}{n} \sum_1^n (E_{ij})^2} \qquad\qquad Eq.\ 3$$

95% Confidence Interval:

$$95\%\ CI = E_{avg} \pm 2\sigma \qquad\qquad Eq.\ 4$$

where σ denotes one standard deviation.

Koivukangas found that low standard deviation may show that the accuracy assessment block works well. Therefore, for the purpose of this thesis, it was decided to use Koivukangas' method to assess the accuracy of the digitization device.

The material used to create the phantom was acrylic plastic due to its very high moisture

resistance and thermal stability. The temperature range in which acrylic plastic can be used without deformation is -40ºC to +70ºC.

1.5 Rationale

Total shoulder arthroplasty (TSA) is the third most common joint replacement and the single most common in the upper limb. While computer- and robot-assisted technologies have enjoyed extensive development for hip and knee replacements, little has been done to study the efficacy of these methods in the upper limb. Thus, the focus of this work is the study and development of a robot-assisted system for total shoulder arthroplasty and related joint resurfacing treatments.

Insufficient instrumentation for the glenoid results in component malalignment, causing loading conditions, which may promote accelerated wear and/or aseptic loosening, and potentially cause humeral instability. Recent focus has been on the development of alignment guides, both implant-specific and patient-specific. Yet the use of these and other jigs precludes the use of minimally invasive techniques, an increasingly important trend in surgical treatments. Leveraging the precision of robotics for TSA may improve implant placement and provide a platform navigated minimally invasive protocols.

Various strategies for robotic assistance control schemes have been employed for joint reconstruction in the lower limb. These include fully active autonomous control, 'active constraint' and 'semi-active' control. In spite of an early checkered history of complications involving some autonomous robots, several contemporary studies have shown that robotic assistance can improve the accuracy of lower limb joint reconstruction without increasing complications. The vast majority of this literature focuses on bone sectioning planes or preparation of the joint bed to accept an implant. As articulated by Van Ham et al. (2005) in the context of hip replacement, "The important factor for the lifetime and the functioning of the prosthesis is the correct orientation of the implanted cup", and some research shows that this concept should be extended to the shoulder (74). However, few computer-navigated or robot-assisted systems for this procedure exist.

1.6   Objective

The overall objective of this thesis was to characterize the accuracy and efficacy of a 7-axis collaborative robot as a manually operated surface digitization device for use in surgical orthopaedic procedures, with special interest in the development of robot-assisted shoulder replacement. Specific objectives to achieve this goal were: 1) to quantify the system's accuracy using an established gold standard assessment protocol, and 2) to quantify the accuracy and efficacy of the robotic digitization method with validation on the glenoid structure.

1.7   Hypotheses

It is hypothesized that using a collaborative robot itself to digitize a glenoid structure will produce average digitization errors of less than 0.5 mm. This level of accuracy would be better than existing intra-operative digitization devices. It is further hypothesized that a novel laser registration method will prove efficacious in reverse-engineering the glenoid structure.

1.8   Thesis Overview

Chapter 2 presents an accuracy assessment of the robot-assisted digitization method within a working volume that encompasses the human glenoid. Chapter 3 is a study quantifying the accuracy of the robot in digitizing cadaveric glenoids, with validation from a 'gold standard' commercial laser reverse-engineering system. Chapter 4 summarizes the conclusions drawn from this work, and recommends future work.

1.9 References

1. Shoulder trauma (fractures and dislocations) [Internet]. Beverly Hills, Michigan: American Academy of Orthopaedic Surgeons; 2007 [updated Sep 2007; cited Oct 17, 2012]. Available from: http://orthoinfo.aaos.org/topic.cfm?topic=A00394.

2. Shoulder joint replacement [Internet]. Beverly Hills, Michigan: American Academy of Orthopaedic Surgeons; 2011 [updated Dec 2011; cited Oct 17, 2012]. Available from: http://orthoinfo.aaos.org/PDFs/A00094.pdf.

3. Shoulder joint anatomy: Gross anatomy [Internet]. New York, NY: Medscape; 2013 [updated Mar 8, 2013; cited Apr 2, 2014]. Available from: http://emedicine.medscape.com/article/1899211-overview#aw2aab6b3.

4. Shoulder dislocations [Internet]. Houston, TX: Houston Methodist Orthopedics & Sports Medicine; 2003; cited Apr 2, 2014]. Available from: http://www.methodistorthopedics.com/shoulder-dislocations.

5. Scapulothoracic joint pathology [Internet]. New York, NY: Medscape; 2012 [updated Sep 18, 2012; cited Apr 2, 2014]. Available from: http://emedicine.medscape.com/article/1261716-overview#aw2aab6b2.

6. Rotator cuff tears [Internet]. Beverly Hills, Michigan: American Academy of Orthopaedic Surgeons; 2011 [updated May 2011; cited Oct 17, 2012]. Available from: http://orthoinfo.aaos.org/topic.cfm?topic=a00064.

7. Kelkar R, Wang VM, Flatow EL, Newton PM, Ateshian GA, Bigliani LU, et al. Glenohumeral mechanics: A study of articular geometry, contact, and kinematics. Journal of Shoulder and Elbow Surgery. 2001;10(1):73-84.

8. Poppen NK, Walker PS. Normal and abnormal motion of the shoulder. J Bone Joint Surg Am. 1976 Mar;58(2):195-201.

9. Howell SM, Galinat BJ, Renzi AJ, Marone PJ. Normal and abnormal mechanics of the glenohumeral joint in the horizontal plane. J Bone Joint Surg Am. 1988 Feb;70(2):227-

32.

10. Benirschke SK, Hansen Jr ST, Sangeorzan MBJ, Smith DG, Brage ME, et al. Total shoulder replacement arthroplasty for shoulder arthritis [Internet]. 2013 [cited Oct 17, 2012]. Available from: http://orthoinfo.aaos.org/topic.cfm?topic=a00064

11. Izquierdo R, Voloshin I, Edwards S, Freehill MQ, Stanwood W, Wiater JM, et al. Treatment of glenohumeral osteoarthritis. J Am Acad Orthop Surg. 2010 Jun;18(6):375-82.

12. Burkhead WZ, Ruark DA. History and development of prosthetic replacement of the glenohumeral joint. In: Williams GR, editor. Shoulder and Elbow Arthroplasty. 1st ed. Philadelphia, PA: Lippincott Williams & Wilkins; 2005. p. 4-9.

13. Matsen FA,III. Total shoulder joint replacement for shoulder arthritis: Surgery with a dependable, time-tested conservative prosthesis and accelerated rehabilitation can lessen pain and improve function in shoulders with arthritis. [Internet]. 2006 May 30 [cited Oct 15, 2012]. Available from: http://depts.washington.edu/shoulder/Handouts/ProcedureHandouts/TSA.pdf.

14. Matsen FA,III, Bicknell RT, Lippitt SB. Shoulder arthroplasty: The socket perspective. Journal of Shoulder and Elbow Surgery. 2007;16(5):S241-7.

15. Matsen FA,III, Clinton J, Lynch J, Bertelsen A, Richardson ML. Glenoid component failure in total shoulder arthroplasty. J Bone Joint Surg Am. 2008;90(4):885-96.

16. Sperling JW, Hawkins RJ, Walch G, Zuckerman JD. Complications in total shoulder arthroplasty. J Bone Joint Surg Am. 2013 Mar 20;95(6):563-9.

17. Bohsali KI, Wirth MA, Rockwood CA. Complications of total shoulder arthroplasty. The Journal of Bone & Joint Surgery. 2006;88(10):2279-92.

18. Strauss EJ, Roche C, Flurin P, Wright T, Zuckerman JD. The glenoid in shoulder arthroplasty. Journal of Shoulder and Elbow Surgery. 2009;18(5):819-33.

19. Schrumpf M, Maak T, Hammoud S, Craig E. The glenoid in total shoulder arthroplasty. Curr Rev Musculoskelet Med. 2011;4(4):191-9.

20. Iannotti JP, Gabriel JP, Schneck SL, Evans BG, Mirsa S. The normal glenohumeral relationships: An anatomical study of one hundred and forty shoulders. The Journal of Bone & Joint Surgery. 1992;74(4):491-500.

21. Churchill RS, Brems JJ, Kotschic H. Glenoid size, inclination, and version: An anatomic study. Journal of Shoulder and Elbow Surgery. 2001;10(4):327-32.

22. Checroun AJ, Hawkins C, Kummer FJ, Zuckerman JD. Fit of current glenoid component designs: An anatomic cadaver study. Journal of Shoulder and Elbow Surgery. 2002;11(6):614-7.

23. Walch G, Badet R, Boulahia A, Khoury A. Morphologic study of the glenoid in primary glenohumeral osteoarthritis. J Arthroplasty. 1999;14(6):756-60.

24. Cofield RH. Bone grafting for glenoid bone deficiencies in shoulder arthritis: A review. Journal of Shoulder and Elbow Surgery. 2007;16(5):S273-81.

25. Iannotti JP, Spencer EE, Winter U, Deffenbaugh D, Williams G. Prosthetic positioning in total shoulder arthroplasty. J Shoulder Elbow Surg. 2005;14(1 Suppl S):111S-21S.

26. Fox TJ, Cil A, Sperling JW, Sanchez-Sotelo J, Schleck CD, Cofield RH. Survival of the glenoid component in shoulder arthroplasty. Journal of shoulder and elbow surgery / American Shoulder and Elbow Surgeons. 2009;18(6):859-63.

27. Throckmorton TW, Zarkadas PC, Sperling JW, Cofield RH. Pegged versus keeled glenoid components in total shoulder arthroplasty. Journal of Shoulder and Elbow Surgery. 2010;19(5):726-33.

28. Lippitt S, Matsen FA,III. Mechanisms of glenohumeral joint stability. Clin Orthop Relat Res. 1993 Jun;(291):20-8.

29. Anglin C, Wyss UP, Nyffeler RW, Gerber C. Loosening performance of cemented glenoid prosthesis design pairs. Clin Biomech. 2001;16(2):144-50.

30. Walch G, Edwards TB, Boulahia A, Boileau P, Mole D, Adeleine P. The influence of glenohumeral prosthetic mismatch on glenoid radiolucent lines results of a multicenter study. The Journal of Bone & Joint Surgery. 2002 Dec 1;84(12):2186-91.

31. Karduna AR, Williams GR, Iannotti JP, Williams JL. Total shoulder arthroplasty biomechanics: A study of the forces and strains at the glenoid component. J Biomech Eng. 1998;120(1):92-9.

32. Anglin C, Wyss UP, Pichora DR. Mechanical testing of shoulder prostheses and recommendations for glenoid design. Journal of Shoulder and Elbow Surgery. 2000; 2000;9(4):323-31.

33. Nho SJ, Ala OL, Dodson CC, Figgie MP, Wright TM, Craig EV, et al. Comparison of conforming and nonconforming retrieved glenoid components. Journal of Shoulder and Elbow Surgery. 2008; 2008;17(6):914-20.

34. Franklin JL, Barrett WP, Jackins SE, Matsen FA,3rd. Glenoid loosening in total shoulder arthroplasty. association with rotator cuff deficiency. J Arthroplasty. 1988;3(1):39-46.

35. Spong MW, Hutchinson S, Vidyasagar M. Robot modeling and control. 1st ed. Hoboken: John Wiley & Sons; 2006.

36. Sciavicco L, Siciliano B. Modelling and control of robot manipulators. New York: Springer; 2000.

37. Kurfess TR. Robotics and automation handbook. CRC press; 2010.

38. Bargar WL. Robots in orthopaedic surgery: Past, present, and future. Clin Orthop. 2007;463:31-6.

39. Adili A. Robot-assisted orthopedic surgery. Surg Innov. 2004 Jun;11(2):89-98.

40. Davies B. A review of robotics in surgery. Proceedings of the Institution of Mechanical Engineers.Part H, Journal of engineering in medicine. 2000;214(1):129-40.

41. Ponnusamy KE, Golish SR. Robotic surgery in arthroplasty. AAOS Now. 2013;7(12):36-8.

42. Pott PP, Scharf H, Schwarz MLR. Today's state of the art in surgical robotics. Computer Aided Surgery. 2005;10(2):101-32.

43. Davies BL, Fan KL, Hibberd RD, Jakopec M, Harris SJ. ACROBOT - using robots and surgeons synergistically in knee surgery. Advanced robotics, 1997. ICAR '97. proceedings., 8th international conference on 1997.

44. Gomes P. Surgical robotics: Reviewing the past, analysing the present, imagining the future. Robot Comput Integr Manuf. 2011 Apr;27(2):261-6.

45. Robotic arm-assisted technology for THA. AAOS Now. 2012:56.

46. Hagag B, Abovitz R, Kang H, Schmitz B, Conditt M. RIO: Robotic-arm interactive orthopedic system MAKOplasty: User interactive haptic orthopedic robotics. In: Rosen J, Hannaford B, Satava RM, editors. Surgical Robotics. Springer US; 2011. p. 219-46.

47. Shoham M, Lieberman IH, Benzel EC, Togawa D, Zehavi E, Zilberstein B, et al. Robotic assisted spinal surgery–from concept to clinical practice. Computer Aided Surgery. 2007;12(2):105-15.

48. FDA approves mazor robot for brain surgery. Medical Device Daily. 2012 Jul 17, 2012:n/a.

49. Garcia E, Jimenez MA, De Santos PG, Armada M. The evolution of robotics research. Robotics & Automation Magazine, IEEE. 2007;14(1):90-103.

50. Angeles J. Fundamentals of robotic mechanical systems: Theory, methods, and algorithms. 3rd ed. New York: Springer; 2007.

51. Hurst K, Phillips R, Viant W, Mobsen A, Sherman K, Bielby M. Review of

orthopaedic manipulator arms. Stud Health Technol Inform. 1998:202-8.

52. Siebert W, Mai S, Kober R, Heeckt PF. Technique and first clinical results of robot-assisted total knee replacement. The Knee. 2002;9(3):173-80.

53. Waurzyniak P. They're here: New collaborative robots lend a helping hand. Manuf Eng. 2013;150(6):49.

54. Davies B. A review of the state-of-the-art of "smart" systems in surgery. Mechatronics and machine vision in practice, 2008. M2VIP 2008. 15th international conference on 2008.

55. Najmaei N, Lele S, Kermani MR, Sobot R. Human factors for robot safety assessment. Advanced intelligent mechatronics (AIM), 2010 IEEE/ASME international conference on 2010.

56. Sadowsky O, Yaniv Z, Joskowicz L. Comparative in vitro study of contact-and image-based rigid registration for computer-aided surgery. Computer Aided Surgery. 2002;7(4):223-36.

57. Horn BK. Closed-form solution of absolute orientation using unit quaternions. J Opt Soc Am A. 1987;4(4):629-42.

58. Besl PJ, McKay HD. A method for registration of 3-D shapes. Pattern Analysis and Machine Intelligence, IEEE Transactions on. 1992;14(2):239-56.

59. Mcdonald CP, Brownhill JR, King GJW, Johnson JA, Peters TM. A comparison of registration techniques for computer- and image-assisted elbow surgery. Computer Aided Surgery. 2007;12(4):208-14.

60. Jackson BG, Rosenberg LB, Schena BM, inventors; Microscribe Llc, assignee. Method and apparatus for tracking the position and orientation of a stylus and for digitizing a 3-D object. US patent US6134506 A. 2000 17 Oct. 2000.

61. Simon DA. Intra-operative position sensing and tracking devices. Proceedings of the

first joint CVRMed/MRCAS Conference; 1997.

62. Birkfellner W, Watzinger F, Wanschitz F, Ewers R, Bergmann H. Calibration of tracking systems in a surgical environment. Medical Imaging, IEEE Transactions on. 1998;17(5):737-42.

63. Schneider M, Stevens C. Development and testing of a new magnetic-tracking device for image guidance. Proc. SPIE 6509, Medical imaging 2007: Visualization and image-guided procedures; February 17, 2007; San Diego, CA. Bellingham, WA: SPIE Digital Library; 2007.

64. Wiles AD, Thompson DG, Frantz DD. Accuracy assessment and interpretation for optical tracking systems. 2004;5367:421.

65. Rohling R, Munger P, Hollerbach JM, Peters T. Comparison of relative accuracy between a mechanical and an optical position tracker for image-guided neurosurgery. Computer Aided Surgery. 1995;1(1):30-4.

66. Koivukangas T, Katisko JPA, Koivukangas JP. Technical accuracy of optical and the electromagnetic tracking systems. SpringerPlus. 2013;2(1):1-7.

67. Mascott CR. Comparison of magnetic tracking and optical tracking by simultaneous use of two independent frameless stereotactic systems. Neurosurgery. 2005 Oct;57(4 Suppl):295,301; discussion 295-301.

68. Koivukangas T. Methods for determination of the accuracy of surgical guidance devices: A study in the neurosurgical region of surgical interest [dissertation]. Oulu, Finland: Ph. D. dissertation, University of Oulu, Finland. ISBN 978-951-42-9904-9; 2012.

69. Grunert P, Darabi K, Espinosa J, Filippi R. Computer-aided navigation in neurosurgery. Neurosurg Rev. 2003;26(2):73-99.

70. Haidegger T, Kazandides P, Rudas I, Benyó B, Benyó Z. The importance of accuracy measurement standards for computer-integrated interventional systems. Workshop on the

role of experiments in robotics research at IEEE ICRA; Anchorage, AK. Genova, IT: EURON GEM Sig; 2010.

71. Hummel JB, Bax MR, Figl ML, Kang Y, Maurer C,Jr, Birkfellner WW, et al. Design and application of an assessment protocol for electromagnetic tracking systems. Med Phys. 2005;32(7):2371-9.

72. Hummel JB, Figl ML, Birkfellner WW, Bax MR, Shahidi R, Maurer CR, et al. Evaluation of a new electromagnetic tracking system using a standardized assessment protocol. Phys Med Biol. 2006;51(10):N205-10.

73. Frantz DD, Wiles AD, Leis SE, Kirsch SR. Accuracy assessment protocols for electromagnetic tracking systems. Phys Med Biol. 2003;48(14):2241-51.

74. Van Ham G, Denis K, Vander Sloten J, Van Audekercke R, Van der Perre G, De Schutter J, Simon JP, Fabry G. A semi-active milling procedure in view of preparing implantation beds in robot-assisted orthopaedic surgery. Proc Inst Mech Eng H. 2005 May;219(3):163-74.

Chapter 2

2 Determination of the accuracy of a 7-axis collaborative robot as a manually operated surface digitizer: with emphasis on robot-assisted surgeries within small working volumes

2.1 Introduction

Collaborative robotics is a recent trend in some surgical procedures – especially total joint replacement or resurfacing – in which a robot-mounted rotary burr cutter is used to machine the cortical and subchondral bone in preparation for a prosthesis (1, 2). Unlike automatic robotic systems, collaborative robot control implies that the user manipulates the robot physically as though it is a tool. For this mode of control, the robot compensates for all external forces, including its own mass gravity weight, so that the surgeon can move the robot freely (3, 4). Typically, the robot's controller is pre-programmed with a pre-operative plan and the robot varies its stiffness as a means of guiding the surgeon to maintain the cutter within the planned region. The more common robotic systems that use this method are the Acrobot (The Acrobot Company Ltd, London, UK) (5) and MAKOplasty (MAKO Surgical Corp, Fort Lauderdale, Florida) (6).

In any computer-navigated or robot-assisted procedure, the pre-operative plan is matched to the patient's anatomy through a coordinate registration process (7). This requires intra-operative digitization of specific osseous anatomy, which is most often, performed using a six degrees-of-freedom (6DOF) tracking system fitted with a contact stylus probe. The surgeon touches the stylus tip to specific osseous features, such as joint articulations and bony prominences in the case of joint replacement and spinal procedures, or craniofacial features in the case of neurosurgery. The coordinate reference frame for the pre-operative plan and all navigation is based on rigid body transformations, which require that any deformations in the relevant anatomical segments are assumed to be negligible.

Most collaborative robots are of an articulated open-chain design with rotary joints. As such, they resemble passive articulated contact digitizing arms such as the Microscribe®

(Immersion Corp, San Jose, California), which have been extensively validated for coordinate measurement and reverse engineering applications (8). An articulated digitizing arm uses rotary encoders at its joints. By measuring the rotational angle of all joints, and knowing the geometry of the links between joints and of the stylus, the location of the stylus tip is resolved relative to the base frame. Then the digitized surface location can be calculated relative to any other reference frame that is known relative to the digitizer's base frame. As collaborative robots also use rotary encoders for their positioning control feedback, it is possible to use any of these devices as a manually operated surface contact digitizer. Currently, optical or electromagnetic 6DOF tracking systems are most widely used in navigated surgical procedures; however, in those procedures where a collaborative robot is already in use, it may be possible to perform the digitizations needed for coordinate registration using the robot itself.

The purpose of this investigation was to quantify the accuracy of manual surface digitization using a collaborative robot. A general method for performing this evaluation in any open-chain collaborative robot was developed, and in this context, the efficacy of this method in surgical applications is discussed.

2.2 Methods

Robot – The robot used was a lightweight robot LWR 4+ (KUKA Robotics GmbH) with KR C2 controller. To achieve the manual digitization of the block, the robot was in a Cartesian impedance controller, so that the LWR 4+ could be operated in collaborative mode to allow the user to move the stylus probe manually. Furthermore, the robot collected the data information in Cartesian form without any transformation needed rather than recording the orientation of each axis that may be less meaningful to the user. The location of each accuracy assessment points were manually digitized using the robot, and the data collection was retained for error analysis calculations.

Stylus Design – Two stainless steel styli were press-fit on opposing sides of a custom Delrin® handle, which was mounted to the robot's end effector (**Figure 2.1**). One stylus had a sharp conical tip while the other had a rounded-tip with radius of 0.74 mm. The radius of the rounded-tip was measured from a magnified high-resolution picture the tip. The sharp tip can be damaging when tracing over an object for digitization, and thus the rounded-tip stylus is more practical. However, there is a small offset error in the calibration method of the rounded-tip stylus (**Figure 2.2**), thus the sharp stylus was used as the gold standard for digitization, since the calibrated position matches its geometric tip when using the pivot vector method. Both tips had a cone angle of 30° and a stylus length of 95 mm from the handle, and each tip was located 160 mm from the center of the end-effector's mounting flange. The tip location of each stylus was calibrated relative to the robot's end-effector coordinate frame using the robot controller's built-in tool calibration procedure with the XYZ 4-point method, as per the manufacturer's documentation (9). A machined 60° conical dimple was used as the pivot point. As such, the sharp stylus tip was calibrated at the dimple's apex, while the rounded stylus was calibrated at the center of its spherical tip radius. The tip locations were determined by the average of 10 calibrations in order to avoid an errant calibration and to quantify calibration variance. Calibrated XYZ coordinates for sharp and rounded-tip stylus were $X = -158.7 \pm 0.31$ mm, $Y = -2.14 \pm 0.34$ mm, $Z = 40.6 \pm 0.34$ mm and $X = 157.7 \pm 0.36$ mm, $Y = 1.92 \pm 0.39$ mm, $Z = 38.9 \pm 0.31$ mm, respectively.
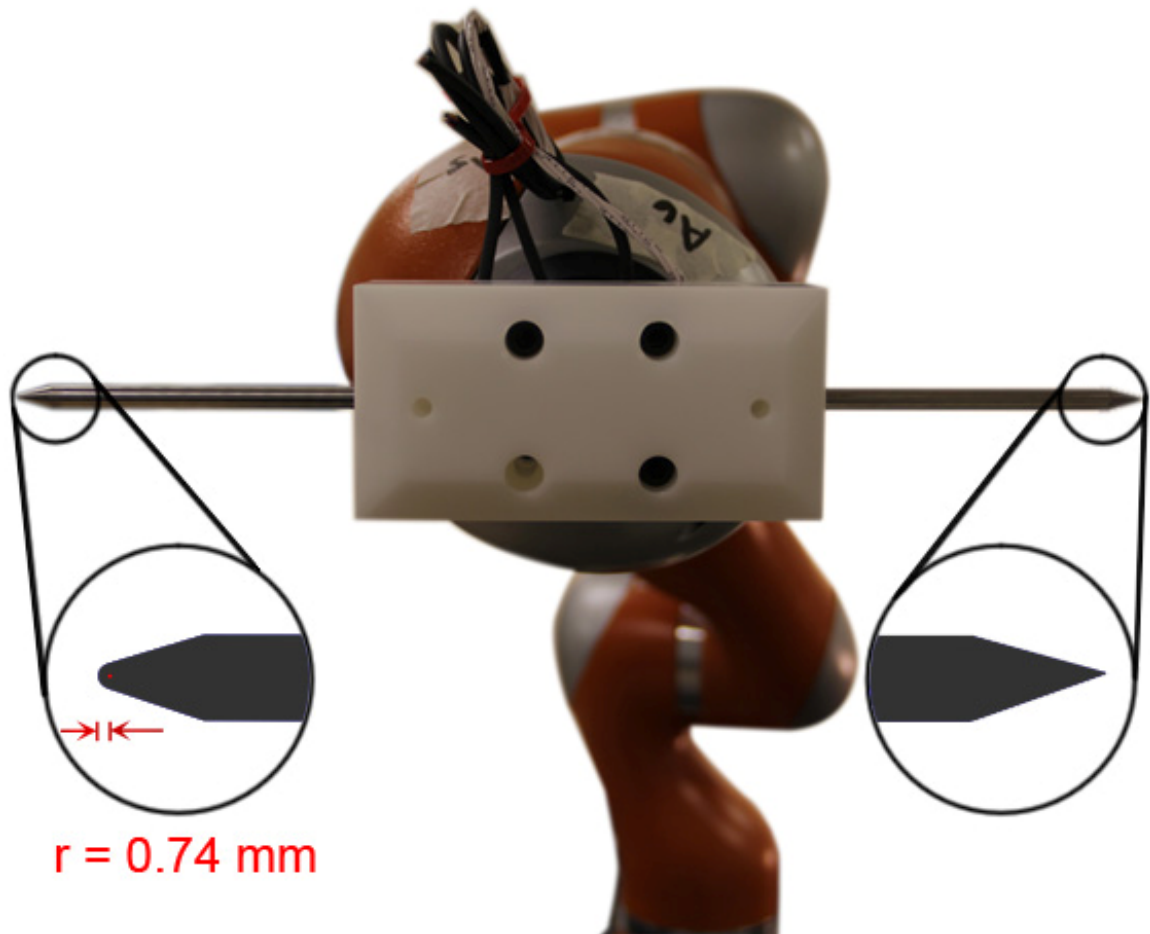
Figure 2.1: Stylus Handle of the Robot

Pictured is a custom-made Delrin handle to manually move the robot to digitize an object. The handle has two styli press-fitted at each end, and is mounted onto the flange of the robot. The left end shows a rounded-tip stylus with a radius of 0.74 mm, and the right end shows a sharp tip stylus.
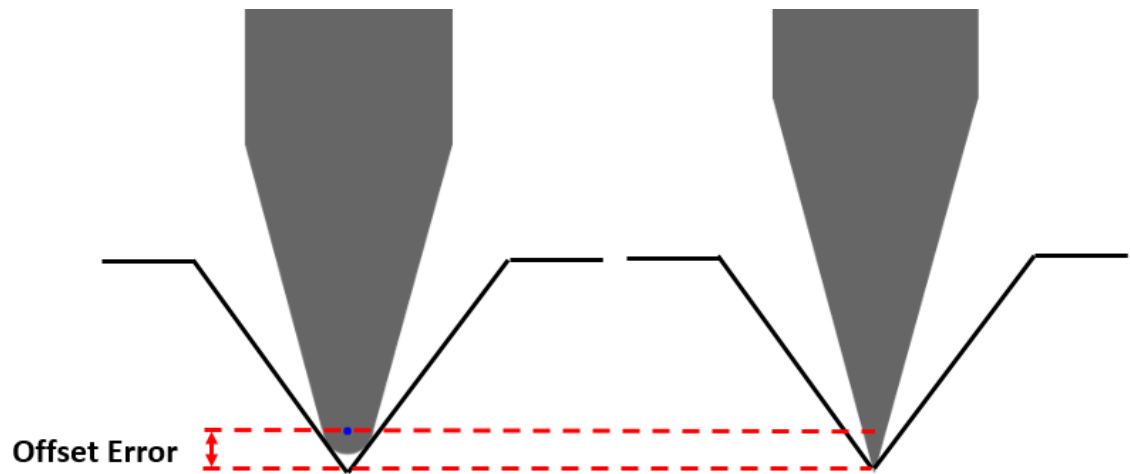
Figure 2.2: Rounded-tip Calibration Error

Calibrating the sharp stylus will result in a calibrated point at the very tip. However, when calibrating the rounded-tip, calibrated point will be at the centre of the rounded tip (blue dot). Therefore there is a small offset.

Accuracy Assessment Blocks – Two master digitization blocks were fabricated from acrylic using a CNC mill (VF4 Vertical Machining Center) with a tolerance of 0.001" (0.0254 mm). Acrylic was used for its thermal stability (10). Accuracy assessment points consisted of conical dimples in which each stylus could be engaged. Each accuracy assessment point was at the depth of each conical dimple. Dimples were made with a cone angle of 60° and were machined on the surfaces of the blocks with 5 mm spacing and a location tolerance of 0.002" (0.0508 mm). One master block (B1) had overall dimensions of 60×60×60 mm, which included the digitized volume of 55×55×55 mm, produced by the 2.5 mm depth of the dimples. On each face, the digitized area is 50×50 mm (**Figure 2.3**), and the distance of the dimples between the opposite face is 55 mm. This block B1 had digitization dimples on 5 faces of a cube with 121 dimples on each face. A second master block (B2) had overall dimensions of 65×65×60, with digitized volume of 55×55×50 mm (**Figure 2.4**). The volume described by the digitization dimples of this block B2 was similar to that of block B1; however, the digitization volume of block B2 was divisible by six separate sections at 10 mm increments, which allowed digitization of the volume inside of the cube in a manner similar to that reported by Koivukangas (2012) (10). Also, the design of block B2 was unable to achieve the digitization of the height of 55 mm due to increments of 10 mm for each layer, as block B1 was created first and the author found that the block B1 had too high of an error, therefore later designed block B2 to only consist of translation. Unlike the design of Koivukangas, which was divided into three equal sections, the six equal sections of our block B2 was designed such that each digitization level was comprised of a single section, which was replaced on the base with the next 10 mm thicker section to achieve the next digitization level. While the Koivukangas design is likely less expensive to fabricate, due to the use of six identical sections, this design minimizes error stack-up since there is always one single assembly interface.
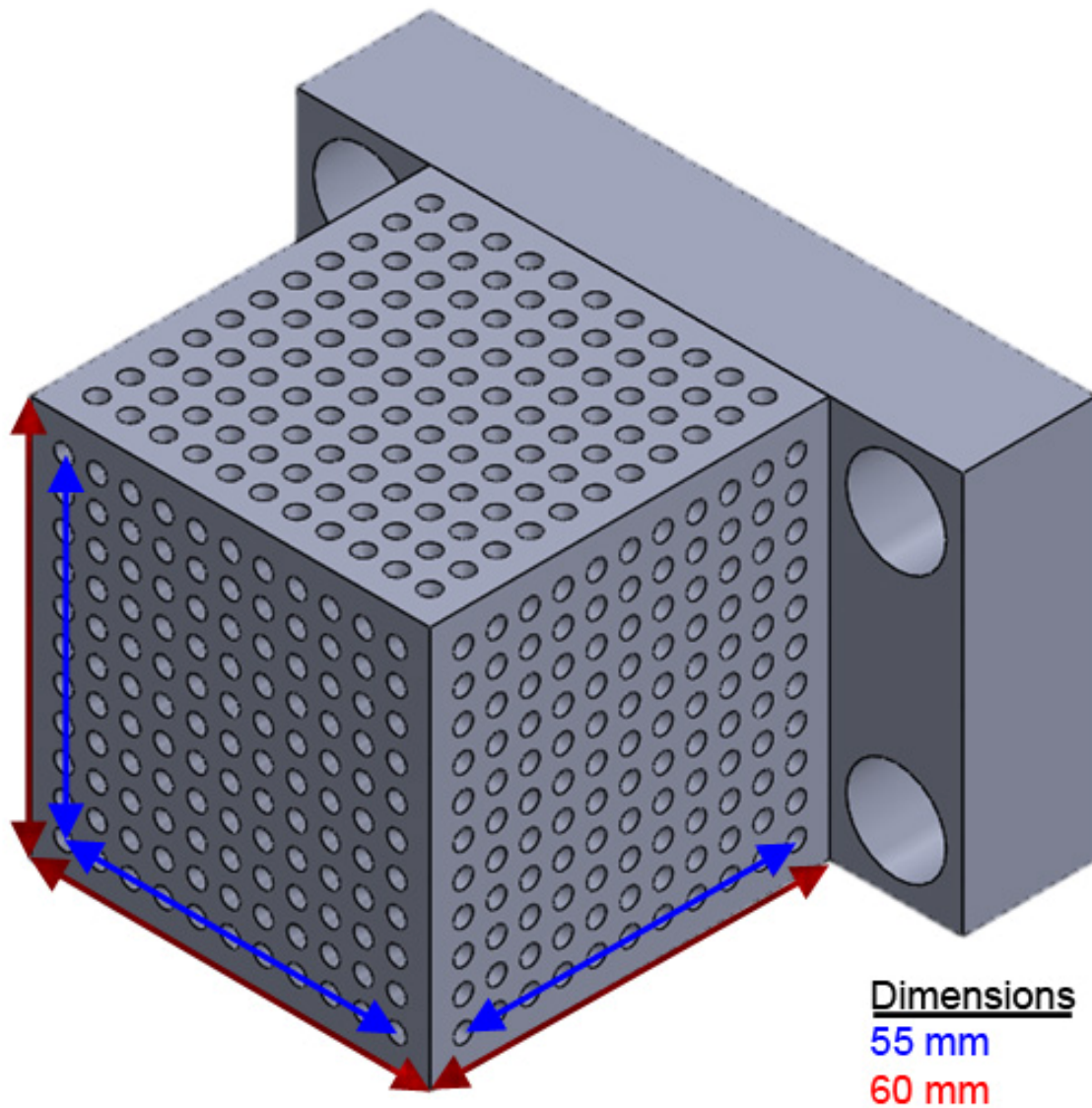
Figure 2.3: An Isometric View of Block B1

Shown is a computer-aided design (CAD) of Block B1 in isometric view. Block B1 is a five-face block with 121 dimple points at 5 mm displacement on each face. B1 has overall block dimensions of 60×60×60 mm, with a digitized volume of 55×55×55 mm. Refer to Appendix D for detailed drawing.
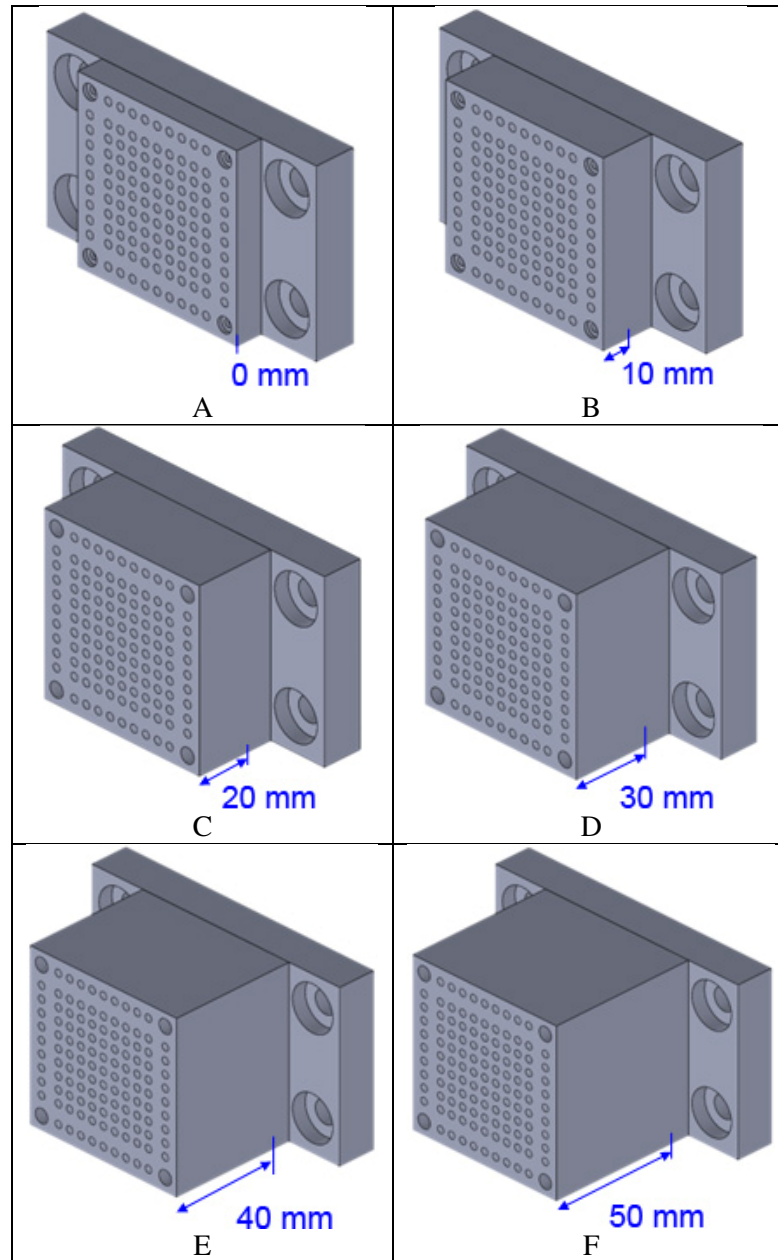
Figure 2.4 a-f: Block B2 with Six Different Layers at 10 mm Displacement

Starting at 0 mm displacement, each CAD model of Block B2 is shown at an increment of 10 mm. Second master block (B2) had overall block dimensions of 65×65×60, with digitized volume of 55×55×50 mm. The outside perimeter of Block B2 coincides with the points of B1 that is adjacent to the face of B2.

The functional difference between the two block designs B1 and B2 was that the dimples on B1 were directed normal to the five available sides of the digitization volume, while all the dimples of B2 were directed in the same direction, away from the block's mounting base. Block B1 requires that the stylus be rotated 180^0 in order to digitize opposite faces of the block, while block B2 allows all perimeter dimples to be digitized with only pure stylus translations. This allowed the determination of whether a wide range of stylus orientations has an impact on digitization accuracy. To accommodate comparison of the digitization volume between the two blocks, the perimeter dimples of block B2 corresponded with the dimple locations of B1. This design required a 7.5 mm gap between the perimeter dimples of B2 and the remaining dimples on each section level. For each section of block B2, there were 81 inner dimples and 36 perimeter dimples.

Measurement Protocol – In order to determine whether the robotic digitization method was orientation-dependent, each dimple location was digitized with three stylus orientations, 0°, 7.5° and 15° from normal to the block surface (**Figure 2.5**). The robot was programmed to maintain the desired angle, relative to the surface of the digitization block, while allowing free translation in collaborative mode. The user manually visited each dimple location with one of the two stylus tips tested, while the calibrated stylus tip location was recorded relative to the robot's base coordinate frame. This relatively small range of stylus angles was distinct from the relatively large range experienced by the stylus when digitizing opposite sides of block B1.

Each block was mounted rigidly to a tower jig, or a vertical aluminum rail (**Figure 2.6**), which allowed positioning horizontally by moving the rail, or vertically by moving the block along the rail. This provided rigid positioning of the blocks anywhere relative to the robot's base frame.
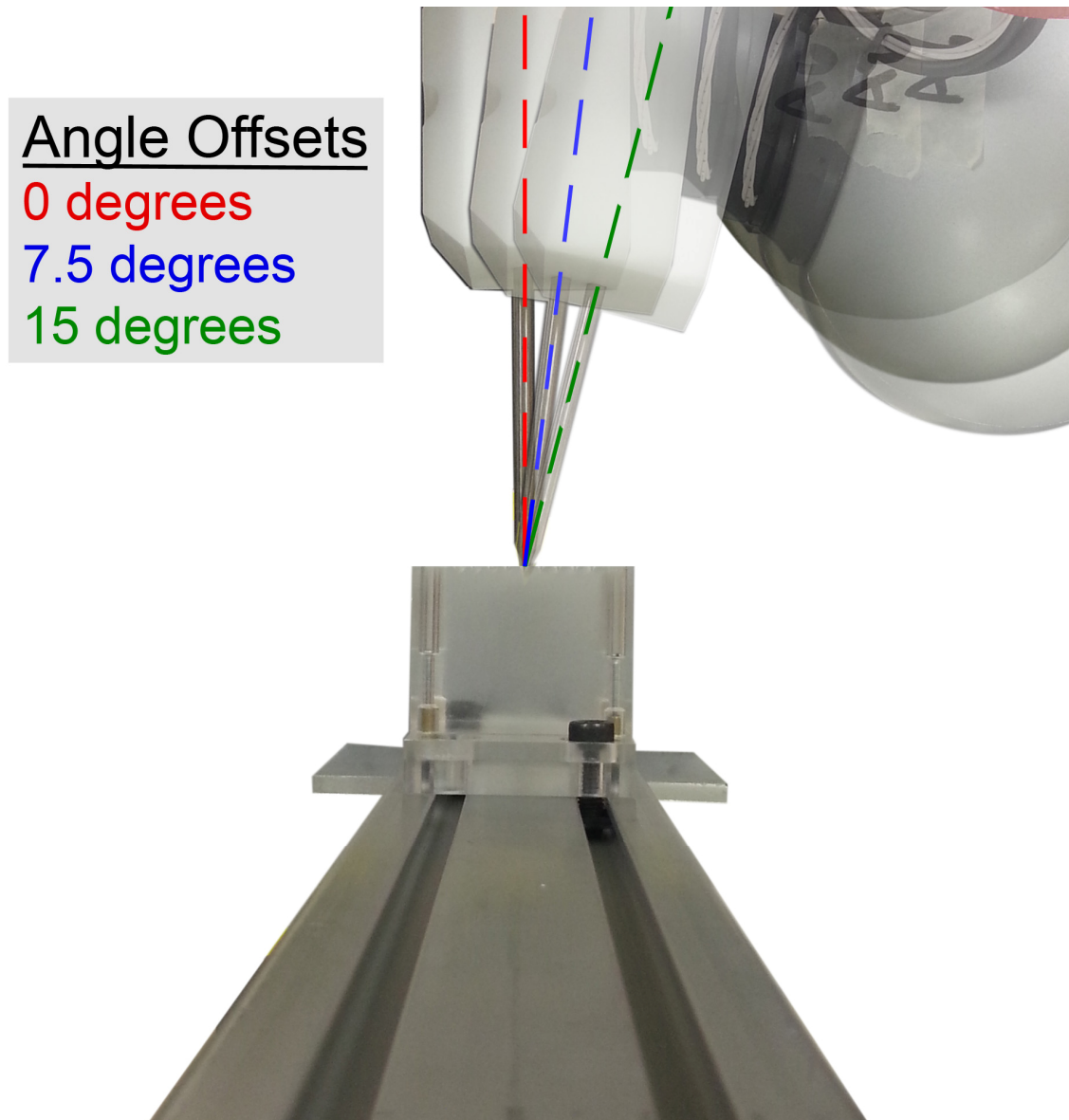
Figure 2.5 Three Different Stylus Orientation

Three different stylus orientations are displayed, at 0°, 7.5° and 15° from normal to the block surface. This procedure is done on each dimple location on the block, to determine whether the robotic digitization method was orientation-dependent. The desired orientations of the stylus are executed and maintained by the robot software, relative to the surface of the digitization block.
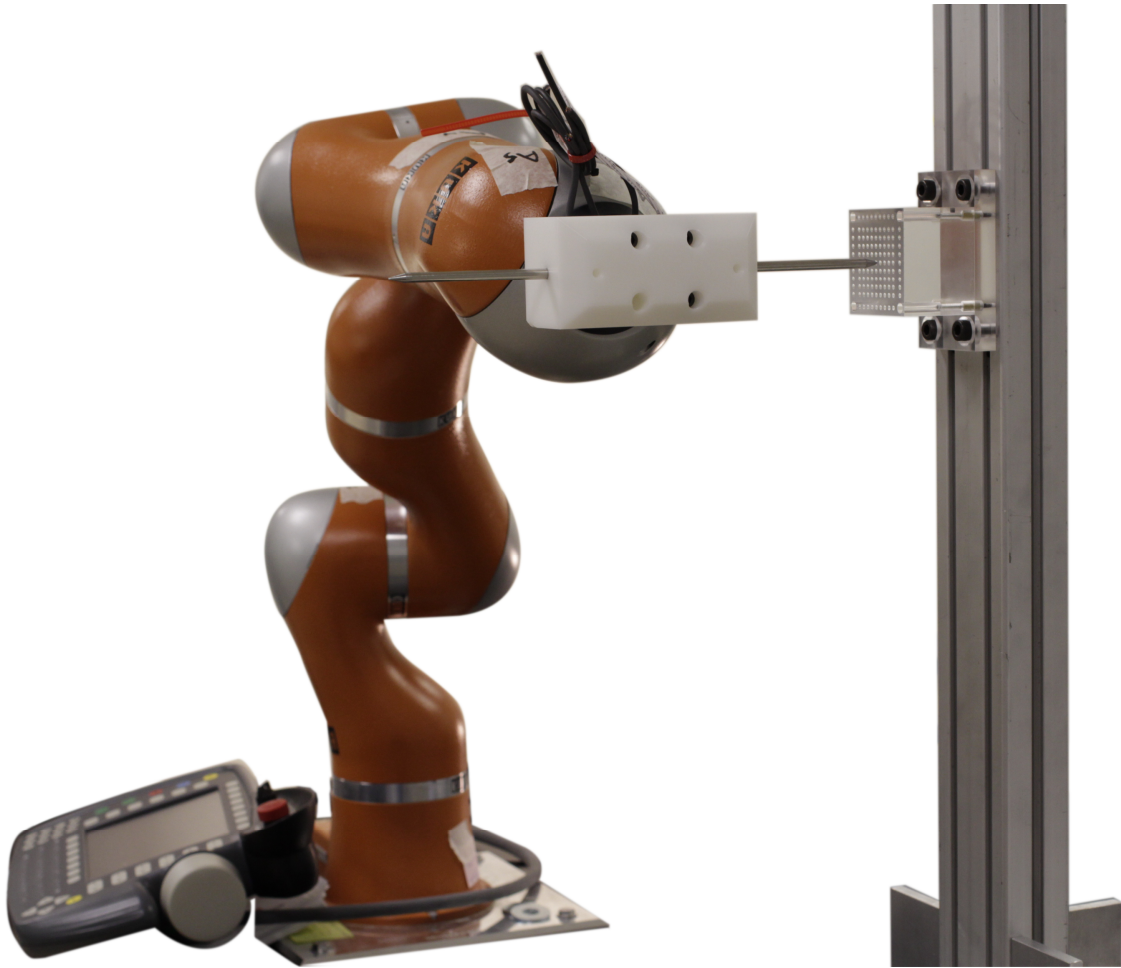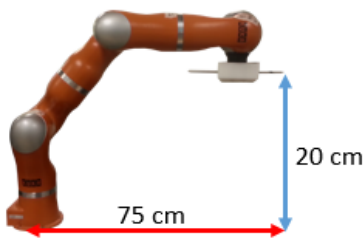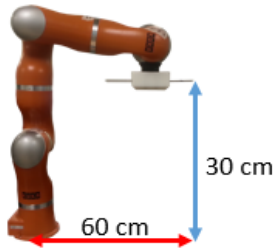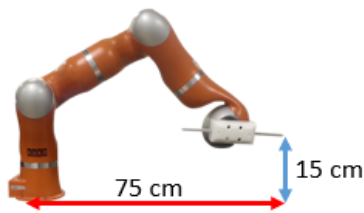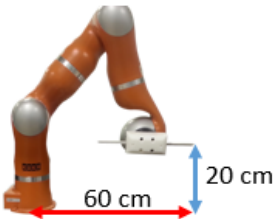
Figure 2.6: The KUKA LWR 4+ Digitization on the Block Mounted onto the Tower Jig

Block B1 or B2 (Block B2 is shown in the picture) can be moved horizontally or vertically to position the block with respect to the robot's frame. One can move the block vertically by mounting the block along the aluminum rail, or tower jig, with four fasteners, and as well as position the block horizontally by moving the tower jig along the firm table, clamped down.

Testing was conducted in four different locations, which were selected as a function of the robot's reach. This was done in order to determine whether different joint configurations have an effect on accuracy. It is known that, for open-chain robots with rotary joints, extending the robot's reach can increase positioning error, therefore the consistency of the robot, in terms of reach and stiffness, is determined. For this paper, if the elbow of the robot is at a right angle, then it is considered as half-reach. If the robot is at about 135 degrees, it is two-third-reach. The first location is about 60 cm away from the robot, at 20 cm high, allowing the robot to be in a half reach, and is in a normal stiffness. Second location is in a two-third-reach, 60 cm away from the robot, at 30 cm high, resulting an increased stiffness. The last two locations are about 75 cm away, at 15 cm and 30 cm high, respectively. The third location is in a half-reach with normal stiffness and the fourth location is in less than half-reach, decreasing stiffness. The joints are fixed in a way that reach and stiffness are correlated for this paper. To simplify the definition of each location, four different words are used to describe the location of the digitization block, which are: close and far, low and high. Therefore, the first, second, third and fourth locations were, close and low, close and high, far and low, and far and high, respectively **(Table 2.1)**.

Table 2.1: Location of the Digitized Area

	Far	Close
High	75 cm — 20 cm	60 cm — 30 cm
Low	75 cm — 15 cm	60 cm — 20 cm

Note: Above picture is only a representation of the location and not the reach of the robot.

Error Analysis – Quantifying the digitization error was based on the method of Koivukangas (11), with the exception of the reference location definition. Koivukangas used one specific digitized dimple location as the reference for all other digitizations. Since any single location measurement is subject to error, we chose to calculate the reference location as the average of all digitized points, thus minimizing the likelihood of the reference location being negatively impacted by an errant measurement. This is prudent, since the robot's error as a function of its position and orientation is the very performance metric that is being tested. The digitization error at each point E_{ij} for each block was calculated as:

$$E_i = \sqrt{(X_i - X_{avg})^2 + (Y_i - Y_{avg})^2 + (Z_i - Z_{avg})^2} - \sqrt{(X_{CAD,i} - X_{CAD,avg})^2 + (Y_{CAD,i} - Y_{CAD,avg})^2 + (Z_{CAD,i} - Z_{CAD,avg})^2} \qquad Eq.\ 5$$

where the variables X, Y and Z denote the three-dimensional coordinates of each point's location. Subscript i denotes the number of dimples in the digitized area. Subscript avg denotes the calculated average reference location. Subscript CAD denotes a 'gold standard' measurement made from the block's computer aided design (CAD). The average error E_{avg} is the average of all the errors at each point in an assessment block. The root mean square (RMS) error E_{RMS} and 95% confidence interval of the n points were also calculated for each block, where n is the number of dimple points in each block B1 and B2.

Average Error:

$$E_{avg} = \frac{1}{n} \sum_1^n E_i \qquad Eq.\ 6$$

RMS Error:

$$E_{RMS} = \sqrt{\frac{1}{n} \sum_1^n (E_i)^2} \qquad Eq.\ 7$$

95% Confidence Interval:

$$95\% \, CI = \, E_{avg} \qquad\qquad Eq. \ 8$$

where σ denotes one standard deviation.

Errors of the stylus were compared by paired-samples T-tests in terms of their descriptive statistics using SPSS software (SPSS V18, IBM Inc., Chicago, IL), as well as the errors of each locations and offsets were compared by repeated measured ANOVA.

2.3   Results

Digitization error for the volumes of Blocks B1 and B2 are shown in **Figure 2.7** and **Figure 2.8**, respectively. Digitization error for the perimeter locations that are common to both Blocks B1 and B2 are shown in **Figure 2.9** and **Figure 2.10**, respectively. A summary of the error metrics defined by equations 1 to 4 is shown in **Table 2.2**. The longest range of errors measured for sharp and rounded-tip styli for block B1 was -2.51 to 2.35 mm, and -1.61 to 2.76 mm, respectively. Similarly, the longest range of error for block B2 was -0.26 to 0.18 mm and -0.26 to 0.19 mm. Generally, for each error metric, the digitization error for Block B1 was one order of magnitude larger than the same metric for Block B2. There was no effect from changing location (i.e. robot joint configuration) (p > 0.05). There was no effect from changing the stylus orientation relative to the block's surface for rotations up to 15° (p > 0.05). There was a statistically significant difference in changing the stylus from sharp tip to rounded tip (p = 0.017). However, the average error of the sharp stylus was 0.15 ± 0.35 mm and rounded-tip stylus was 0.29 ± 0.40 mm accuracy.

Volume Digitization Error with Wide Stylus Rotation Allowed: Block B1
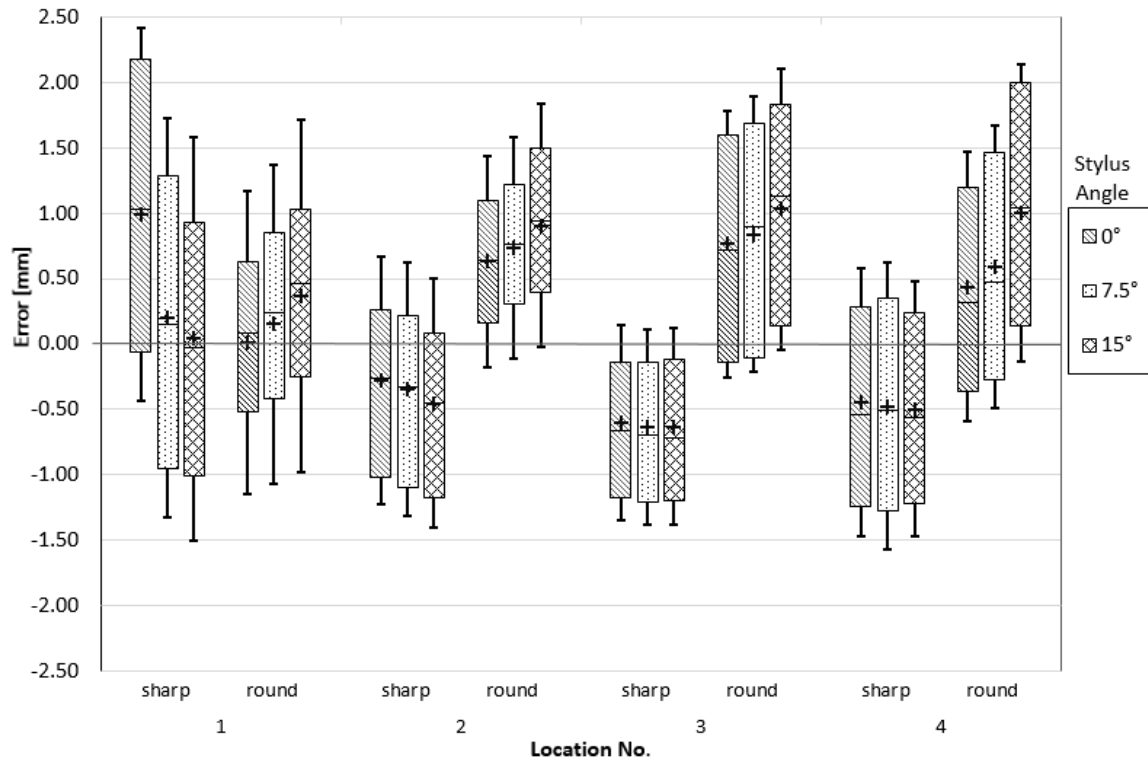
Figure 2.7: Volume Digitization Error of Block B1

Volume digitization error is the difference between the block digitization and the ideal CAD model. This box plot is the volume digitization error of block B1, with the stylus rotating $\pm\ 180^0$ to digitize each face. Average errors (black cross) range from -0.6 to 1.1 mm. The box plot whiskers represent 1 standard deviation and all other box plot features are standard. Each consecutively numbered location was defined as close and low, close and high, far and low, and far and high, respectively.

Volume Digitization Error with Stylus Rotation Constrained: Block B2
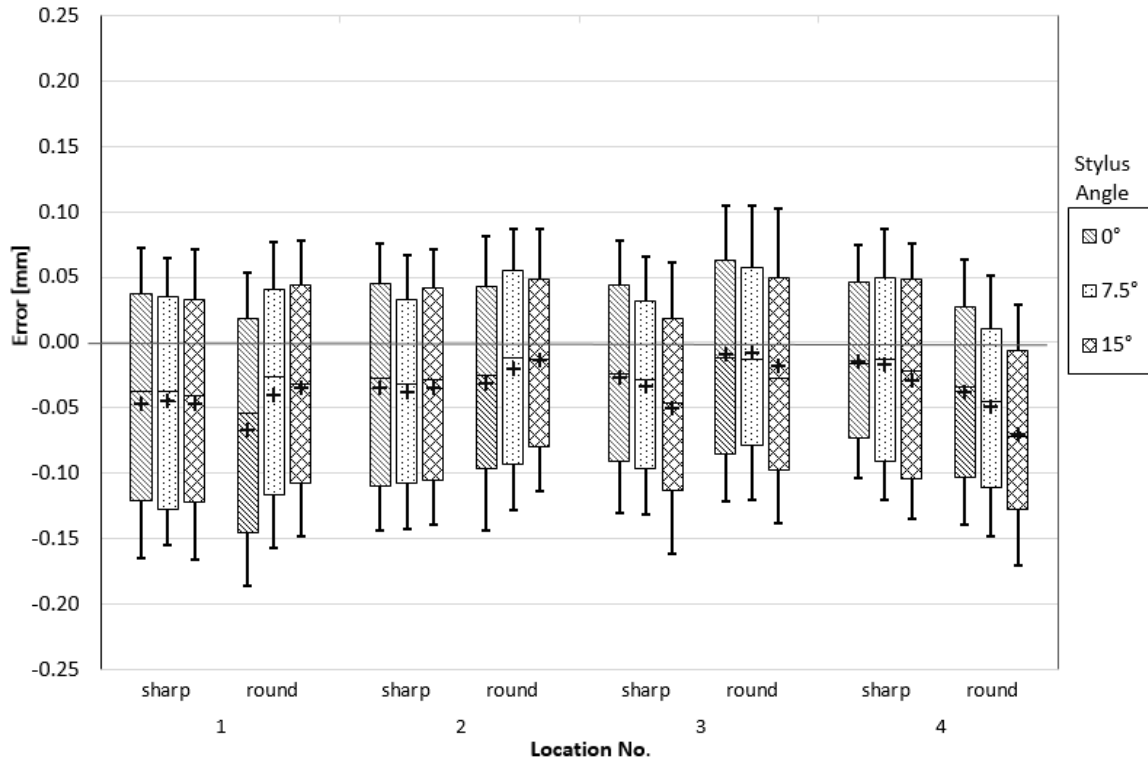
Figure 2.8: Volume Digitization Error of Block B2

Volume digitization error of block B2 with the robot maintaining its configuration, keeping the styli fixed throughout the trial in one location. The average errors (black cross) were less than 0.06 mm. Notice the axis change, B2 having a smaller scale than B1. The box plot whiskers represent 1 standard deviation and all other box plot features are standard. Each consecutively numbered location was defined as close and low, close and high, far and low, and far and high, respectively.

Perimeter Digitization Error with Wide Stylus Rotation Allowed: Block B1
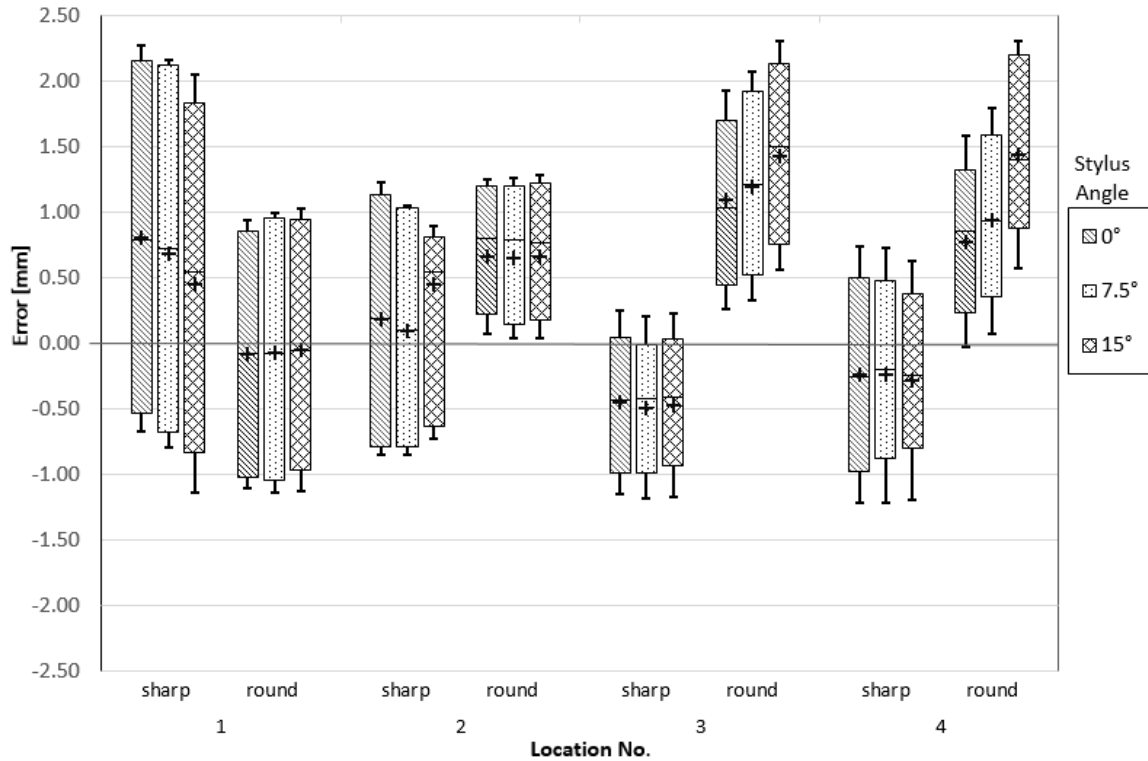
Figure 2.9: Perimeter Digitization Error of Block B1

Perimeter digitization error is the distance between the outer perimeter of B1 and the ideal CAD model using the stylus orientation of 180^0. Errors generally are higher than full volume digitization, due to less digitized points are being averaged out. Average errors (black cross) range from -0.5 to 1.4 mm. The box plot whiskers represent 1 standard deviation and all other box plot features are standard. Each consecutively numbered location was defined as close and low, close and high, far and low, and far and high, respectively.

Perimeter Digitization Error with Stylus Rotation Constrained: Block B2
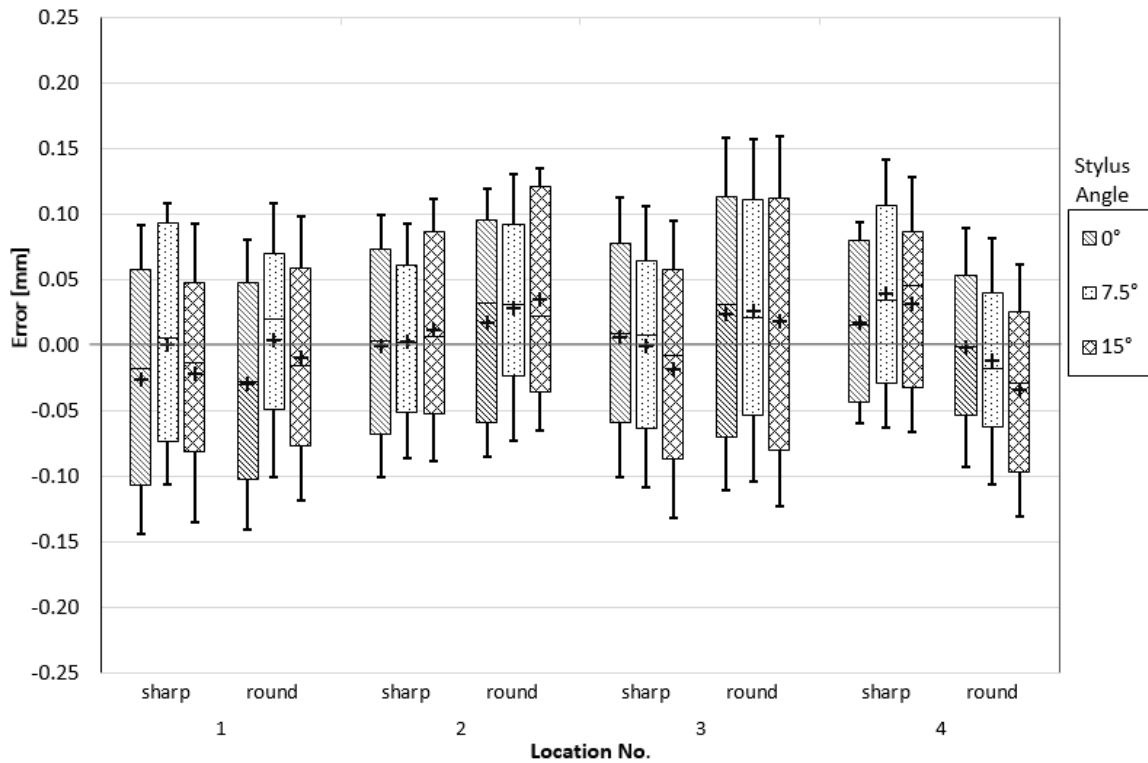
Figure 2.10: Perimeter Digitization Error of Block B2

Block B2 is the stylus rotation maintained in one direction. Also notice the axis change when comparing B1 and B2 plots. This box plot shows a significantly better accuracy. Average errors (black cross) range from -0.03 to 0.04 mm. The box plot whiskers represent 1 standard deviation and all other box plot features are standard. Each consecutively numbered location was defined as close and low, close and high, far and low, and far and high, respectively.

Table 2.2: Summary of Error Metrics for Both Digitization Blocks

Block	Stylus Angle [deg]	Error [mm]							
		Sharp Stylus				Rounded Stylus			
		Average	±1SD	RMS	95% CI	Average	±1SD	RMS	95% CI
B1	0	-0.08	1.22	1.20	-2.51, 2.35	0.46	1.05	1.14	-1.64, 2.56
	7.5	-0.32	1.14	1.18	-2.60, 1.97	0.58	1.09	1.23	-1.61, 2.76
	15	-0.39	1.10	1.17	-2.58, 1.81	0.46	1.05	1.14	-1.64, 2.56
B2	0	-0.03	0.11	0.11	-0.24, 0.18	-0.04	0.11	0.12	-0.26, 0.19
	7.5	-0.03	0.10	0.11	-0.24, 0.18	-0.03	0.11	0.11	-0.25, 0.19
	15	-0.04	0.11	0.12	-0.26, 0.18	-0.03	0.11	0.12	-0.26, 0.19

2.4 Discussion

The locating performance of a robot is generally reported as its repeatability in positioning rather than its accuracy, which is partly because a robot's accuracy is greatly impacted by its changing joint configuration. In the case of open chain rotary joint robots, the joint configuration refers to the combination of joint rotations that produce the given end-effector pose. Since a robot's position feedback is derived from the rotation that it measures at each joint in its open chain, then joint rotation measurement errors can stack up from the base to the end-effector, and some joint configurations produce more error stack up than others. Generally, configurations that produce higher bending loads, such as extended reaching, may challenge the stiffness of the robot's links and other constructs, thus reducing the predictability of end-effector positioning. This effect is generally worse when a joint's rotation axis is parallel to the torsion axis generated by the net load distal to the joint. Thus, the position accuracy is a function of the combination of joint rotations (i.e. configuration) which produce a given end-effector position. Some robots, like the 7-axis robot tested here, can achieve an end-effector position through more than one configuration of joint rotations, which further complicates the matter.

This study found that the magnitudes of average error and variability can be quite low; less than 0.04 ± 0.11 mm, when using a collaborative robot within a working volume of 55×55×55 mm, refer to Appendix A for determining the average error and variability. However, some specific considerations must be made in order to achieve this level of performance. We found that unspecified orientations of the end-effector can increase this positioning error and its variability by one order of magnitude. Large rotations and translations of the end-effector, while digitizing the Block B1 volume, were the greatest source of digitization error. However, small changes in orientation of the tool (i.e. stylus), up to 15°, had no significant effect when digitizing either block volume. These results indicate that, while some relative rotation may facilitate access without impacting performance, end-effector rotations should be limited to 15° within the working volume so that the stylus, or other calibrated tool, varies little in its approach vector.

The finding that digitizing normal to the surface did not improve accuracy is in contradiction to Milne and Lee (1999), who showed that significantly less digitization error was realized when the stylus was maintained normal to the digitized surface (12). Milne and Lee evaluated an electromagnetic tracking system with significantly less precision than the robot tested here; thus, the discrepancy is likely due to greater calibration error from that tracker. Theoretically, and especially when using a sharp stylus tip, there should be no increased error caused by small angles to the surface. Moreover, this has not been borne out in more contemporary evaluations of next-generation tracking systems.

There was no significant difference in error as a function of changing the location of the working volume, indicating that all robot configurations tested were equivalent, within the one-half to two-thirds reaches that were tested. While reach and joint configuration, as well as the location of the working volume relative to the robot's base frame, were not significant factors in this study, it should be emphasized that one should not expect the error performance of one working volume to be applicable elsewhere. The way to interpret these results is: The validated positioning error and repeatability inside of a specified working volume is relative to the center of that volume, and is not generally transferrable. This further implies that moving the end-effector to a different validated

working volume requires a redefinition of the reference frame to the center of the current working volume; thus, the measurements within one validated working volume cannot be made relative to a reference frame defined inside of a different working volume, even if that too was validated. Thus, stored definitions may be referenced as a function of location of the working volume.

The comparison of Blocks B1 and B2 did not isolate large rotations from large translations of the end-effector, and thus we cannot comment specifically on which was the greatest source of error. However, this distinction is somewhat moot since the approach vector cannot be achieved while maintaining one or the other constant. While large changes in translation may also contribute to the large errors, we found that it is best to minimize changes in the direction of the approach vector, while making translations sufficient to address the working volume.

A strength of this study, compared with previous work involving master digitization objects, was the use of two high-precision blocks with corresponding points. This allowed comparison between digitization accuracy using widely different approach vectors, which is a departure from most previous work using peg boards or other apparatus that focus more on varying location rather than orientation.

One of the limitations for this project is that digitizations were performed by only one user. Therefore it is not a good representation of the surgeon population for accuracy assessment. Also, the specimen count is relatively low, which may not provide sufficient statistical power.

Contact stylus probes that are used to digitize anatomy intra-operatively generally have a rounded tip. We included a sharp-tipped stylus in our tests as a 'gold standard' in terms of calibration and highly conforming physical contact between the stylus tip and the cone tip of the machined dimples in the digitization blocks. Moreover, a rounded stylus requires further considerations in its calibration and calculation of the true contact location when digitizing, which may conceivably affect its accuracy and added to our rationale for testing both. Our results showed that there was a statistically significant difference between the sharp and rounded stylus tips we used, however the average

accuracy of the rounded-tip was less than 0.30 mm. Of course, this result will be limited by the radius of a rounded tip, since a radius above some amount related to the robot's positioning accuracy and to the application's desired accuracy, will certainly preclude any assumption of equality with a sharp-tipped stylus.

This study found that the positioning error, when using a collaborative open chain robot, can be within levels that are acceptable in many fields where manual collaborative positioning or navigation relative to osseous anatomy are used, including joint arthroplasty, spine surgery and neurosurgery (13, 14). This information is likely also relevant to robotic surgical systems that perform navigated bone machining from a pre-operative plan, since these systems also rely on the accuracy of the robot's position feedback to locate a tool tip that has been previously calibrated relative to the robot's end-effector frame. Collaborative bone reshaping systems, such as MAKOplasty (6), may potentially be utilized as a digitizer for locating anatomical reference points needed in the process of registering the pre-operative plan to the patient's osseous anatomy. The results of this study suggest that these systems may also benefit from some amount of rotation constraint on tool orientation.

We tested only one collaborative robot, which is not necessarily representative of the general state of the technology, nor of specific systems that are currently in use for surgical applications. However, the method we employed is relevant to all collaborative open chain robots and is a simple and effective means of quantifying the accuracy of any similar robotic system within a specific working volume. This method is also useful for determining the most reliable mounting location and range of joint configurations that minimize positioning error. The robot tested in this study is not currently used in any surgical procedures that we know of; however, KUKA does manufacture a 7-axis robot that is essentially identical to the model tested, both in form and in function, which is advertised as a platform for OEM integration of surgical systems. As industry is moving toward integrating collaborative robots into increasingly more surgical procedures, it will be important to have standardized evaluation methods that can be applied to specific procedure setups. This can be a valuable tool for site personnel to periodically confirm positional accuracy and variability of the system throughout its operating life.

2.5 References

1. Jakopec M, Rodriguez y Baena F, Harris SJ, Gomes P, Cobb J, Davies BL. The hands-on orthopaedic robot "acrobot": Early clinical trials of total knee replacement surgery. IEEE Trans Robotics Autom. 2003;19(5):902-11.

2. Gomes P. Surgical robotics: Reviewing the past, analysing the present, imagining the future. Robot Comput Integr Manuf. 2011 Apr;27(2):261-6.

3. Hagn U, Konietschke R, Grebenstein M, Warpup R, Haslinger R, Frommberger M, Hirzinger G, Jörg S, Passig G, Bahls T, Nothhelfer A, Hacker F, Le-Tien L, Albu-Schäffer A. The DLR MIRO: A versatile lightweight robot for surgical applications. Int J Ind Robot. 2008 Jan;35(4):324-36.

4. Albu-Schäffer A, Ott C, Hirzinger G. A unified passivity-based control framework for position, torque and Impedance control of flexible joint robots. Int J Robot Res. 2007;26(1):23-39.

5. Davies B. A review of the state-of-the-art of "smart" systems in surgery. Mechatronics and machine vision in practice, 2008. M2VIP 2008. 15th international conference on 2008.

6. Hagag B, Abovitz R, Kang H, Schmitz B, Conditt M. RIO: Robotic-arm interactive orthopedic system MAKOplasty: User interactive haptic orthopedic robotics. In: Rosen J, Hannaford B, Satava RM, editors. Surgical Robotics. Springer US; 2011. p. 219-46.

7. Horn BK. Closed-form solution of absolute orientation using unit quaternions. J Opt Soc Am A. 1987;4(4):629-42.

8. Enciso R, Shaw AM, Neumann U, Mah J. Three-dimensional head anthropometric analysis. Proc.SPIE. 2003;5029:590-7.

9. KUKA system software 5.6 lr: Operating and programming instructions for system integrators. 5th ed. Augsburg, DE: KUKA Laboratories GmbH; 2012.

10. Koivukangas T. Methods for determination of the accuracy of surgical guidance devices: A study in the neurosurgical region of surgical interest [dissertation]. Oulu, Finland: Ph. D. dissertation, University of Oulu, Finland. ISBN 978-951-42-9904-9; 2012.

11. Koivukangas T, Katisko JPA, Koivukangas JP. Technical accuracy of optical and the electromagnetic tracking systems. SpringerPlus. 2013;2(1):1-7.

12. Milne A, Lee J. Error analysis of a direct current electromagnetic tracking system in digitizing 3-dimensional surface geometries. Biomed Sci Instrum. 1999;35:23-8.

13. Shoham M, Lieberman IH, Benzel EC, Togawa D, Zehavi E, Zilberstein B, Roffman M, Bruskin A, Fridlander A, Joskowicz L, Brink-Danan S, Knoller N. Robotic assisted spinal surgery–from concept to clinical practice. Computer Aided Surgery. 2007 2007;12(2):105-15.

14. Davies B, Rodriguez F, Harris S, Jakopec M, Barrett A, Gomes P, Cobb J. An overview of the acrobot® robotic surgical system for minimally invasive unicompartmental knee arthroplasty. J Biomech. 2006;39(1 Suppl):S211.

Chapter 3

3 Evaluation of a 7-Axis Collaborative Robot as a Bone Surface Digitizer: With Validation in an *In-Vitro* Glenoid Model

3.1 Introduction

The frequency of robot-assisted surgery has been increasing in recent years. In 2010, it was reported that the number of robot-assisted procedures performed worldwide have tripled since 2007 (1). Spong et al. (2006) defined a robot as "a reprogrammable, multifunctional manipulator designed to move materials, parts, tools, or specialized devices through variable programmed motions for the performance of a variety of tasks (2)." This definition describes an autonomous mode, which is common in manufacturing, and was notably employed by the ROBODOC robotic orthopaedic surgical system (3). However, more contemporary orthopaedic surgical robots have employed a collaborative mode approach, in which the robot arm is compliant to forces applied by the surgeon's hand, and moves in response while compensating for the robot's mass and nullifying the gravity load vector (4, 5). Systems like the Acrobot (The Acrobot Company Ltd, London, UK) (6) and MAKOplasty (MAKO Surgical Corp, Fort Lauderdale, Florida) (7) utilize this collaborative mode to machine cortical and subchondral bone with a burring tool in preparation for joint replacement (8, 9).

Some robot-assisted procedures in orthopaedics, craniofacial and neurosurgery applications require localization to the patient's bony anatomy for robot navigation, which is most often accomplished by defining bone-fixed coordinate frames (10). Most of these procedures utilize a tracking system to digitize the coordinates of osseous features in order to generate the coordinate frames needed for robot navigation (11). The actual recording of the osseous surface topology is generally performed with a contact stylus probe outfitted with a tracking device. Most tracking systems in surgical use are optical, which require an unobstructed line-of-sight to all the trackers (12), which can be obtrusive to the surgical team and interfere with the workflow.

In robot-assisted surgical procedures that utilize a collaborative robot, it may be possible to employ the robot itself as the bone surface digitizer. These robots can report their end-effector location relative to their native coordinate frame. Thus by outfitting the end-effector with a stylus probe and calibrating the tip location with respect to the robot's end-effector, a collaborative robot can readily be used as a manually operated localizer, or surface contact digitizer, similar to current optical tracking methods. The accuracy of such a construct has not been reported; thus, the purpose of this study was to quantify the accuracy of a robotic bone digitization method, and to provide validation in an *in-vitro* model relevant to clinical joint replacement (i.e. shoulder arthroplasty).

3.2   Methods

A 7-axis robot (LWR4+, KUKA Robotics Canada Ltd., Mississauga, ON) was used as the articulated robot arm for this study. The robot's end-effector was outfitted with a 95 mm long stylus probe with a rounded-tip (0.74 mm radius). The tip location of the stylus was calibrated relative to the robot's end-effector coordinate frame and the robot was programmed to output the tip location relative to its native base frame. The LWR4+ was operated in collaborative mode (i.e. gravity compensated), allowing an investigator to move the stylus probe manually.

A three-dimensional (3D) laser scanner (3D Scanner HD, NextEngine Inc., Santa Monica, CA), with specified accuracy of 0.127 mm and spatial resolution of 4 400 points per square inch, was used to provide the gold standard digitization of the specimen's articular surface (13).
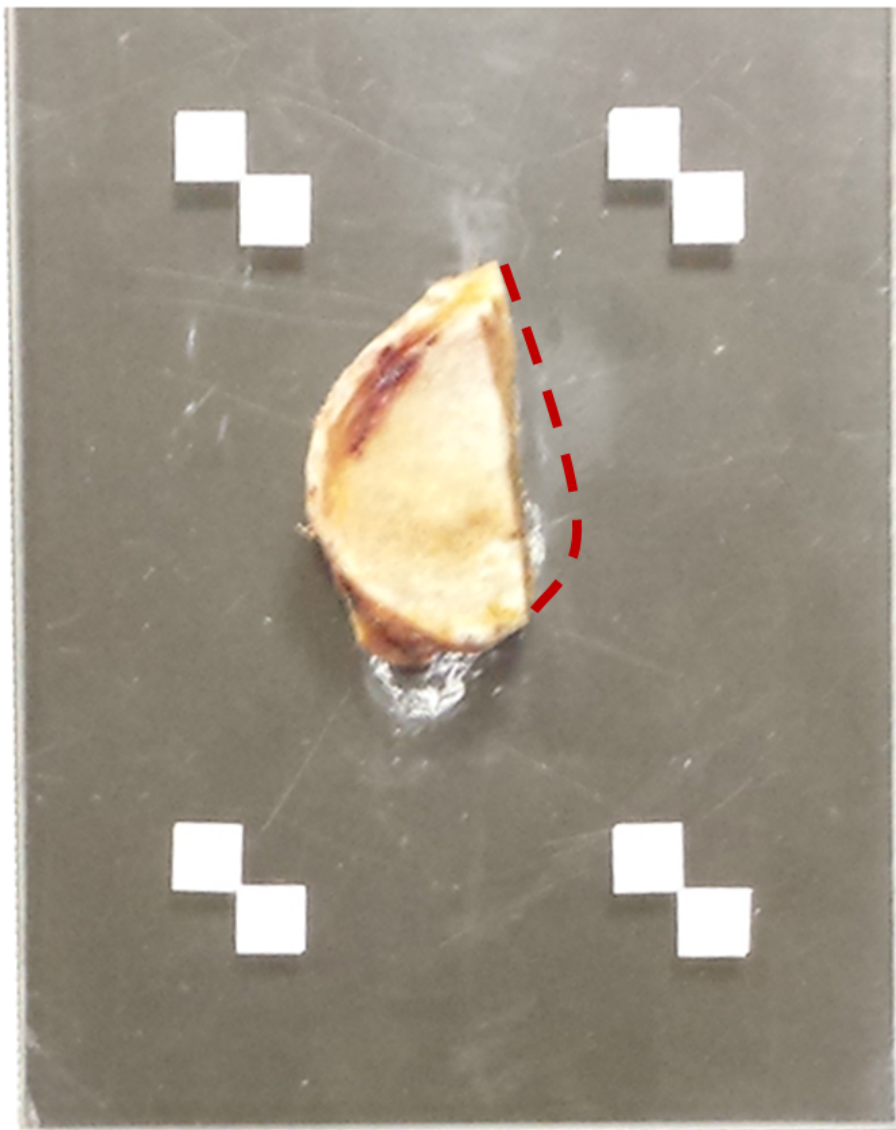
Figure 3.1: Glenoid Acrylic Base Set Up

Glenoid cadaveric specimen mounted to transparent acrylic base with four optical fiducial markers. Four specimens were tested, each with a 30% anterior defect to simulate a realistic surgical case. The red dashed line indicates the native perimeter of the intact glenoid.

3.2.1   Testing protocol

Four previously fresh-frozen cadaveric glenoids (68.5 ± 12.7 years old, 4 males, 4 right) were used. A 30% anterior defect was removed from all glenoids to simulate a realistic amount of bone loss due to degenerative arthritis, which would often be indicated in a total shoulder arthroplasty procedure. These specimens were removed of the soft tissue surrounding the glenoid, and were cut using a sagittal saw to separate the glenoid from the scapula. The glenoids were prepared by rubbing with a paper towel to give a matte surface finish for improved laser retro-reflection. Each glenoid was mounted onto a transparent acrylic base, which was not detectable by the laser scanner (**Figure 3.1**). Four fiducial markers were affixed to the base. Each marker was constructed from standard white paper (0.10 ± 0.01 mm thick) in checkered interference pattern, the shape of a typical checker style optical location marker, in which the intersection of square corners indicated the fiducial location. The colour white was chosen for a maximum reflection the laser scan. These fiducial locations could be measured by both the robotic stylus and the laser scanner.

Two robot digitization methods were conducted for each glenoid. For the first method (Orientation Free), the stylus was free in all 6DOF and the user, having complete manual control over translation and rotation, maintained the stylus approximately perpendicular to the glenoid surface. For the second digitization method (Orientation Locked), the robot was programmed to maintain a medially-oriented stylus, while allowing the user to translate the stylus (i.e. 3DOF). Approximately 6 000 - 9 000 points per glenoid were collected. Locations of the four fiducial markers were also manually digitized using the robot by touching the stylus tip to the corner intersection of each fiducial. Ten digitized points were averaged in order to reduce variability.

Laser scans were measured using ParaView (Kitware, Inc., Clifton Park, NY). As for the robot digitization, fiducial locations were determined using the intersection of the two square label corners. Since the laser scan exhibited some point cloud scatter, this was done by creating best-fit vectors on the internal sides of each square (**Figure 3.2**). The fiducial location was then defined as the average location of the four vector intersections.
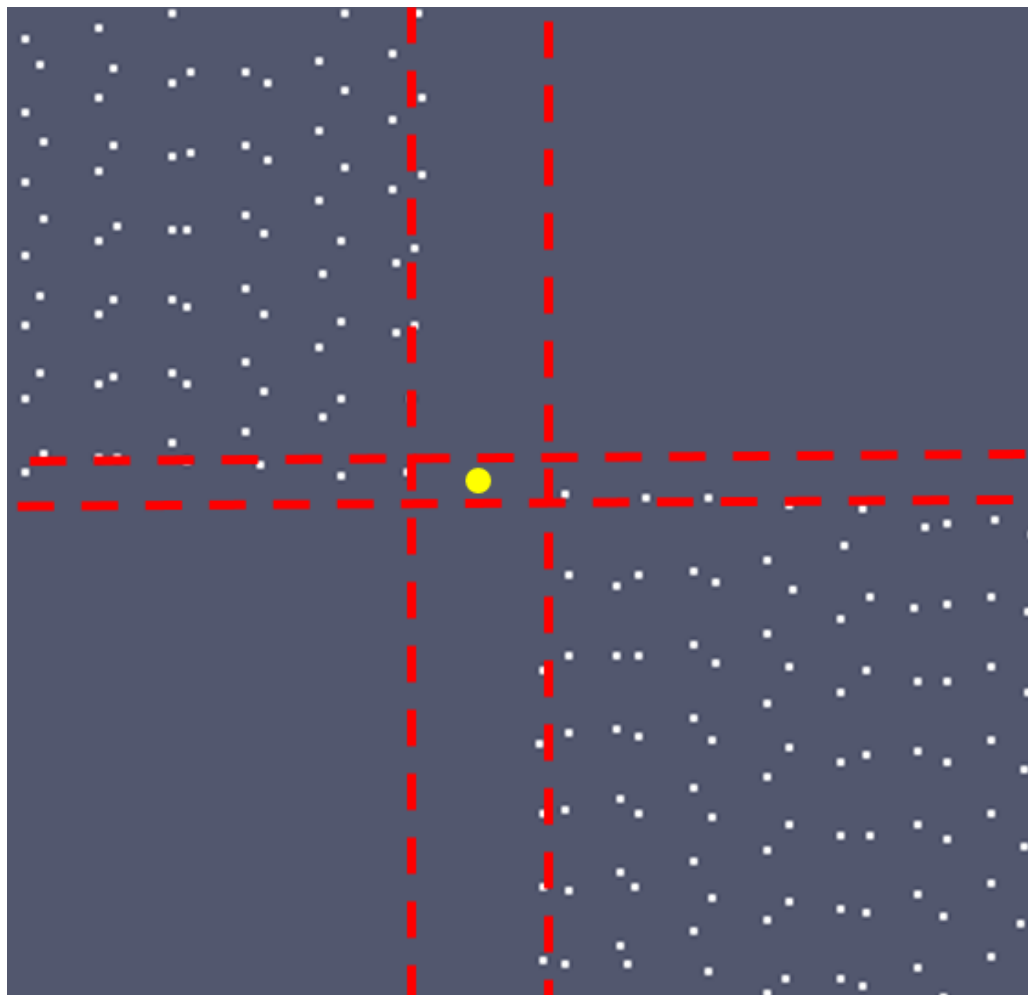
Figure 3.2: An Illustration of the Spatial Calculation to Determine the Fiducial Marker

An illustration of the method to determine the center of a fiducial marker from a laser scan point cloud. Vectors (red dashed lines) were fit to the points that comprise the intersecting edges. The fiducial center (yellow dot) was then the average location of the four vector intersections. This method assumes that any factors causing point cloud errors affect all vertical edges equally in both squares, and similarly for horizontal edges. This method also works in the case where edges overlap due to dilation (not shown).

After fiducial locations were determined from both modalities, a co-registration was performed using paired-point registration, in order to evaluate both robot and laser surface digitizations in a common coordinate frame (14). The fiducial points from the robot digitization and the laser scanner were co-registered using custom code made with VTK Version 5 (Visualization Toolkit, Kitware Inc., Clifton Park, NY) (15), which reported the transformation matrix and a fiducial registration error (16). The transformation matrix was used to transform the robot digitization to a fiducial reference frame in the laser's native coordinate frame.

The robot-assisted digitization was surface fit using a Radial Basis Function (MATLAB 7, The MathWorks, Inc., Natick, MA), which interpolated the point clouds to create a surface that had similar point density as the laser scanned surface (gold standard). The two surfaces were compared and errors between the two surfaces were represented by residual distances between them using a previously developed algorithm, and visualized using proximity maps (17). The residual distance algorithm was developed in a custom software written with VTK by Lalone et al. In this software, the minimum distances were calculated using a nearest point-to-point distance algorithm, where the points correspond to the vertices within each triangular mesh. The algorithm first lists the Cartesian coordinates of all points on the laser scan and robot digitization of glenoid surface models, then compares the list of opposing surfaces to determine which points are closest in proximity. Finally, the residual distance between these closest points is then calculated, and the average residual distance error is reported (17). Errors of the Orientation Locked and Orientation Free digitization methods were compared by paired-samples T-tests in terms of their descriptive statistics using SPSS software (SPSS V18, IBM Inc., Chicago, IL).

3.3 Results

The mean Fiducial Registration Error (FRE) for all trials was 0.17 mm, with a maximum of 0.23 mm (**Figure 3.3**). The average residual error of the glenoid model for the Orientation Locked and Orientation Free methods resulted in 0.27 ± 0.21 mm and 0.37 ± 0.27 mm, respectively (**Figure 3.4**). Residual errors were visualized using proximity maps (**Figure 3.5**), which showed that distance errors were 0 to 1 mm within the articular

regions. The Root Mean Square (RMS) of the residual error was between 0.26 and 0.54 mm for all trials, with only two trials above 0.50 mm. All errors for each specimen and methods are reported in **Table 3.1.** The average errors across the four specimens for Orientation Locked and Orientation Free methods are 0.27 and 0.37 mm, respectively. There were no differences between the Orientation Locked and Orientation Free methods in terms of residual error ($p = 0.10$), spread (i.e. 1 standard deviation; $p = 0.13$), RMS ($p = 0.09$), or FRE ($p = 0.88$).
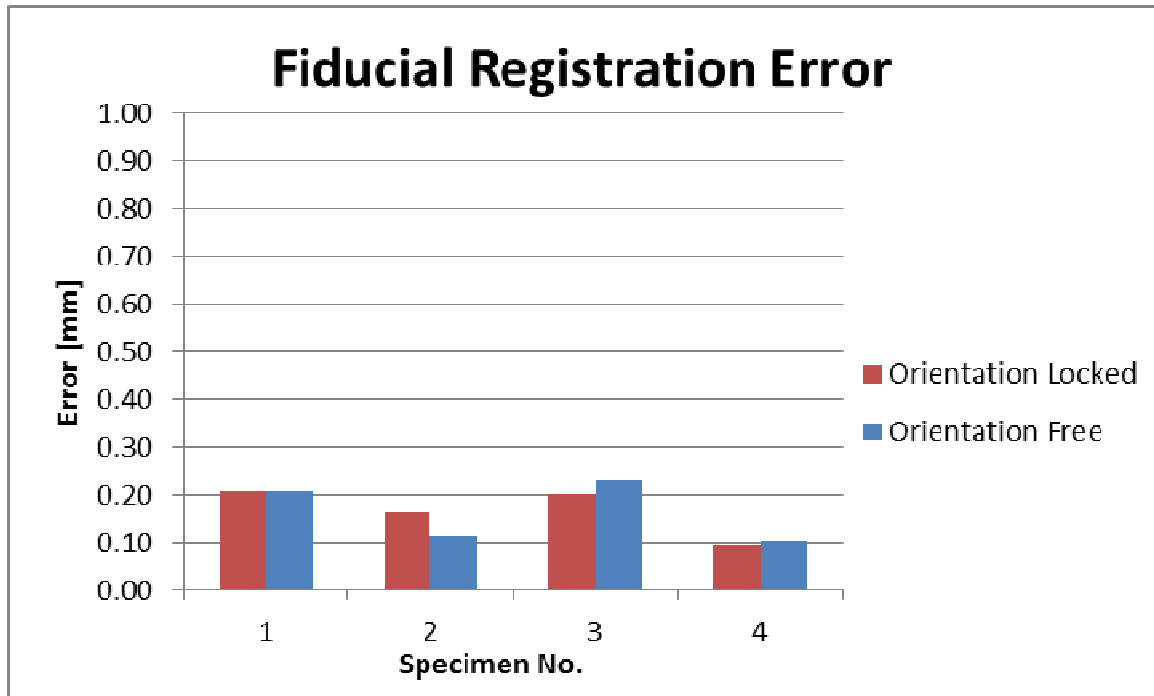
Figure 3.3: Fiducial Registration Error using Paired Point Registration

Fiducial registration error is the root-mean-square error in fiducial alignment between the laser scan and robot digitization. Fiducial registration was done for all specimens using paired point registration. Registration error was less than 0.25 mm for all trials, with an average error of 0.17 mm.
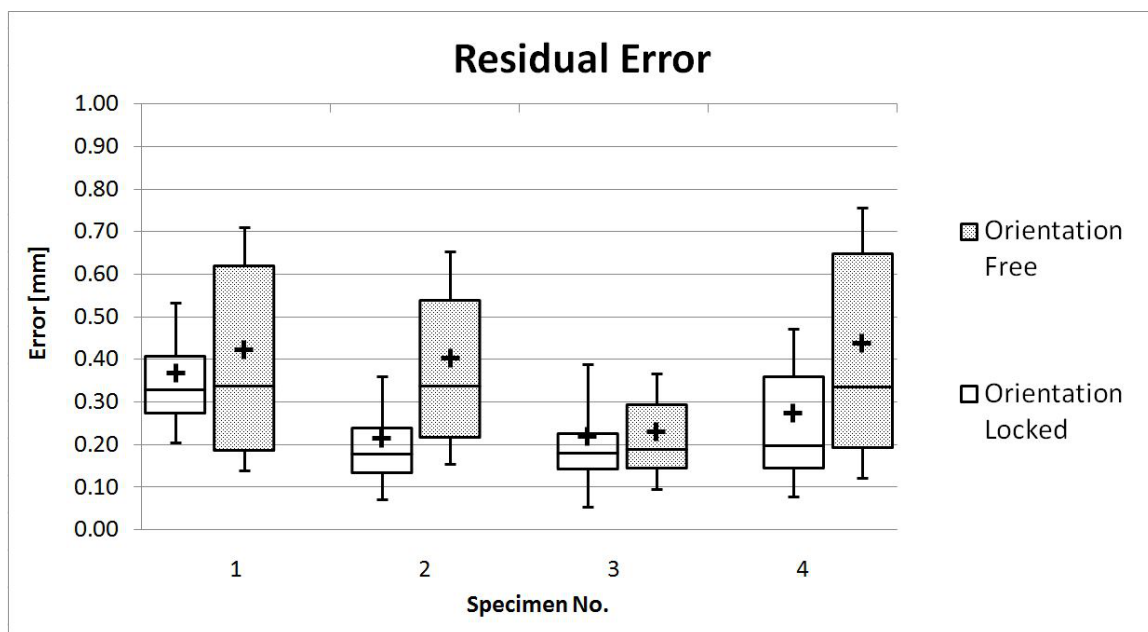
Figure 3.4: The Residual Error between Laser Scan and Robot Digitization

The residual error is the inter-surface distance between the laser scan (gold standard) and the manually-performed robot digitization. Average errors (black cross) were less than 0.5 mm in all trials. The box plot whiskers represent 1 standard deviation and all other box plot features are standard. There was no difference between the Orientation Free and Orientation Locked digitization methods in terms of any descriptive statistic ($p > 0.05$).
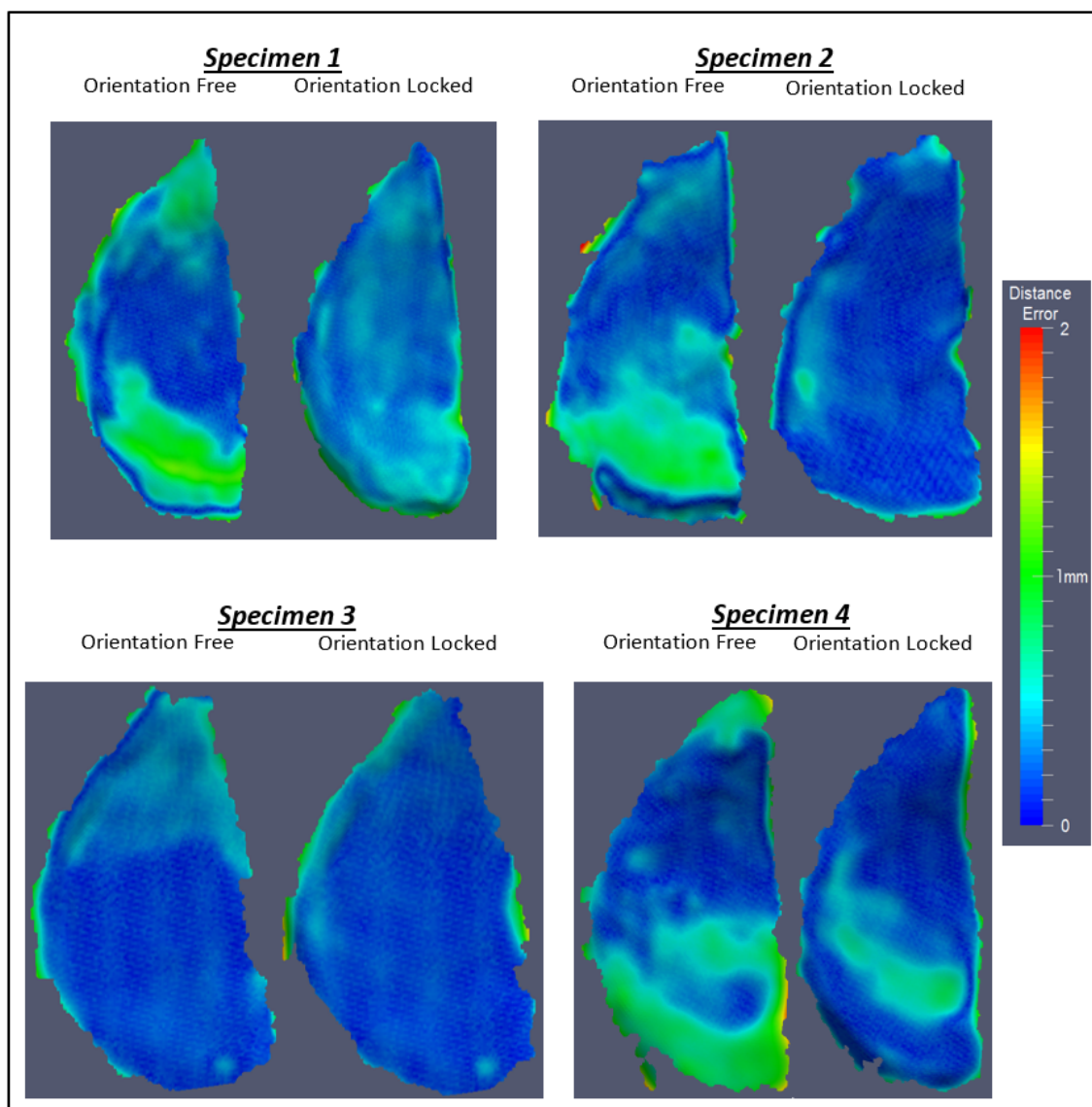
Figure 3.5: Proximity Maps of Residual Distance Error

Proximity maps showing residual distance error as a function of location. Error of the manually-performed robot digitization was 0 to 1 mm within the articular region for all four specimens.

Table 3.1 Summarized Error Results of each Specimen for each Method

	30% Anterior Glenoid Defect							
	Orientation Free				Orientation Locked			
Specimen No.	1	2	3	4	1	2	3	4
Fiducial Registration Error [mm]	0.208	0.161	0.198	0.095	0.207	0.114	0.227	0.104
Average Residual Error [mm]	0.424	0.404	0.230	0.438	0.368	0.216	0.220	0.273
Standard Deviation [mm]	0.286	0.250	0.136	0.318	0.164	0.144	0.168	0.197
Root Mean Square [mm]	0.511	0.475	0.267	0.541	0.402	0.260	0.277	0.337

These specimens are listed in Appendix B.

3.4 Discussion

The manually performed robot-assisted surface digitization produced errors less than 0.50 mm on average per specimen, which is sufficient in most procedures and certainly suitable in orthopaedic procedures, which was the cadaveric model used here. The median error was less than 0.35 mm and the mean error was greater than the median error in all eight trials, which indicates that the error is not normally distributed, but rather that the majority of measurements had error magnitudes less than the mean. Thus, there were relatively fewer measurements in each trial, which skewed the mean higher, but these few were greater in error magnitude. Moreover, each of the lower quartiles are smaller than their corresponding upper quartiles, further indicating that error values in the higher range have greater spread. From these observations, we can conclude that there were some errors around 1 mm, but that the majority were less than 0.5 mm.

Normal stylus calibration of a rounded stylus would produce a calibrated point located in the center of the spherical tip. This would manifest as a slight dilation of the digitized surface, since the calibrated point would always be offset above the surface. In order to avoid this, we offset the calibrated point distally by one radius of the tip sphere, bringing it to the most distal tip surface of the stylus. Given the rounded geometry of the stylus tip, it is likely that the calibrated point was not in contact with the digitized surface when the stylus was not perpendicular to the surface, which would theoretically increase digitization error. This was tested by comparing the Orientation Locked and Orientation Free methods. There was no difference in error between both methods. This indicates that stylus orientation is not a factor for a stylus calibrated using our technique and that no further compensation is required, such as calculating stylus deflection as used by some Coordinate Measurement Machines (CMM) (18). This is stated with the caveat that oblique stylus angles were not tested in this study.

The high number of surface points that we digitized does not represent typical digitization density in most intra-operative procedures. Rather, we collected high-density digitizations for mapping error over the entire available articular surface. Since each digitized point is independent, then any pixel on the error map can be interpreted independently, which makes these results relevant for protocols that require even a small

number of points or digitized locations.

Robotic digitization is relevant to procedures that use articulated robots, such as MAKOplasty (7) and Acrobot (19), as it can be incorporated with the pre-operative plan. Robots have been extensively studied and used in the lower extremity, where their improved precision and accuracy of implant placement and bone reshaping has been shown (20). Although significant inroads have not been made into upper extremity procedures, the results of this study show that robot assistance may be advantageous in total shoulder arthroplasty, where malalignment and aseptic loosening of the glenoid component remains a leading cause of implant failure requiring revision surgery (21-23).

In robotic procedures where a digitizer is used for registration of the pre-operative plan, it may be an attractive option to perform the digitization using the robot itself. Digitizing in the robot's native coordinate frame may be used to reduce the number of coordinate transformations, thus reducing mathematical precision error, which is generally a significant source of registration error. This is notwithstanding the fact that a tracking system is still required for applications in which intra-operative movement of the patient's anatomy must be tracked in real-time. A trackerless method may be more suitable for procedures which do not require movement tracking, such as some craniofacial and neurosurgical procedures in which the anatomy is fixed by spatial frames relative to a robot's base frame, as is the case with the Neuromate (Renishaw Ltd.) and the Pathfinder (Prosurgics Ltd.) (24, 25).

Manual digitization using a collaborative robot is similar to using a passive linkage contact stylus digitizer, which is utilized in some surgical navigated systems. This is not implying that collaborative robots should replace passive linkage digitizers in all circumstances, but rather that passive linkages may not be required in applications where a collaborative robot is already employed. The same may be said for optical and other tracking systems where the tracker is primarily used as a digitizer.

In 3 of the 4 specimens, the variability was greater when using the Orientation Free method; however, this was not statistically significant. For these specimens, this variability was concentrated mostly in the inferior articular region. This was not likely

due to robot accuracy, but rather the operator's ability to navigate the curvature of the inferior rim while reorienting the robot's end-effector. Further study, including inter-observer reliability, would have to be conducted to determine the precise reason. Such investigations, specific to anatomy, would be required to determine also, if it is more reliable to avoid or mathematically discount certain regions if they are associated with higher digitization variability.

The simulation of a 30% anterior defect was a strength in this study since the accuracies of the registration algorithms used are negatively impacted by a reduction in the amount of digitized area; thus, our conclusions of suitable accuracy are conservative, given that 30% is relatively large defect. Moreover, the simulated defect provides relevance to the glenoid model, since most total shoulder arthroplasty procedures are indicated by significant bone loss due to degenerative bone disease, mainly from osteoarthritis and rheumatoid arthritis.

We have presented a construct for digitizing a bony surface using a collaborative robot and evaluated its accuracy in a cadaveric shoulder model. As this method is readily applied to existing articulated surgical robots, it may be adopted into current procedures. Additionally, it may facilitate the move to robot-assistance in procedures where robots are not currently used, but that could benefit from their precision and accuracy, such as shoulder arthroplasty.

3.5 References

1. Barbash GI, Glied SA. New technology and health care costs -- the case of robot-assisted surgery. N Engl J Med. 2010 Aug 19;363(8):701-4.

2. Spong MW, Hutchinson S, Vidyasagar M. Robot modeling and control. 1st ed. Hoboken: John Wiley & Sons; 2006.

3. Adili A. Robot-assisted orthopedic surgery. Surg Innov. 2004 Jun;11(2):89-98.

4. Hagn U, Konietschke R, Grebenstein M, Warpup R, Haslinger R, Frommberger M, Hirzinger G, Jörg S, Passig G, Bahls T, Nothhelfer A, Hacker F, Le-Tien L, Albu-Schäffer A. The DLR MIRO: A versatile lightweight robot for surgical applications. Int J Ind Robot. 2008 Jan;35(4):324-36.

5. Albu-Schäffer A, Ott C, Hirzinger G. A unified passivity-based control framework for position, torque and Impedance control of flexible joint robots. Int J Robot Res. 2007;26(1):23-39.

6. Davies B, Jakopec M, Harris SJ, Rodriguez y Baena F, Barrett A, Evangelidis A, Gomes P, Henckel J, Cobb J. Active-constraint robotics for surgery. Proceedings of the IEEE. 2006;94(9):1696-704.

7. Hagag B, Abovitz R, Kang H, Schmitz B, Conditt M. RIO: Robotic-arm interactive orthopedic system MAKOplasty: User interactive haptic orthopedic robotics. In: Rosen J, Hannaford B, Satava RM, editors. Surgical Robotics. Springer US; 2011. p. 219-46.

8. Gomes P. Surgical robotics: Reviewing the past, analysing the present, imagining the future. Robot Comput Integr Manuf. 2011 Apr;27(2):261-6.

9. Jakopec M, Rodriguez y Baena F, Harris SJ, Gomes P, Cobb J, Davies BL. The hands-on orthopaedic robot "acrobot": Early clinical trials of total knee replacement surgery. IEEE Trans Robotics Autom. 2003;19(5):902-11.

10. Clark TC, Schmidt FH. Robot-assisted navigation versus computer-assisted

navigation in primary total knee arthroplasty: Efficiency and accuracy. ISRN Orthop. 2013;2013:1-6.

11. Mavrogenis AF, MD, Savvidou OD, MD, Mimidis G, MD, Papanastasiou J, MD, Koulalis D, MD, Demertzis N, MD, Papagelopoulos, Panayiotis J,MD, DSC. Computer-assisted navigation in orthopedic surgery. Orthopedics (Online). 2013 Aug 2013;36(8):631-42.

12. Cleary K, Peters TM. Image-guided interventions: Technology review and clinical applications. Annu Rev Biomed Eng. 2010;12(1):119-42.

13. Sholts SB, Flores L, Walker PL, Wärmländer SK. Comparison of coordinate measurement precision of different landmark types on human crania using a 3D laser scanner and a 3D digitiser: Implications for applications of digital morphometrics. Int J Osteoarchaeol. 2011;21(5):535-43.

14. Horn BK. Closed-form solution of absolute orientation using unit quaternions. J Opt Soc Am A. 1987;4(4):629-42.

15. Schroeder W, Martin K, Lorensen B, Sobierajski L, Avila R, Law C. The visualization toolkit. 2nd ed. New York: Prentice Hall; Kitware Inc.; 1998.

16. Maurer C.R. J, Fitzpatrick JM, Wang MY, Galloway R.L. J, Maciunas RJ, Allen GS. Registration of head volume images using implantable fiducial markers. IEEE Trans Med Imag. 1997;16(4):447-62.

17. Lalone EA, McDonald CP, Ferreira LM, Peters TM, King GW, Johnson JA. Development of an image-based technique to examine joint congruency at the elbow. Comput Methods Biomech Biomed Engin. 2013 Mar;16(3):280-90.

18. Hocken RJ, Pereira PH. Coordinate measuring machines and systems. 2nd ed. Hoboken: CRC Press; 2011.

19. Davies B, Rodriguez F, Harris S, Jakopec M, Barrett A, Gomes P, Cobb J. An overview of the acrobot® robotic surgical system for minimally invasive

unicompartmental knee arthroplasty. J Biomech. 2006;39(1 Suppl):S211.

20. Howe RD, Matsuoka Y. Robotics for surgery. Annu Rev Biomed Eng. 1999 Aug;1(1):211-40.

21. Deutsch A, Abboud JA, Kelly J, Mody M, Norris T, Ramsey ML, Iannotti JP, Williams GR. Clinical results of revision shoulder arthroplasty for glenoid component loosening. J Shoulder Elbow Surg. 2007;16(6):706-16.

22. Raphael BS, Dines JS, Warren RF, Figgie M, Craig EV, Fealy S, Dines DM. Symptomatic glenoid loosening complicating total shoulder arthroplasty. HSS J. 2010 Feb;6(1):52-6.

23. Walch G, Young AA, Boileau P, Loew M, Gazielly D, Molé D. Patterns of loosening of polyethylene keeled glenoid components after shoulder arthroplasty for primary osteoarthritis: Results of a multicenter study with more than five years of follow-up. J Bone Joint Surg Am. 2012 Jan 18;94(2):145-50.

24. Eljamel MS. Validation of the PathFinder neurosurgical robot using a phantom. Int J Med Robot Comput Assist Surg. 2007 Dec 1;3(4):372-7.

25. Li QH, Zamorano L, Pandya A, Perez R, Gong J, Diaz F. The application accuracy of the NeuroMate Robot—A quantitative comparison with frameless and frame-based surgical localization systems. Computer Aided Surgery. 2002;7(2):90-8.

Chapter 4

4 Conclusion and Future Directions

The objectives stated in Chapter 1 are revisited. Conclusions regarding the general outcome in Chapter 2 and 3 are reviewed. Future research potential and clinical significance of the work concludes this thesis.

4.1 Conclusions

In Chapter 2, precision-machined master blocks, with dimensions sufficient to encompass a human glenoid structure (i.e. approximately 50×50×50 mm), were fabricated in order to quantify digitization accuracy and variability using an established method. Based on literature review, the effects of three factors were tested: 1) rounded-tip versus sharp tip stylus, 2) stylus orientation relative to the digitized surface, and 3) robot joint configurations.

The geometry of the sharp-tip stylus facilitates tip calibration using the pivot method, whereas the rounded-tip stylus requires a constant tip offset, which is not always guaranteed to coincide with the surface contact point. Thus, it was hypothesized that the sharp-tip stylus would produce less digitization error. There was indeed a statistically significant difference in error between the sharp-tip and rounded-tip styli, 0.15 ± 0.35 mm and rounded-tip stylus was 0.29 ± 0.40 mm, respectively (p = 0.017). Therefore, the collaborative robot digitization methods will provide better accuracy in reverse-engineering applications using a sharp-tip stylus, taking precautions to avoid scoring from the sharp stylus. However, error using the rounded-tip stylus was still less than 0.5 mm, which is generally considered suitable for most orthopaedic applications. Furthermore, a rounded-tip is safer and not damaging to cartilage and other soft tissues. Thus, it was concluded that the collaborative robot, outfitted with a rounded-tip stylus, can be a suitable manual digitization system for quantifying surfaces similar in volume to the human glenoid.

There was no effect from stylus angles of up to 15° off perpendicular relative to the

digitized surface; however, large rotations in which the stylus was rotated 180° to digitize opposing sides of the volume, increased errors and variability by one order of magnitude. This was likely caused by increased errors from the robot's joint encoders. This result indicates that, while maintaining the stylus tip within this tested volume can produce acceptable levels of error, inverting the stylus causes the robot's end-effector to traverse a much wider space, which significantly increases digitization error. Therefore, the range of end-effector motions should also be constrained within the working volume to achieve the reported accuracy. This is relevant to robotic joint resurfacing systems like MAKOplasty, which also incorporate collaborative robotics.

Chapter 3 reported an evaluation of the collaborative robot as a manual bone surface digitizer with validation in an *in-vitro* glenoid model. Two stylus orientation methods were tested. In one, the stylus was free in all six degrees-of-freedom (6DOF). In the second, the robot was programmed to constrain the stylus to a medial orientation, thus allowing only translations. There was no statistically significant difference between both methods, which in agreement with Chapter 2, indicates that the stylus need not be perpendicular to the digitized surface. In comparison with a 'gold standard' laser scanner, the robotic digitizations produced errors generally less than 0.50 mm, and no single point digitization had an error greater than 1 mm.

In conclusion, collaborative robotics may be useful as localization or reverse-engineering devices. Moreover, the registration fiducials were successful at registering laser scans with contact stylus digitizations. In the context of glenoid replacement or resurfacing, the system tested performed well, with errors less than 0.5 mm, as originally hypothesized. Notwithstanding the fact that the equipment tested may not be used clinically, the evaluation methods presented here can be used to quantify the accuracy and variability of any collaborative robot-assisted digitization method.

4.2 Future Directions

This thesis evaluated the accuracy of the KUKA robot as a digitizer, and the results were in favour of using the robot itself as a digitizer. This creates more opportunities to explore the collaborative robot as an assist in surgical procedures. Glenoid component

complications continue to be the leading cause for revision surgery, and further research on the collaborative robot is required. Therefore, the objective of future plans should include: 1) to explore minimally invasive techniques, 2) to develop a robotic glenoid preparation, 3) to evaluate the accuracy of the robot equipped with a bone burr, 4) to create a force feedback system to limit any complications and 5) use the robot digitization as a tracking system.

There is a high interest in the minimally invasive approach, as it limits the complications of the post-operative surgery. Minimally invasive surgery in orthopaedic applications may reduce the amount of blood loss, hospital stays, soft-tissue disruptions and physiotherapy. This approach may also be favourable for cosmetic reasons, as the incision is much smaller, which limits the length of surgical scars. Therefore, the reamer used to resurface the glenoid needs to be smaller to fit through a smaller incision, as the current diameter reamer is about 3 cm. The reamer is a one-time procedure, in which surgeons simply ream out the bones and then start preparing the bone for glenoid component placement. This may reduce the accuracy of component placement alignment. Therefore, the ream and run procedure should be changed to include a smaller milling bit, which introduces the next objective: to develop a robotic glenoid preparation.

A robot-assisted glenoid preparation involves preoperative planning. After obtaining a computed tomography (CT) scan of the patient's anatomy, the virtual model of the implant will be superimposed to determine the negative area that needs to mill the bones in order to precisely place the implant. Therefore, the robot will need to have a software that involves the milling path. Extensive research is required to in this topic, as there are many ways to create a milling path algorithm; the goal is to find the optimal algorithm so that bone removal is minimal. After the optimal milling algorithm is found, the robot will digitize the glenoid before, during and after the milling process to ensure that the milling process is according to the preoperative plan. Additional study is needed to ensure that the robot digitizer is integrated in the milling path algorithm in case the glenoid is moved.

Thirdly, an accuracy assessment is needed to determine if the robot equipped with a bone burr is comparable to the accuracy of the robot with stylus. This can reduce operation

time as one does not need to change end effector from digitization to milling process. Moreover, reducing the amount of end effector changes needed can simplify the surgical procedure, keep the operation organized, and reduce the cost of equipment.

The robot system in the bone and joint field should have a force feedback; it is beneficial to detect excessive force to avoid any issues. For example, while milling the bone to prepare the glenoid bone bed, the scapula may move, as the scapula is a floating bone. The force feedback should sense this change, and readjust to the current frame for a proper milling path. Comprehensive testing is necessary, as it is unknown how accurate the force feedback is during the milling procedure, as well as how much applied force is needed to mill on a bone.

Lastly, using the robot digitizer as a tracking system limits the registration error as the number of coordinate transformations is reduced. More specifically, digitizing in the robot's native coordinate frame reduces the number of coordinate transformations, consequently reducing mathematical precision errors, which are generally a significant source of registration error.

Appendices

Appendix A: Location Measurement Variability as a Function of Robot Joint Configuration

Introduction

A 7-axis KUKA lightweight robot (LWR4+, KUKA Robotics Canada Ltd. Mississauga, ON) is often redundant since there is more degrees-of-freedom than needed for a task. For example, a human arm can write on a table with their elbow down, however with the extra DOF, the human can write with the elbow up if desired. Furthermore, redundancy occurs when there are more than one configuration to complete a task, where the freedom in joint space is usually greater than required for the task (1). To resolve redundancy, the controls are decomposed to task space and null space (2). A task space is dealing with a 3D Cartesian position or a force vector, where a null space determines the position of the robot's elbow. A null space allows a robot to move dexterously, however it can contribute to position error as shown in Cortesao's paper (2) where he showed that task space robots achieved less than 1 mm error, and null space robots achieved approximately 3 mm. While doing the previous testing, it was found that there was an increased error when doing extreme orientations, even though the KUKA lightweight robot has a marketed repeatability value of 0.05 mm. Moreover, this accuracy does not tell the user which configuration of the robot it was used, or how the configuration affects the accuracy. This procedure will determine the variability of the centre point while the robot is pivoting about a defined point.

Methods

Two different methods to determine the variability were: a) to change the null space while the end effector was fixed and rotated internally, and b) to move the robot arm freely and manually pivot about the defined radius ball. The end effector of the robot was fitted with a 1¼" (31.75 mm) diameter pipe reducer, with an end cap mounted on the end effector. The size of the ball that was mounted onto the tower jig was 28 mm radius. The end effector must be in contact with the ball before recording any values.

For both procedures, the end effector of the robot was calibrated using the robot controller's built-in tool calibration with the XYZ 4-point method, as per the manufacturer's documentation (3). This method requires pivoting on the hemi-sphere, keeping the pipe and the hemi-sphere in contact, and recording four different end-effector poses. A least-squares algorithm calculates the tip offset coordinates relative to the end-effector frame. The calibrated point is the pivot point, which was the centre of the hemi-sphere. The two protocols were defined in a software for the robot.

In the first method, the elbow configuration of the robot could be changed while maintaining the end effector's position. Therefore, the null space was activated in Cartesian stiffness controller by setting the Cartesian spring stiffness high, and the axis-specific spring stiffness low (**Figure A.1** and **Figure A.2**). The software also retained data points, as ten points were recorded, two of these points had the elbow configuration upright at 0 degrees, two points where the elbow was rotated 45° to the right, two points to the left, two points rotated 90° to the right as well as two points to the left.

The second method had a similar procedure as before, except the configuration of the robot is stiff and there is a rotation (yaw and pitch) about a fixed point when recording points. As a result, the second program was set to have a normal axis-specific spring stiffness, and no Cartesian stiffness (**Figure A.3**). The software recorded the end effector twice at 0°, ±45° and ±90°, allowing the orientation of the stylus to have a range of 180°.

The variability was calculated by the standard deviation of all recorded points in Cartesian form, as well as using MATLAB (MATLAB R2011b, The MathWorks, Inc., Natick, MA) to compute the distance of each point to the centroid (**Figure A.4**). This program in MATLAB outputted the average error distance, standard deviation and RMS of the distance from all the points to the centroid. The code in MATLAB was as follows:

```
xyz_bar = mean(xyz);
M = bsxfun(@minus,xyz,xyz_bar);
d = sqrt(sum(M.^2,2)); % distances to centroid

mean(d)
std(d)
sqrt(mean(d.^2))
```
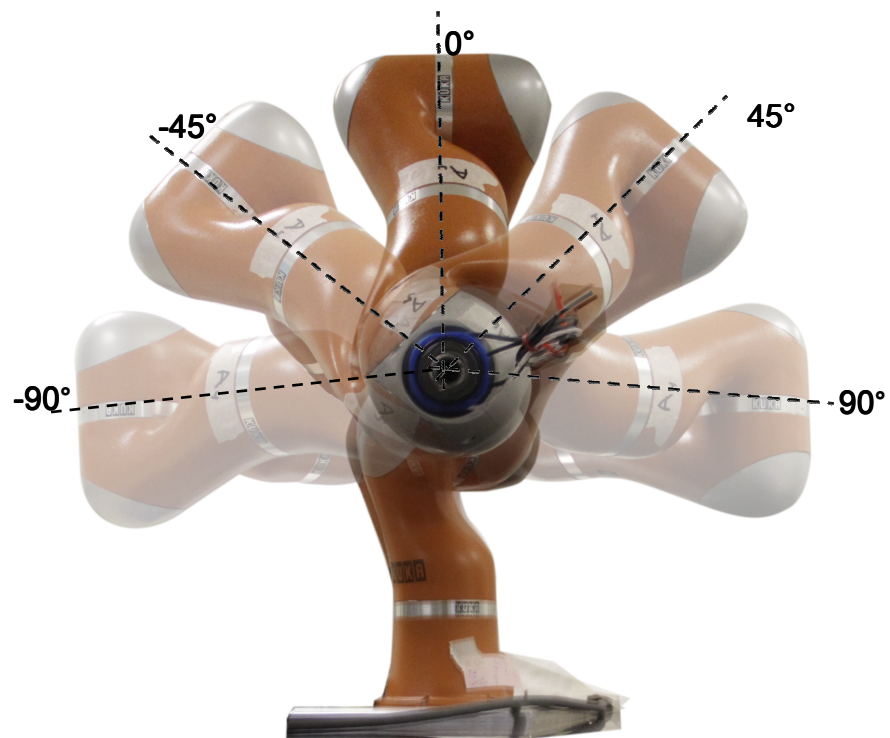
Figure A.1: Different Elbow Configuration of the Robot

A front view of the robot shows five different configurations tested to determine the variability when changing the null space.
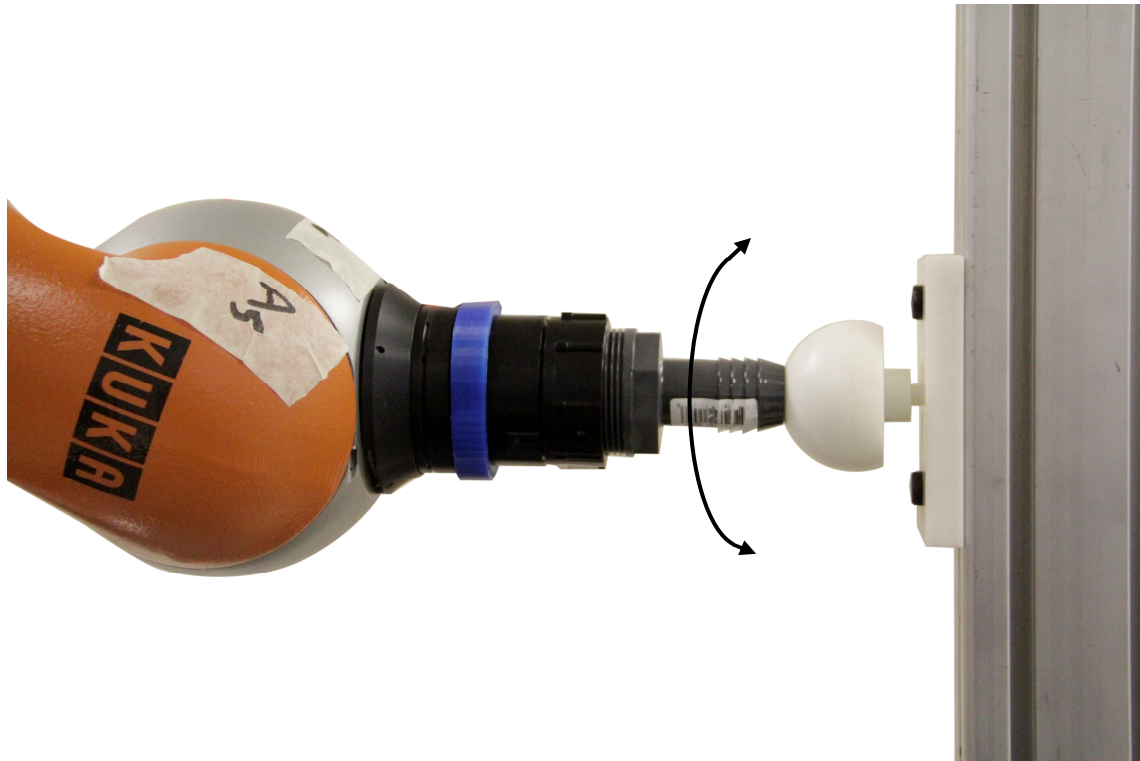
Figure A.2: A Side View of the Robot with Different Elbow Configuration

The stylus is maintained at its rotation about fixed point, and when the configuration changes, the stylus rotates internally.
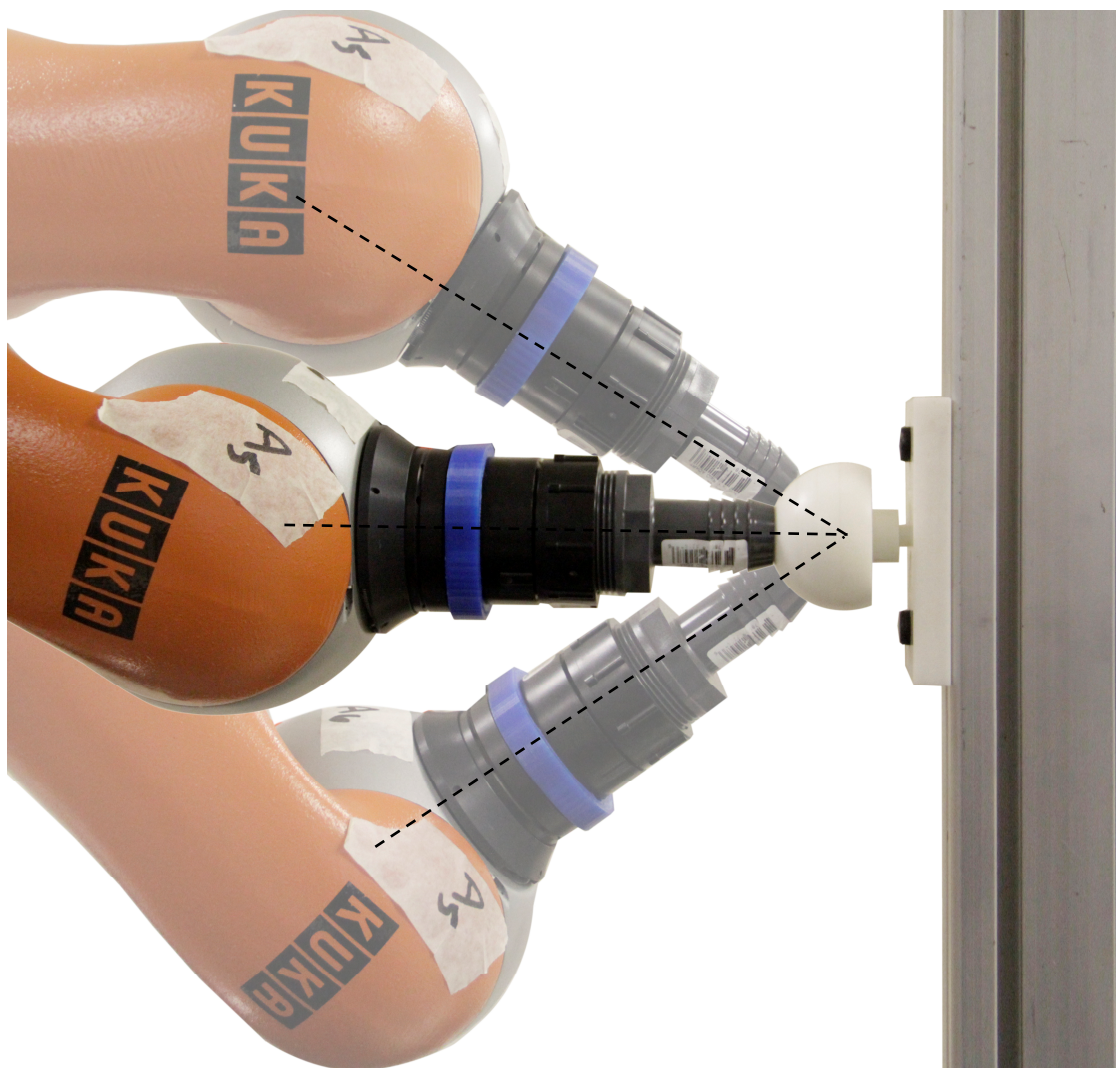
Figure A.3: A Side View of the Robot Stylus Rotating at a Fixed Point

The stylus is rotated about a fixed point. The blue dotted line shows that the stylus is pivoting about a centre of the sphere.
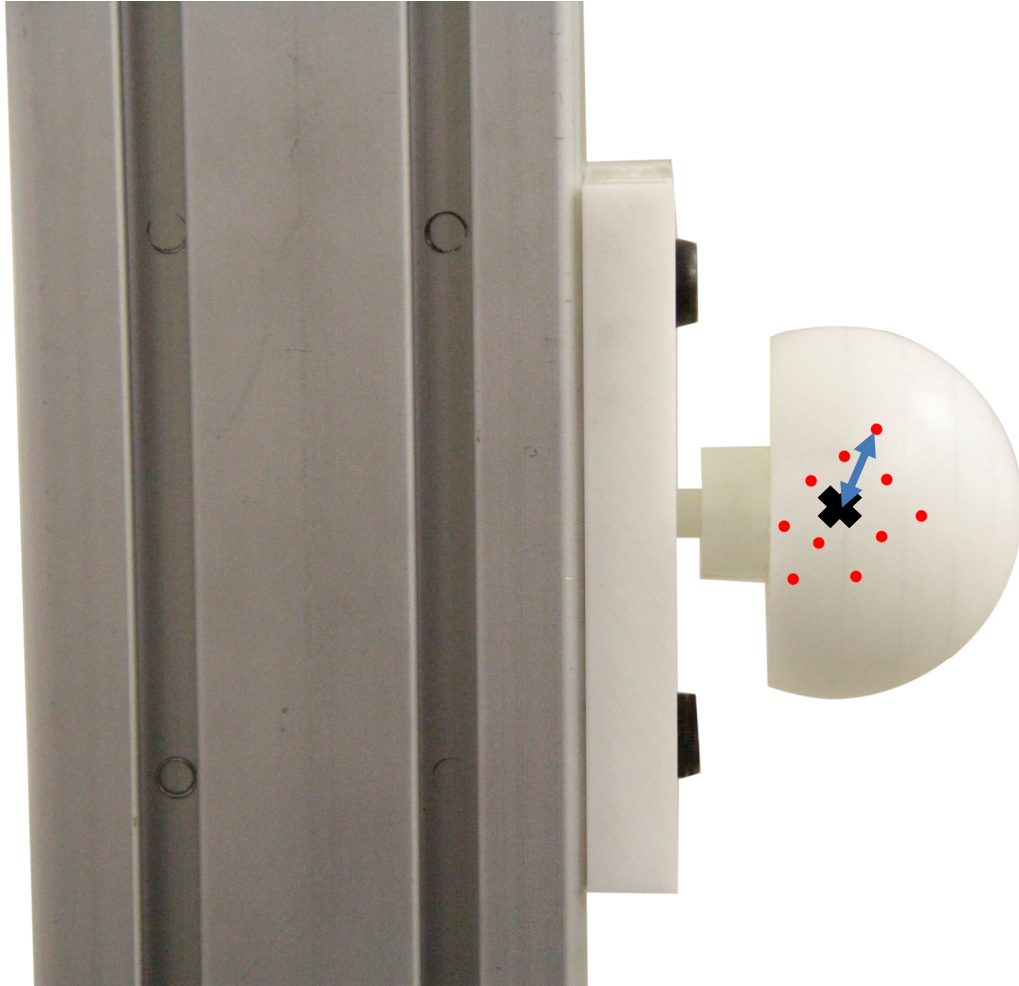
Figure A.4: Determination of the Variability in the Hemi-Sphere

A picture of a hemi-sphere attached to a post to show how the recorded points (red) will be used to determine the variability. The centroid point, marked in black "X", is the average of all recorded points, and the blue arrow represents the distance error between the centroid and the selected point.

Results

Results are shown in **Table A.1**, where changing the null space while the stylus is in place produced a larger variability than moving the stylus around.

Table A.1: Side-by-side Comparison Between Each Technique

Technique 1 - changing the null space [mm]		Technique 2 - changing the orientation of end effector [mm]	
Standard Deviation in Cartesian Form		Standard Deviation in Cartesian Form	
x	2.27	x	1.40
y	0.63	y	1.60
z	2.11	z	0.81
Distance to Centroid Error		Distance to Centroid Error	
Average	2.78	Average	1.88
Standard Deviation	1.20	Standard Deviation	1.15
RMS Error	3.00	RMS Error	2.18

Changing the elbow or the null space show the most change, which can be the significant source of error.

Discussion

There can be many factors contributing to this error, such as recording position of the end effector in stiffness control mode may not be as accurate as in position control mode. Moreover, the stiffness control mode has more parameters such as Cartesian stiffness and damping, as well as axis-specific stiffness and damping. This can be tested by using the master digitization block as described in Chapter 2.

The second technique is composed of task space and null space; however, the null space in this technique had a much smaller range of motion than the first technique, which can explain why the results in the second technique have smaller errors than the first technique. Therefore, it is recommended to keep the null space minimal to reduce the error, and only use null space when needed.

Appendix B: Specimen Information

Specimen Description

Specimens were procured following the guidelines of our institution and the government regulatory agencies.

Table B.1: Description of all Specimens

Specimen	Serial #	Gender	Age	BMI	Weight (lbs)	Height (in)
1	09-12055R	Male	73	18	124.4	69
2	11-03075R	Male	84	20	125	66.5
3	11-08024R	Male	55	28	203	71
4	11-06005R	Male	62	21	137	68

Mean age: 68.5 ± 12.7 years

Appendix C: Robot Specification Data Sheet

All the information from this Specification Data Sheet were obtained from the
documentations of the 7-axis lightweight KUKA robot.

Table C.1: Basic Data

Type	Lightweight Robot LWR 4
Number of axes	7
Volume of working envelope	1.84 m^3
Repeatability (ISO 9283)	±0.05 mm
Weight	approx. 16 kg
Protection classification of the robot	IP 20 ready for operation, with connecting cables plugged in (according to EN 60529)
Protection classification of the in-line wrist	IP 20
Sound level	< 75 dB (A) outside the working envelope
Mounting position	Any
Surface finish, paintwork	CRP, paintwork: orange; base frame enclosure: orange

Table C.2: Ambient Temperature and Conditions

	Temperature	Condition
Operation	0 °C to +30 °C (273 K to 303 K) Relative air humidity ≤90% No condensation permissible.	• Free from inflammable dust, gases and liquids • Free from aggressive and corrosive gases and liquids
Storage and transportation	-10 °C to +60 °C (263 K to 333 K) Relative air humidity ≤75% No condensation permissible.	• Free from flying parts • Free from spraying liquids • Free from electromagnetic loads, e.g. from welding equipment or high-frequency converters

Table C.3: Axis Data

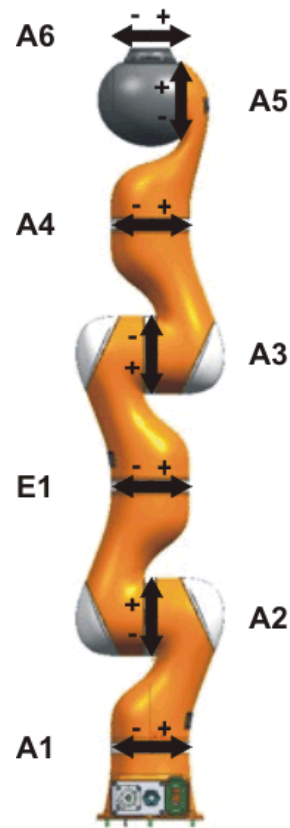| Axis	Range of motion	Velocity without payload	Maximum torque
A1 (J1)	+/-170°	112.5 °/s	200 Nm
A2 (J2)	+/-120°	112.5 °/s	200 Nm
E1 (J3)	+/-170°	112.5 °/s	100 Nm
A3 (J4)	+/-120°	112.5 °/s	100 Nm
A4 (J5)	+/-170°	180.0 °/s	100 Nm
A5 (J6)	+/-120°	112.5 °/s	30 Nm
A6 (J7)	+/-170°	112.5 °/s	30 Nm

Figure C.1: Robot Axes

Figure C.1 shows a drawing of the robot in a candle position, and axis notations are specified accordingly.
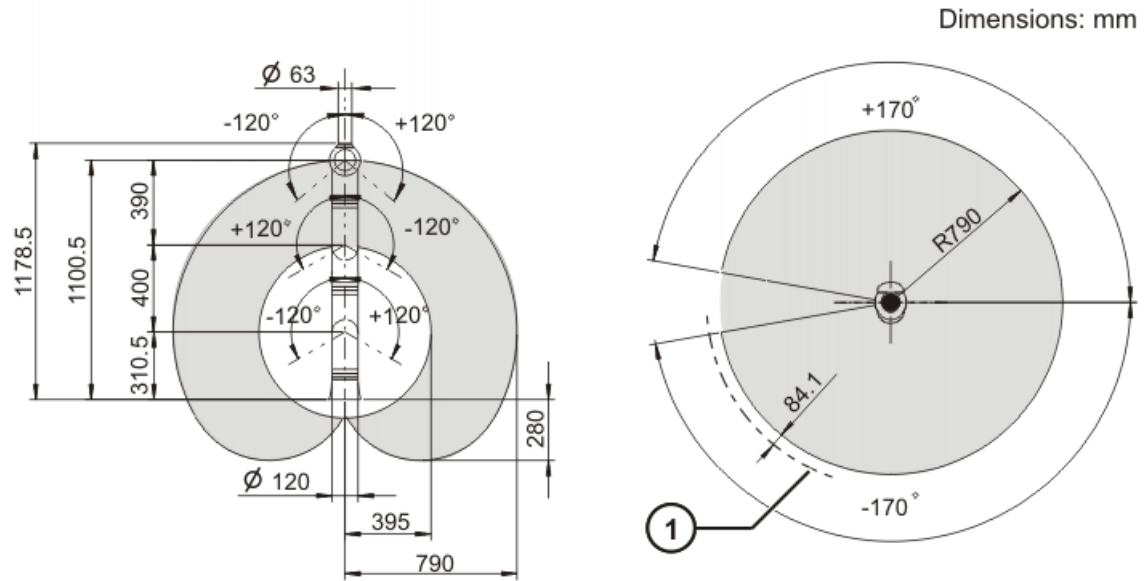
Figure C.2: Working Envelope

Figure C.2 shows a picture of the maximum range of motion of the KUKA robot. Notation 1 represents interference radius.

Table C.4: Mounting Flange

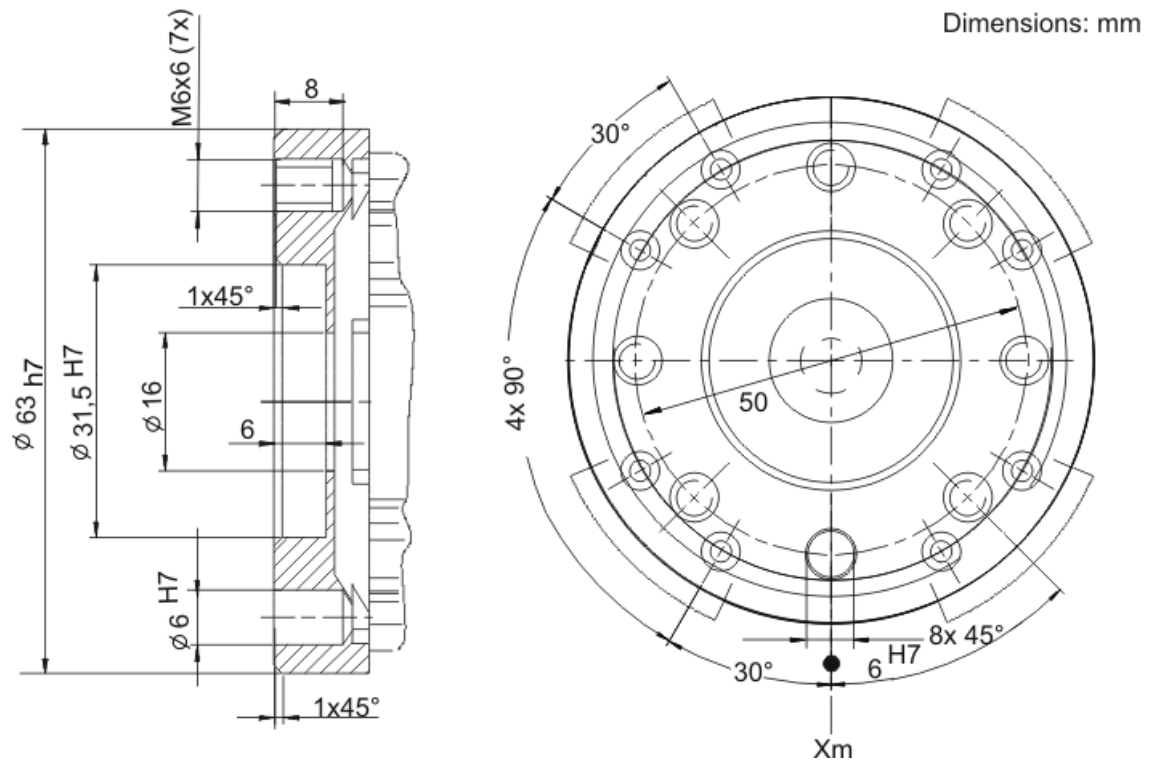| Mounting flange	DIN ISO 9409-1-A50
Strength class	10.9
Screw size	4 x DIN6912-M6
Depth of engagement	5 mm
Locating element	6 H7

Figure C.3: Mounting Flange

The dimensions of the mounting flange in the end-effector of the robot is shown in **Figure C.3**. Variable Xm represents the position of the locating element.

Figure C.4: Loads Acting on the Mounting Base

Notations of each force and moments are shown in **Figure C.4**. The specified forces and moments already include the payload and the inertia force (weight) of the robot.

Table C.5: Type of Loads Acting on the Mounting Base

Type of load	Force/torque/mass
F_v = vertical force	F_{vmax} = 396 N
F_h = horizontal force	F_{hmax} = 215 N
M_k = tilting moment	M_{kmax} = 306 Nm
M_r = torque	M_{rmax} = 204 Nm
Total mass for load acting on the mounting base	22 kg
Robot	approx. 16 kg
Total load (rated payload)	7 kg

Table C.6: Cartesian Stiffness Controller: Parameterization (3)

	Stiffness				Damping			
	Min.	Max.	Default	Unit	Min.	Max.	Default	Unit
X								
Y		5 000	2 000	[N/m]				[N*s/m]
Z	0.01				0.1	1.0	0.7	
A								
B		300	200	[Nm/rad]				[Nm*s/rad]
C								

Table C.7: Axis-specific Stiffness Controller: Parameterization

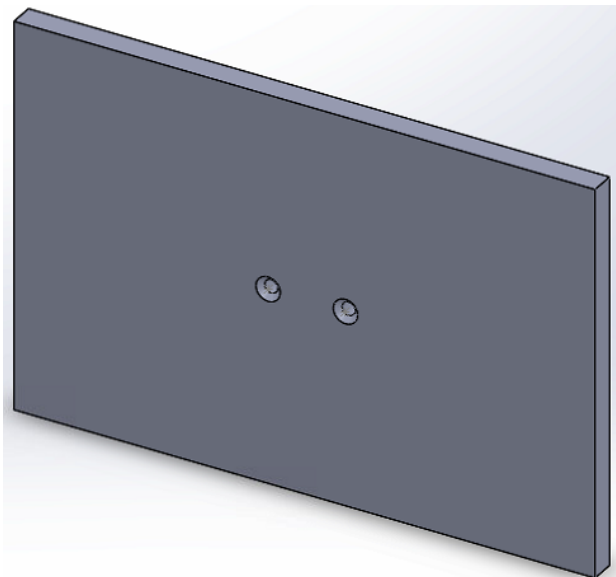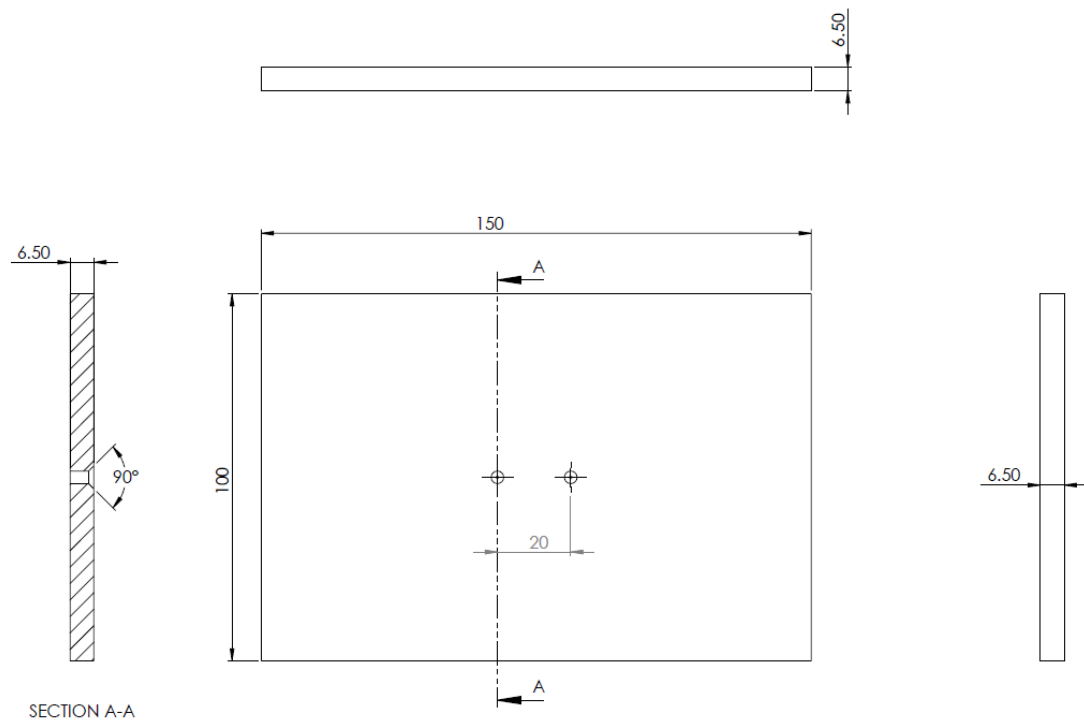|	Stiffness [Nm/rad]			Damping [Nm*s/rad]		
	Minimum	Maximum	Default	Minimum	Maximum	Default
A6						
A5						
A4						
A3	0.01	2 000	1 000	0.1	1.0	0.7
E1						
A2						
A1						

The definition of damping value for both **Table C.6** and **C.7** are as follows:

- Damping value 0: undamped vibration (not recommended)
- Damping value 0.7: default setting
- Damping value 1: completely damped vibration (no overshoot)

Note that excessive stiffness in Cartesian (Position stiffness > 5,000 or Rotation stiffness > 300) or in axis-specific (> 2,000) or damping (> 1) in stiffness control can cause the robot to buzz. Damage to the industrial robot may result.
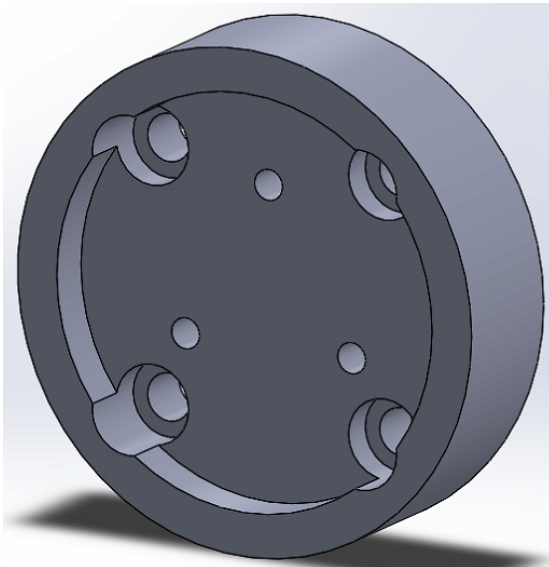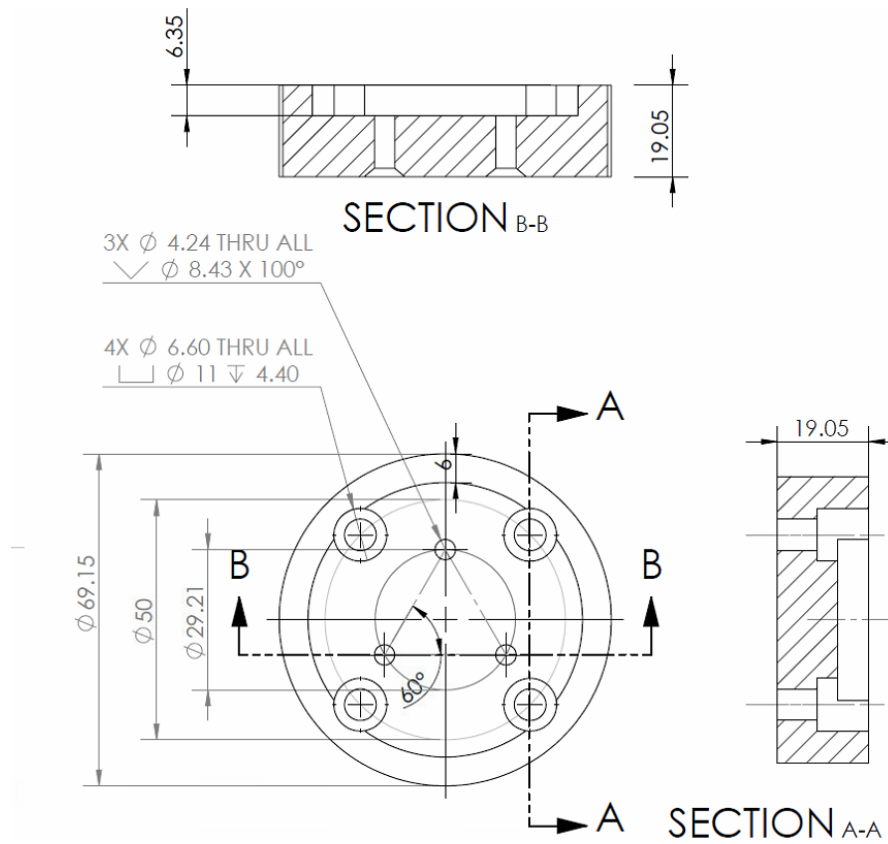
Appendix D: Mechanical Drawings

D1: Acrylic Base Board for Glenoid
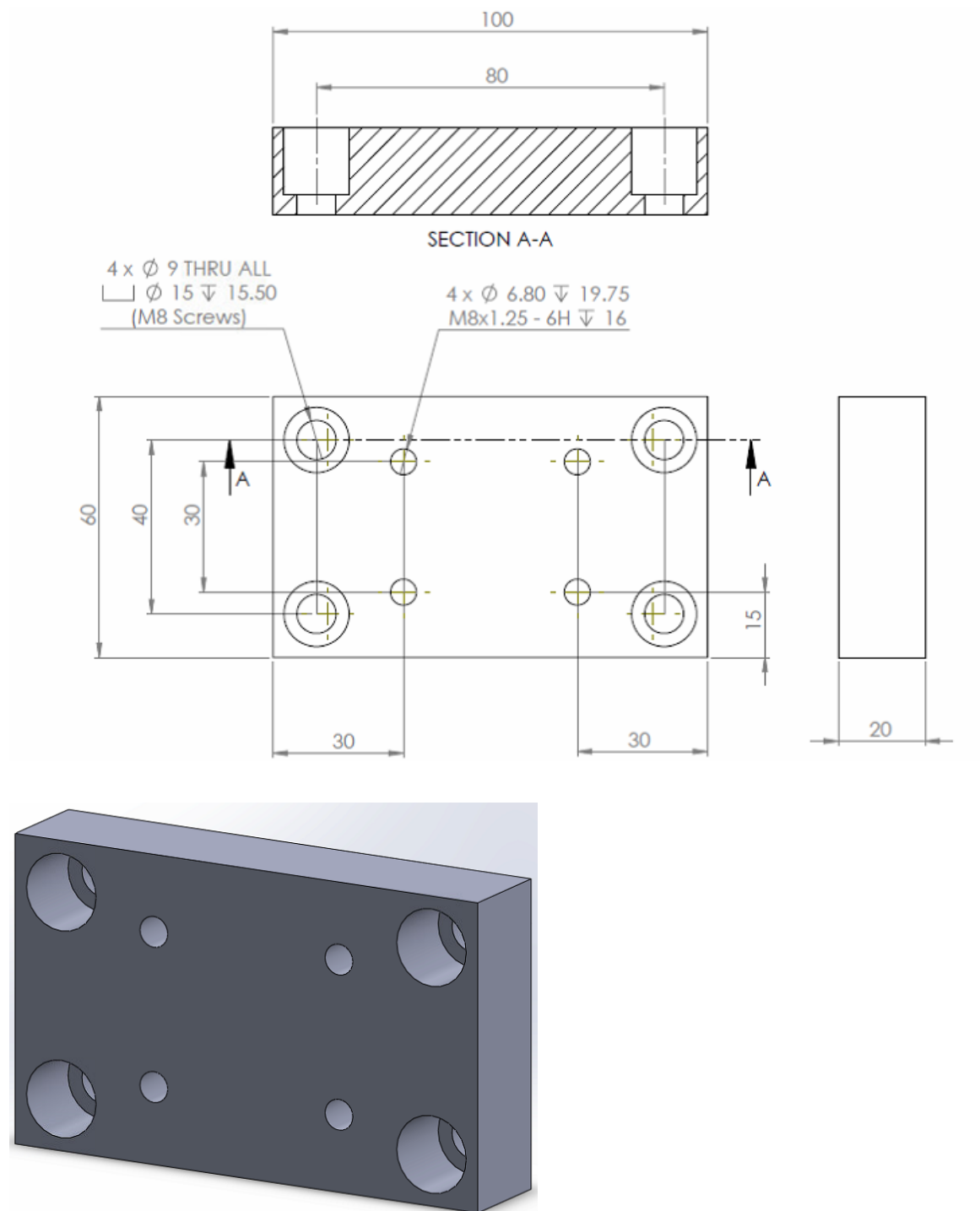

Dimensions in [mm]

D2: End Effector Mount Base for Pipe Reducer

SECTION B-B

6.35

19.05

3X Ø 4.24 THRU ALL
∨ Ø 8.43 X 100°

4X Ø 6.60 THRU ALL
⊔ Ø 11 ↧ 4.40

A

B

B

Ø 69.15

Ø 50

Ø 29.21

60°

A

19.05

SECTION A-A

Dimensions in [mm]

D3: Mount Board for the first Accuracy Assessment Digitization Block

SECTION A-A

4 x Ø 9 THRU ALL
Ø 15 ⊽ 15.50
(M8 Screws)

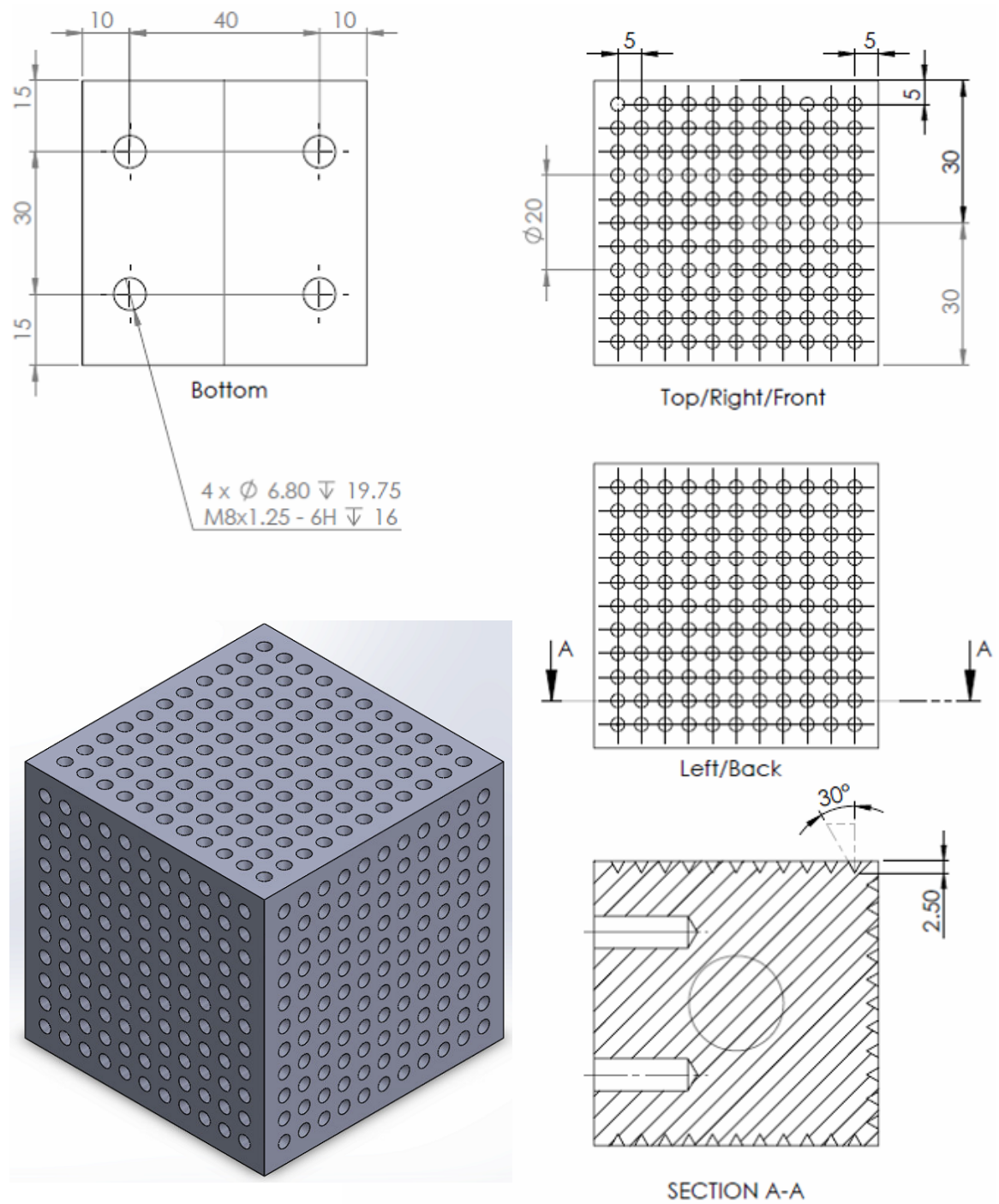4 x Ø 6.80 ⊽ 19.75
M8x1.25 - 6H ⊽ 16

100

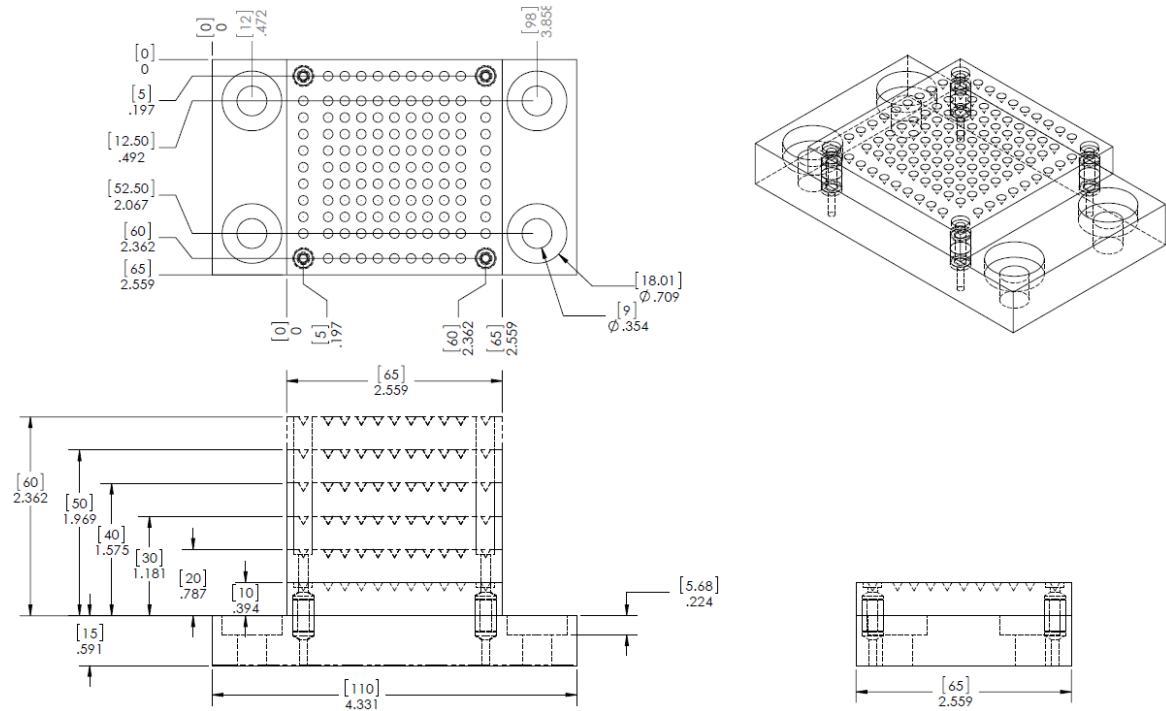80

60

40

30

30

30

15

20

Dimensions in [mm]

D4: First Accuracy Assessment Digitization Block

Dimensions in [mm]

D5: Second Accuracy Assessment Digitization Block

Dimensions in Squared Bracket in [mm]

Otherwise in [inches]

D6: Peg Base
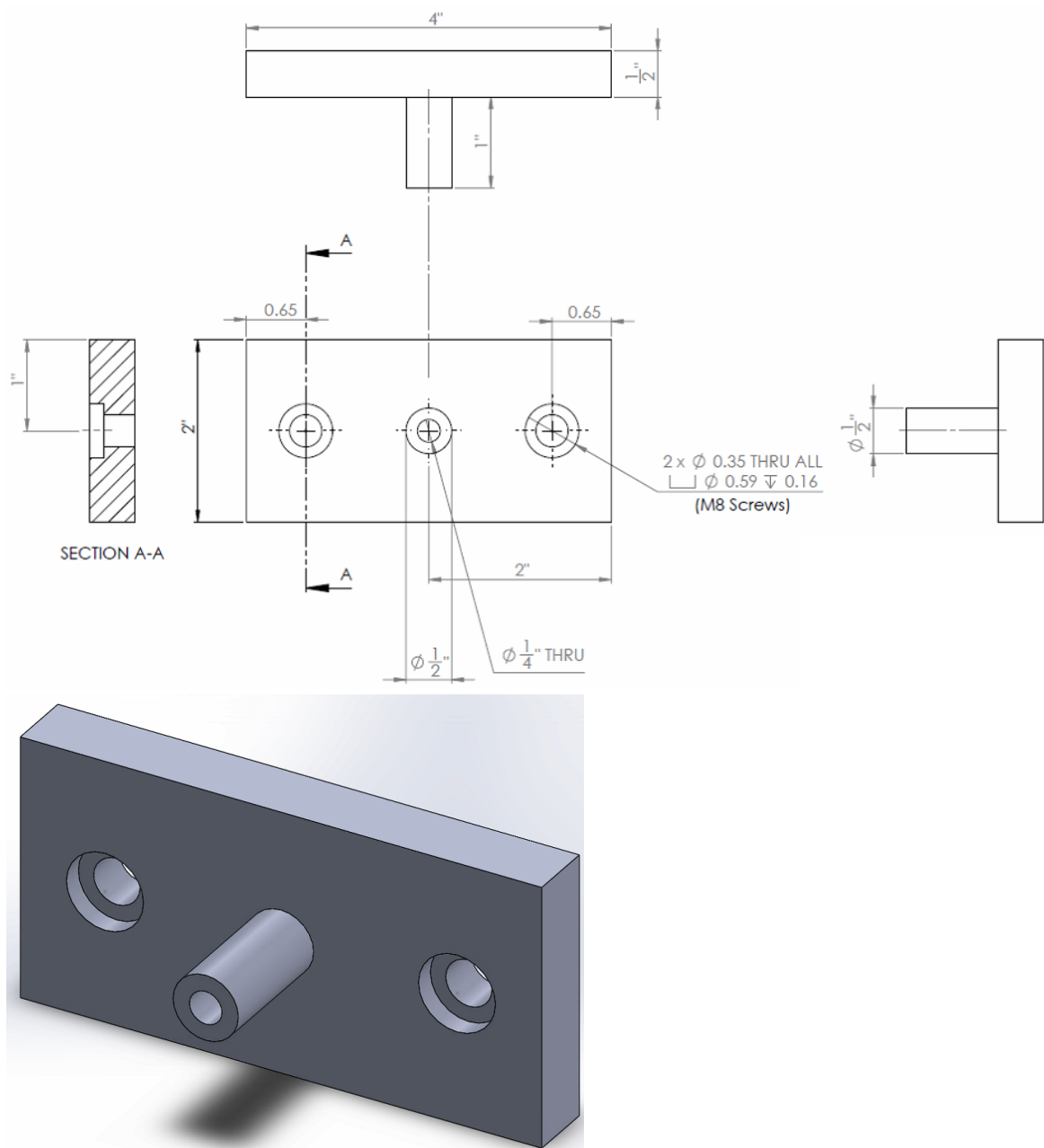
Dimensions in [inches]

D7: Handle for Two Styli

2 x Ø 0.20 ↧ 1¼"
1/4-20 UNC ↧ 1½"

4 x Ø 0.26 THRU ALL
⌴ Ø 0.43 ↧ 0.96

R0.22

SECTION A-A

1½"

1¼"

2½"

2½"

1¼"

5"

1½"

Ø 1.97 (50mm)

5"

SECTION B-B
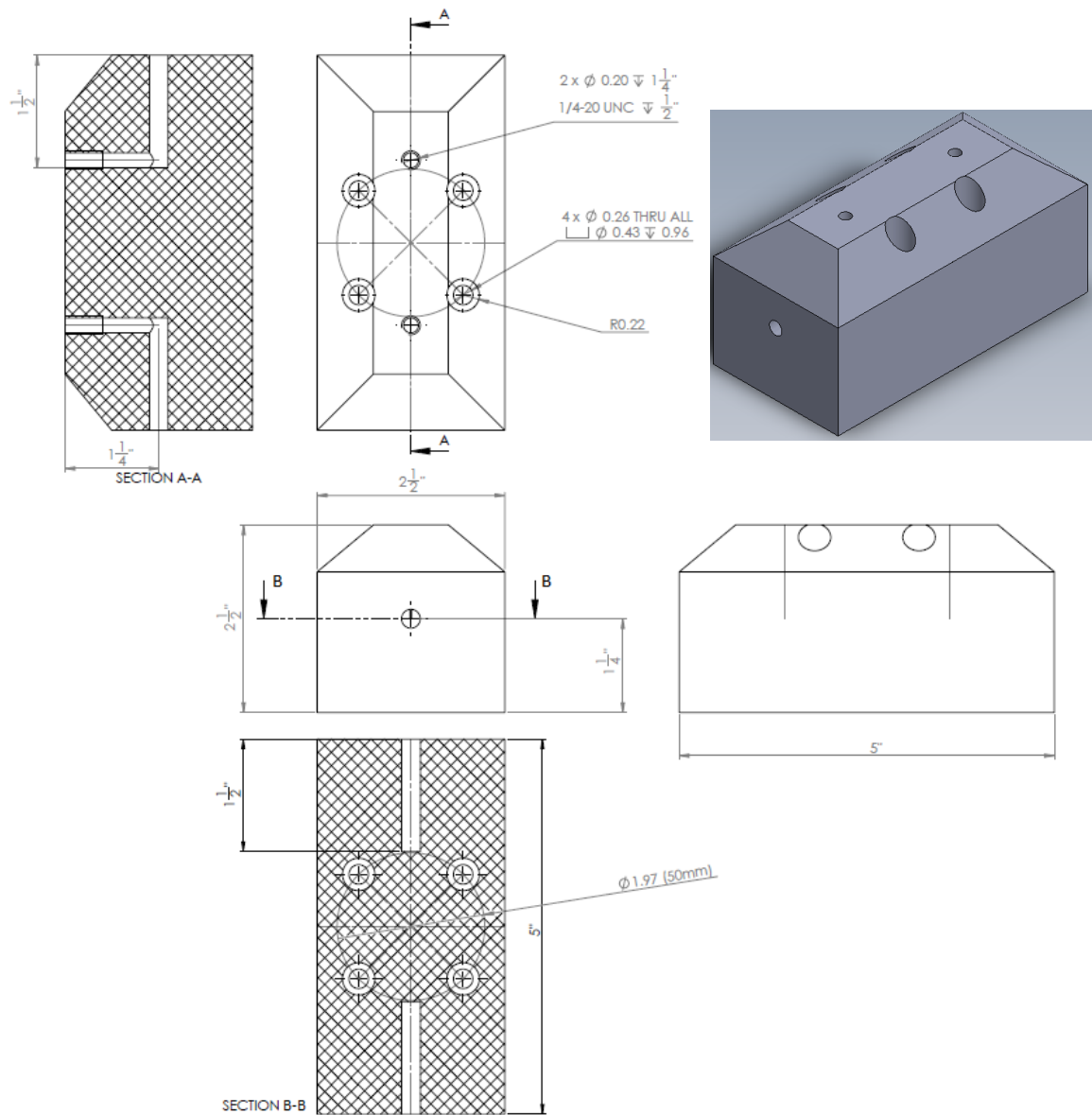
Dimensions in [inches] otherwise specified.

D8: Styli

(A) Rounded Tip Stylus

Rounded Tip
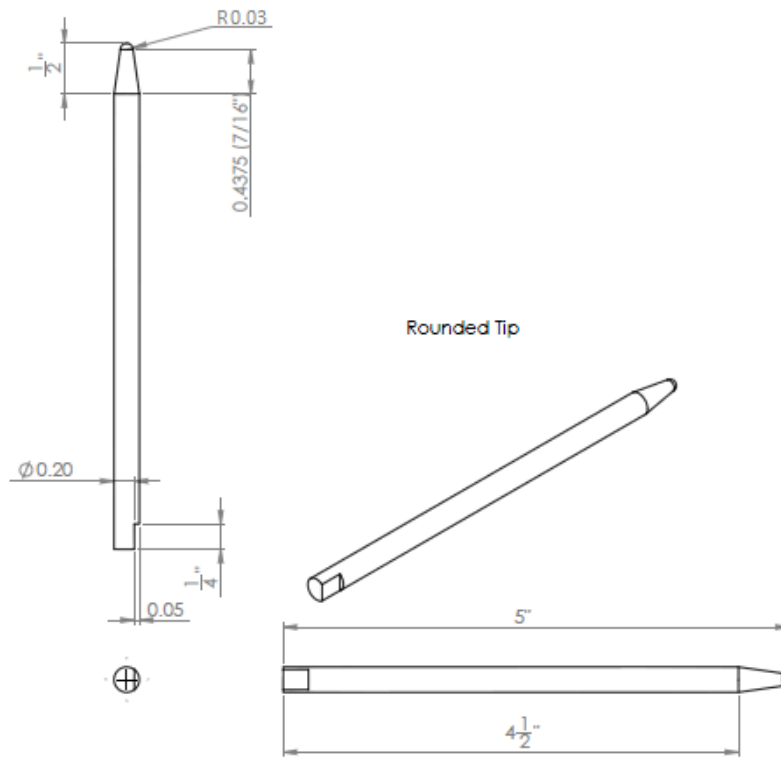
(B) Sharp Tip Stylus
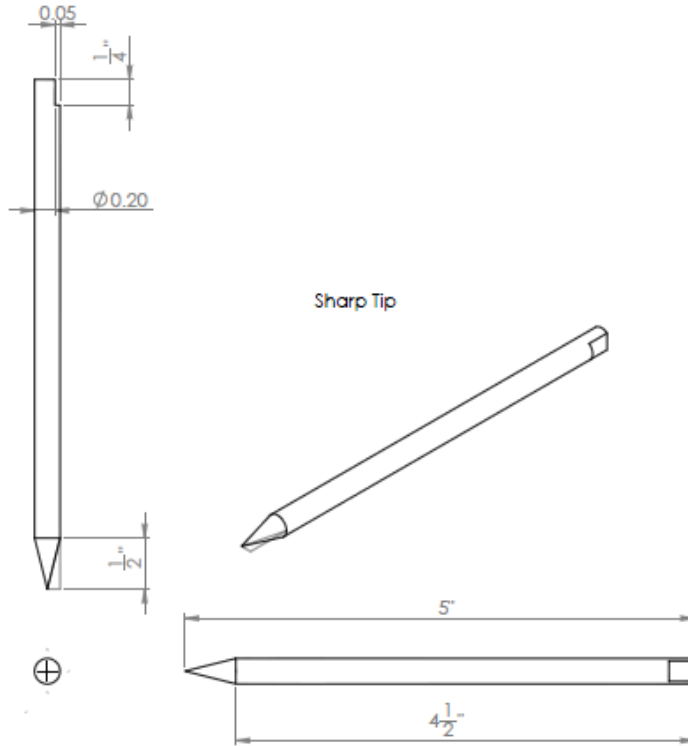
Dimensions in [inches] otherwise specified.

References

1. Towell C, Howard M, Vijayakumar S. Learning nullspace policies. IEEE; 2010.

2. Cortesao R, Zarrad W, Poignet P, Company O, Dombre E. Haptic control design for robotic-assisted minimally invasive surgery. Intelligent robots and systems, 2006 IEEE/RSJ international conference; 2006.

3. KUKA system software 5.6 lr: Operating and programming instructions for system integrators. 5th ed. Augsburg, DE: KUKA Laboratories GmbH; 2012.

Curriculum Vitae

Sara Zimmo BESc

The Hand and Upper Limb Centre Research ‖ St. Joseph's Health Care

Musculoskeletal Health Research & Graduate Program in Biomedical Engineering
‖ Western University

EDUCATION

Sep. 2012 – Present	**MESc in Biomedical Engineering** Western University, London, Ontario, Canada *Supervisor: Dr. Louis Ferreira*
Jan. 28 – 31, 2013	**Certificate in Advanced Robot Programming V5.x** KUKA College, Shelby Township, Michigan, USA *Instructor: James Rude*
Jan. 21 – 24, 2013	**Certificate in Basic Robot Programming V5.x** KUKA College, Shelby Township, Michigan, USA *Instructor: Jeffrey James*
Sep. 2009 – Jun.2012	**Certificate in Technological Entrepreneurship** Western University, London, Ontario, Canada
Sep. 2008 – Jun.2012	**BESc in Electrical and Computer Engineering** With Wireless Communications Option Western University, London, Ontario, Canada

---

POSITIONS

Sep. 2012 – Present	**Graduate Research Assistant** Graduate Program in Biomedical Engineering Western University, London, Canada *Supervisor: Dr. Louis Ferreira*

TEACHING EXPERIENCE

Jan. 2014 – Apr. 2014	**Graduate Teaching Assistant** MME 2213b Engineering Dynamics Department of Mechanical & Materials Engineering Western University, London, Canada

Sep. 2013 – Dec. 2013	**Graduate Teaching Assistant** MME 2259a Product Design and Development Department of Mechanical & Materials Engineering Western University, London, Canada
Jan. 2013 – Apr.2013	**Graduate Teaching Assistant** MME 4452b Robotics and Manufacturing Automation Department of Mechanical & Materials Engineering Western University, London, Canada
Sep. 2012 – Dec. 2012	**Graduate Teaching Assistant** ES 1050 Intro. Engineering Design and Innovation Studio Faculty of Engineering Western University, London, Canada

---

MANUSCRIPTS IN PREPARATION FOR SUBMISSION

1) Zimmo SS, Lalone EA, Ferreira LM. Evaluation of a 7-Axis Collaborative Robot as a Bone Surface Digitizer: With Validation in an In-Vitro Glenoid Model. 2014.

2) Zimmo SS, Ferreira LM. Determination of the accuracy of a 7-axis collaborative robot as a manually operated surface digitizer: with emphasis on robot-assisted surgeries within small working volumes. 2014.

ABSTRACTS, POSTERS AND PRESENTATIONS

1) Zimmo SS, Ferreira LM. Robot-Assisted Shoulder Arthroplasty: A Minimally Invasive Approach. *BME Seminar at Western University*, London, Ontario, December 2013. (Presentation)

2) Zimmo SS, Ferreira LM. Minimally Invasive Surgery using Robotic Glenoid Milling. *London Health Research Day*, London, Ontario, March 2013. (Poster)

3) Zimmo SS, Lalone EA, Ferreira LM. Evaluation of a Gravity Compensated 7-Axis Robot a Manual Digitizer of Osseous Anatomical Landmarks for Intra-Operative Robot-Assisted Orthopaedic Procedure. *Talks on Fridays at Lawson Health Research Institute*, London, Ontario, November 2013. (Presentation)

4) Zimmo SS, Lalone EA, Ferreira LM. Evaluation of a Gravity Compensated 7-Axis Robot a Manual Digitizer of Osseous Anatomical Landmarks for Intra-Operative Robot-Assisted Orthopaedic Procedure. *Annual Meeting of Society of Robotic Surgery*, Orlando, Florida, November 2013. (Poster)

5) Zimmo SS, Lalone EA, Ferreira LM. Evaluation of a Gravity Compensated 7-Axis Robot a Manual Digitizer of Osseous Anatomical Landmarks for Intra-Operative Robot-Assisted Orthopaedic Procedure. *BME Seminar at Western University*, London, Ontario, December 2013. (Presentation)

6) Zimmo SS, Lalone EA, Ferreira LM. Evaluation of a Gravity Compensated 7-Axis Robot a Manual Digitizer of Osseous Anatomical Landmarks for Intra-Operative Robot-Assisted Orthopaedic Procedure. *Annual Bone and Joint Injury Repair Conference*, London, Ontario, January 2014. (Poster)

7) Zimmo SS, Lalone EA, Ferreira LM. Evaluation of a 7-Axis Robot as a Bone Surface Digitization Device. *The 60th Annual Meeting of the Orthopaedic Research Society*, New Orleans, Louisiana, March 2014. (Poster)

8) Zimmo SS, Lalone EA, Ferreira LM. Evaluation of a Gravity Compensated 7-Axis Robot as a Manual Digitizer of Osseous Anatomical Landmarks for Intra-Operative Robot-Assisted Orthopaedic Procedures. *Combined Annual Meeting of the American Orthopaedic Association and Canadian Orthopaedic Association*, Montreal, Ontario, June 2014 (Poster)

MEETINGS ATTENDED

1) London Health Research Day, London, Ontario, March 2013

2) The Annual Bone and Joint Retreat, London, Ontario, May 2013.

3) The Annual Meeting of Society of Robotic Surgery, Orlando, Florida, November 2013.

4) The Annual Bone and Joint Injury Repair Conference, London, Ontario, January 2014.

INVITED TALKS

1) Discovery Day at Western, part of the TD Discovery Days in Health Sciences program, organized through the Canadian Medical Hall of Fame and Western, at St. Joseph's Health Care, London, Ontario, May 2013. (Demonstration)

2) London Museum School program, organized by the London Heritage Council, Canadian Medical Hall of Fame, and the Lawson Health Research Institute, at St. Joseph's Health Care, London, Ontario, May 2013. (Demonstration)

3) Roth | McFarlane Hand and Upper Limb Centre Renaming at St. Joseph's Health Care, London, Ontario, September 2013. (Demonstration)

4)   Museum School Tour, organized by the Lawson Health Research Institute, at St. Joseph's Health Care, London Ontario, October 2013. (Demonstration)

HONOURS AND AWARDS

2011 – 2012   **Dean's Honour List**
Awarded to a full time student who has maintained an average of 80% or more

2009   **Ontario Volunteer Service Award**
Award in recognition of commitment to volunteerism from the Ontario Minister of Citizenship and Immigration

2008 – 2009   **Western Scholarship of Distinction**
Awarded upon admission to Western students who have an admission average of 85-89.9%

2007   **Muslim Association of Canada – Most Active Youth Scholarship**
Nominated and awarded for being active in many community involvements

---

RELEVANT GRADUATE COURSES

Fall Term 2012   ECE 9513A Robot Control

Winter Term 2013   BIOMED 9502B Engineering Analysis of Physiological System
BIOMED 9550B Principles of Communication and Knowledge

Fall Term 2013   MSK 9000A Biomedical and Bioengineering Concepts

Winter Term 2014   MSK 9100B Fundamental Concepts in Clinical and Health Services Research

---

LEADERSHIP and VOLUNTEER ACTIVITIES

Sep. 2012 – Present   **Radio Talk Host and Organizer**
Weekly look at issues, events and news about the Islamic Faith
Muslims Live! on CHRW94.9FM
Western University, London, Ontario, Canada

Sep. 2011 – Present   **MAC Give President**
Outreach to larger community to help the needy
Outreach Department
Muslim Association of Canada, London, Ontario, Canada

Apr. 2014 – Present   **Internal Media Relations**
Sub-committee responsible for creating, designing and
maintaining media outreach
London Muslim Mosque, London, Ontario, Canada

Sep. 2013 – Apr. 2014   **BME Treasurer**
Graduate Program in Biomedical Engineering
Western University, London, Ontario, Canada

Jan. 2014 – Mar. 2014   **#WinterRefugee Committee Organizer**
Responsible for raising awareness and money for the
Syrian Refugees during winter
London, Ontario, Canada

Feb. 2013 – Apr. 2013   **Chief Returning Officer**
Appointed by the President to administer the elections
process
Muslim Students' Association
Western University, London, Ontario, Canada

Sep. 2012 – Apr. 2013   **Senior Executive**
Muslim Students' Association
Western University, London, Ontario, Canada

Mar. 2013   **Open House Volunteer**
Robot and Automation Laboratory
Western University, London, Ontario, Canada

Aug. 2012   **Summer Camp Councillor**
Spiritual and Recreational Camp for Muslim Teenagers
Muslim Association of Canada London Chapter, London,
Ontario, Canada

Sep. 2011 – Apr. 2012   **VP Finance Executive with Signing Authority**
Muslim Students' Association
Western University, London, Ontario, Canada

Sep. 2005 – Jun. 2012   **Guider/Leader of Girl Guides of Canada**
Various Groups (88th Sparks, 120th Brownies, 88th Guides
and 55th Rangers)
Westmount District, London, Ontario, Canada

Mar. 2012	**Open House Volunteer**
	Electrical Engineering Communication Laboratory
	Western University, London, Ontario, Canada
Sep. 2010 – Apr.2011	**Athletic Manager**
	Responsible for running various recreational activities for the club members
	Muslim Students' Association
	Western University, London, Ontario, Canada
Jul. 2010	**Summer Camp Councillor**
	Spiritual and Recreational Camp for Muslim Teenagers
	Muslim Association of Canada London Chapter, London, Ontario, Canada